Energy-Saving Melting and Revert Reduction Technology (E-SMARRT)
Task 5.3: Casting Porosity-Free Grain Refined Magnesium Alloys
Final Technical Report

Award Number DE-FC36-04GO14230
Project Period: (January 2004 – June 2013)

Case Western Reserve University
10900 Euclid Avenue
Cleveland, OH 44106

David Schwam, Principal Investigator
Phone: 216-368-6499
Email: dxs11@case.edu

Contributors:
Xuejun Zhu, Postdoctoral Trainee
Daniel Druyor, MS Student
Richard Tomazin, Research Engineer

August 12, 2013

Acknowledgements

Acknowledgement: This report is based upon work supported by the U. S. Department of Energy under Award No. DOE award DE-FC36-04GO14230.

Table of Contents

List of Tables

List of Figures

Executive Summary

The objective of this project was to identify the root causes for micro-porosity in magnesium alloy castings and recommend remedies that can be implemented in production.

Three casting magnesium alloys were used to determine the causes of porosity that is a common problem in the magnesium casting industry. These alloys were AM50A, AM60A, and AZ91D, and all were grain refined with C_2Cl_6. Gas porosity was found to have little effect if proper degassing methods and foundry practices were used. It was found that sound gating practice, directional solidification towards the riser and generous risering should always dominate in order to produce sound castings. In sand cast magnesium, thermal gradients were found to be an important indicator of heat transfer in the mold. A minimum thermal gradient was found for each alloy that would produce sound castings. There were 2.02°C/cm for AM50A, 1.99°C/cm for AM60A, and 1.97°C/cm for AZ91D. If these gradients are met or exceeded when an area of the casting reaches 50°C below the liquidus for the alloy, the casting will be free of shrinkage porosity in that area. The cooling rates measured during casting magnesium alloys in a pre-heated step permanent mold ranged from 12°F/min in the three inches thick step to 200°F/min in the one inch step. The effect of the cooling rate on the grain size and the mechanical properties was noticeable but not substantial.

Grain refining with C_2Cl_6 had a marked effect on the grain size of the permanent mold step casting. It reduced it by 10-15% in AM50A and by a factor of six in AZ91E from 300 μm to around 55 μm. The mechanical properties of both permanent mold cast AZ91E and AM50A were improved by grain refinement. The most prominent increase was in the elongation of AM50A that more than doubled from 8% to 17%.

Computer simulation of porosity was conducted for a well gated commercial wheel casting. The simulation did not predict significant porosity in the wheel. The mechanical testing of tensile specimens excised from the wheel indeed confirmed good properties, in line with the specifications for this alloy. Evidence of minimal micro-porosity was detected in sections cut from the wheel and investigated under optical microscopy. This finding confirms the key role played by utilizing optimal gating and risering practices in minimizing porosity in magnesium castings.

1 Introduction

Magnesium and its alloys are important structural metals due to their high strength to weight ratio. This allows the production of light weight components with similar mechanical properties to their heavier alloy counterparts. The automotive industry in particular is very interested in ways to reduce the gross weight of vehicles to increase fuel efficiency. With shrinking global oil reserves and the associated increase in gasoline prices, magnesium alloy castings are quickly becoming an economical means of weight reduction in the many sectors of industry including automotive. Table 1.1 shows the tensile strength to density ratio of various structural materials commonly found in automobiles (1).

Table 1 Tensile strength to density ratio for various metals found in automobile construction (2, 3, 4)

Material	Ultimate Tensile Strength (MPa)	Density (g/cm^3)	Ratio ($MPa/g/cm^3$)
Magnesium (AZ91D)	230	1.81	127
Aluminum (A390)	310	2.72	114
Steel (1020, hot rolled)	475	7.87	60

Magnesium alloy die castings produced for automotive use reached over 82,000 tons and are predicted to reach production levels of 250,000 tons by 2015 (5). In 2002, fuel savings due to lightweight aluminum and magnesium cast parts in automobiles were estimated to be over 719 million dollars (6). This energy savings has been the driving force for a renewed interest in lightweight alloy castings including magnesium.

Magnesium has other advantages over other structural metals. Two of these are very important for the die casting industry. The first is the fact that magnesium alloys can be die cast over four times faster than aluminum alloys. Die life is also greatly increased due to the lower incidence of soldering to die surfaces. Since die replacement costs and production rate greatly impact the die casting industry, cost savings in these areas are essential and can greatly impact profitability (7). Another advantage is that magnesium is easier to machine than aluminum. This leads to reduced tooling costs as the life of machine tools increases. Magnesium can also be machined much faster than aluminum, leading to time savings and increased throughput. Finally, magnesium alloys can be machined dry, eliminating the costs associated with using and disposing of lubricants.

Significant research, including this work, has been funded by the U.S. Department of Energy in hopes of further improvement of light metal castings. As research and development continues, magnesium castings with improved properties will be able to replace more of the total weight of vehicles, further increasing energy cost savings and thus reducing the dependence of the United States on foreign oil sources.

2 Literature Review

2.1 Magnesium and its Alloys

Magnesium is a silvery-white metal first produced in metallic form in 1808 by Sir Humphrey Davy. Industrial scale production began in 1886 in Germany. It is the lightest structural metal, with a density of 1.7g/cm3 (8). Magnesium is one of the most common elements in the earth, comprising about 2.5% of the earth's crust. Worldwide magnesium production is expected to exceed 500,000 metric tons annually by 2015 (9).

Magnesium is refined from sea water and magnesium-containing minerals. The most common means of refining involves electrolysis of magnesium chloride salt. Thermal cracking of magnesia (MgO) is a lesser used method. Most magnesium produced today is used to alloy with aluminum (40-45%). The magnesium additions to aluminum alloys increase the strength without adversely affecting the ductility. Roughly 35% is used in the production of magnesium cast parts, and the remainder is used in the desulfurization of iron and steel as well as various other applications. Magnesium is an important alloying element in ductile iron, which causes the graphite to nucleate into spherical particles rather than flakes. A small percentage is used in electrochemical applications such as sacrificial anodes in cathodic protection.

The alloys used in this study were AM50A, AM60A, and AZ91D. The first two letters in the standard ASTM magnesium alloy naming convention indicate the two principal alloying elements, arranged in order of decreasing percentage. The two following digits represent rounded-off percentages of the two principal alloying elements. The final letter (if present) is used to differentiate between different alloys with the same base composition. A temper designation is placed at the end if required. Table 2 shows the compositions of the alloys used in this study. Table 3 shows selected thermal properties for each alloy.

Table 2 Compositions of the alloys used in this study. (*) minimum. Please see Tables 13, 14, and 15 in the appendix for the full specifications for each alloy.

Alloy	Aluminum (wt %)	Manganese (wt %)	Zinc (wt %)
AM50A	5.0	0.13 *	0.0
AM60A	6.0	0.13 *	0.0
AZ91D	9.0	0.13 *	0.7

Table 3 Selected thermal properties for magnesium alloys. (2)

Alloy	Liquidus (°F/°C)	Solidus (°F/°C)	Thermal Conductivity (W/m-K)	Heat Capacity (J/g-C)	Heat of Fusion (J/g)
AM50A	1150/620	1022/550	65	1.02	368
AM60A	1140/615	1010/545	61	1.00	370
AZ91D	1100/595	878/470	73	1.05	373

Aluminum is the primary alloying element present in the alloys listed above. It serves to increase the mechanical properties and corrosion resistance, as well as to lower the reactivity of the melt with oxygen. Aluminum is relatively soluble in magnesium as shown in the Al-Mg phase diagram in Figure 1.

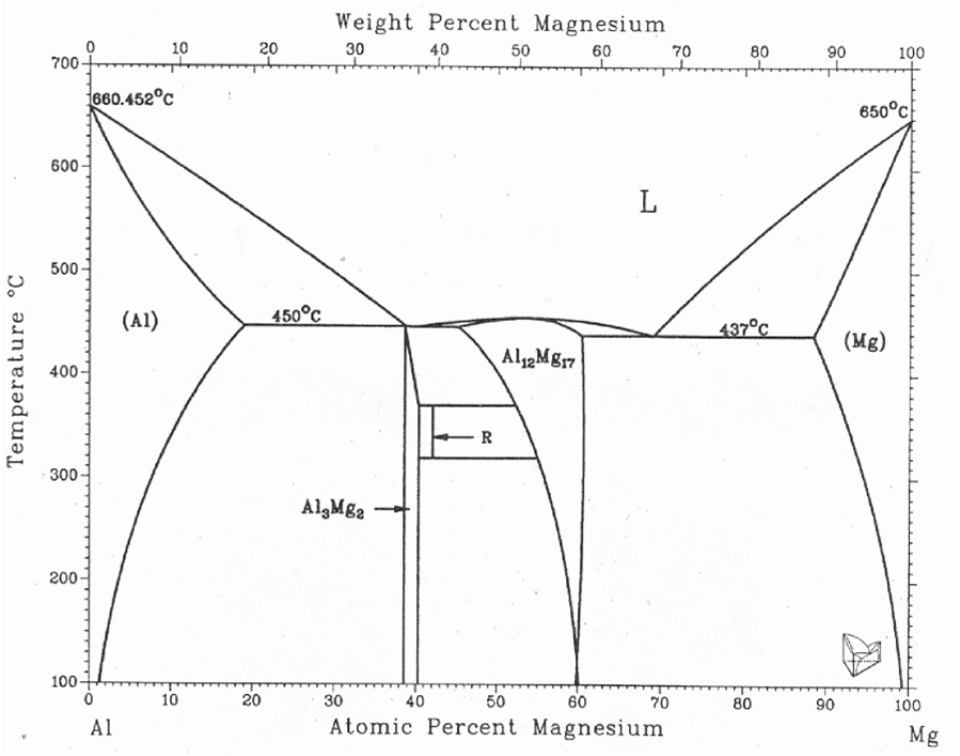

Figure 1 The aluminum-magnesium phase diagram (10)

As can be seen in Figure 1, all of the studied magnesium alloys are hypoeutectic. The first phase to solidify is a magnesium-rich α. phase followed by the formation of a lamellar eutectic structure composed of Al12Mg17 and α.

The manganese content in all of these alloys helps to improve the corrosion resistance and lower the activity of the alloy. Manganese also ties up any iron contaminants in the melt, eliminating it as a detrimental species. This is very important because magnesium is almost always melted in steel crucibles. Since corrosion resistance is a primary concern in many applications, the levels of critical impurities must be kept below certain minimums. These impurities include iron, nickel and copper. These impurities are so detrimental due to their low (even vanishingly small) solubility in solid magnesium. These metals come out of solution to form particles in the magnesium matrix. Such particles, when on or near the surface of a part, act as a cathode in an electrochemical cell which coupled with an aqueous environment accelerates the corrosion of the surrounding magnesium. This is due to the fact that iron, nickel, and copper are all more noble than magnesium on the galvanic series.

All three of these alloys are used primarily in the die casting industry. AZ91B and AZ91D are the most commonly used alloys due to their high strength and excellent corrosion resistance (AZ91D only, since AZ91 B has lesser restriction on contaminant content and thus less corrosion resistance). AM60A and AM60B are used in applications where greater ductility is desired. Despite the lower aluminum content of these alloys compared to AZ91, the tensile strength is only slightly lower. AM60 also provides excellent corrosion resistance (2).

2.2 Magnesium Melting and Melt Handling Techniques

Magnesium alloys have a melting point near 600°C (this varies slightly with alloy composition). They have a fairly low heat capacity and broad solidification range. This presents special problems during the casting of these alloys, as will be discussed later. Since magnesium is so reactive, it presents many unique challenges in its processing.

Magnesium is well known for its flammability and high burning temperature, which makes it dangerous in the foundry setting if not handled correctly. The auto-ignition temperature, the temperature at which it will spontaneously combust in the presence of oxygen, for magnesium is about 455°C, requiring protective measures at any temperature above this. Magnesium burns in excess of 1,982°C, making it very difficult to extinguish. Water and CO_2 both dissociate when brought in contact with burning magnesium, usually causing an explosion which only serves to scatter the burning magnesium. The only method for extinguishing a fire is to starve it of oxygen. Typically, fluxes and/or gases such as Halon ($CBrClF_2$) and sulfur hexafluoride (SF_6) suffice.

Magnesium alloys must be melted in non-ceramic crucibles due to their highly reducing nature. Molten magnesium would strip the oxygen atoms from the oxides in a ceramic crucible, destroying it as well as contaminating the melt. This is why most magnesium melting occurs in low-carbon steel crucibles. The iron is very slow to dissolve and what little does is tied up by the manganese content of the melt. The furnace must also be covered to shield the melt from an oxygen atmosphere. The oxide film that forms on the surface of any magnesium melt is only slightly protective and very easily disturbed, allowing oxygen to permeate the oxide and thus allowing burning at the oxide-melt interface. Therefore, the surface of the melt must always be protected from oxygen contact.

Two main methods are used to protect the melt from oxidizing. The first is the use of fluxes, magnesium and fluoride salts that melt to produce a protective layer that floats on the melt. Fluxes are also used in the refining and cleaning of the melt. These salts make oxides and contaminants clump up and sink to the bottom of the crucible or ladle to form a heel of sludge. This 'sludge' is cleaned from the crucible between heats. Typical flux composition is approximately 49% $MgCl_2$, 27% KCl, 20% $BaCl_2$, and 4% CaF_2. The magnesium and potassium chloride salts give the mixture a low eutectic; the fluoride gives surface wettability and chemical reactivity with magnesium oxide; and the heavy barium chloride salt increases the density to facilitate mixing and sludging for the separation of dross and oxide inclusions.

The second method is the so-called fluxless process, where a cover gas is used to displace oxygen away from the melt surface. In the past, sulfur dioxide gas (SO_2) was used to protect the melt from oxidizing. However, sulfur dioxide is poisonous in large amounts and foul smelling, so its use has been all but discontinued. More common in modern magnesium casting is the use of a cover gas mix. This gas mixture most commonly consists of 1% sulfur hexafluoride (SF_6), carbon dioxide (CO_2), and dry air (11, 12). The gas is heavy and displaces oxygen from the melt surface, and can also be used to purge molds, ladles, and other handling equipment. Research is currently

underway to find a suitable replacement for SF_6 because of environmental concerns. Certain Halon replacements such as 3M's Novec 612 currently show the most promise (13).

Magnesium alloy casting also requires special ladles and other handling equipment. In aluminum casting, the steel ladles and skimmers are coated in a ceramic material to protect them from the highly reactive melt. This protects the equipment from corrosion and the melt from contamination. In magnesium casting these items are not coated due to the low rate of reaction with the steel. In fact, ceramic coated equipment should never be used with magnesium alloys because of the high reaction rate with the oxides in the ceramic coatings. Low carbon (< 0.12%) steels with low nickel and copper content (< 0.10%) are generally used for magnesium handling tools and equipment. It is standard practice to use the same steel alloy for both crucibles and handling equipment.

2.3 Magnesium Alloy Casting

Despite its reactive nature, magnesium can be cast in the same ways as most other metals. This includes die casting, permanent mold casting, sand casting, investment casting, thixomolding, injection molding, and even lost-foam casting. Most of the casting performed for this study used no-bake sand casting techniques. In no-bake sand casting, silica sand is mixed with a two-part organic binder. After the sand is packed into a mold pattern, the binder hardens and the mold is ready for casting in a relatively short period of time. Sand casting of magnesium alloys is slightly different than that for other metals. Since magnesium reacts very quickly with the moisture and oxygen trapped in the mold, something must be added to the sand and binder mixture to react with the oxygen before the molten magnesium can. In the past it was common practice to add 1-2 wt% sulfur to the sand and binder mixture. On pouring, the sulfur would react with the oxygen in the mold and create SO_2, which acts as a protective cover gas. While sulfur works very well, there are obvious drawbacks to its use, such as the noxious fumes generated in the process. A good replacement for sulfur in sand molds is potassium fluoborate (KBF_4) in the same proportions. When added to the sand mixture, it produces the same oxygen scavenging effect as sulfur, but without the noxious fumes. Potassium fluoborate acts by decomposing and reacting with the oxygen.

2.4 Optimizing Mechanical Properties of Magnesium Cast Parts

As with any material system, magnesium alloys have widely varying mechanical properties depending on many process parameters. Of primary concern to the automotive industry are ultimate tensile strength (UTS), yield strength (YS), and ductility expressed as percent elongation. The most important quality parameters in magnesium alloys are melt quality, grain size, porosity level, and heat treatment. Due to the fact that most die castings are not heat treated, heat treatment of these alloys will be considered to be beyond the scope of this investigation. Table 4 shows industry-obtainable mechanical properties for the AM50, AM60A, and AZ91D alloys.

Table 4 Mechanical properties for the studied magnesium alloys in the as-cast (F) condition.

Alloy	UTS (MPa)	YS (MPa)	% Elongation	Hardness (Brinell)	Poisson's Ratio
AM50A-F	228	124	15	60	0.35
AM60A-F	241	131	13	65	0.35
AZ91D-F	230	150	3	63	0.35

The first and foremost way to control mechanical properties in magnesium castings is to ensure a clean, and oxide-free melt. Oxide or flux inclusions (only applicable in the flux-based melting and handling processes) can have a devastating impact on magnesium alloy mechanical properties. Certain other contaminants can both directly and indirectly affect properties. Thus proper foundry practice and safety procedures should be observed while casting magnesium alloys.

Once a clean melt is assured, the next most important factor in determining the final properties of magnesium alloy castings is grain size. Mechanical strength is related to the grain size via the Hall-Petch relation (14, 15):

$$\sigma_0 = \sigma_i + kD^{-1/2} \qquad \text{(Equation 2.1)}$$

Where σ_0 is the yield stress; σ_i is the friction stress, or overall resistance of the crystal to dislocation movement; k is the locking parameter, or hardening contribution of grain boundaries; and D is the grain diameter. The value of the locking parameter is material dependent, thus some materials respond strongly to grain refining, while others do not.

The strength of magnesium alloys has been shown to be about four times more sensitive to grain size than aluminum with a value of k equal to $280 MPa \cdot m^{1/2}$ (16).

Knowing this, the best way to strengthen a high quality magnesium casting is to lower the average grain size. This is also known as grain refining. The simplest way, in theory, to reduce the grain size in a casting is to rapidly solidify it. Magnesium has another advantage in that it has a low heat capacity (1.02 J/g-C) and low heat of fusion (370 J/g) compared to other structural alloys. (Please see Table 3 for exact values for each magnesium alloy). This means less heat will have to be removed to solidify the casting. This fact has led to very high strength magnesium die castings due in part to the rapid solidification inherent in the die casting process. (This low heat of fusion is also responsible for the much faster casting times as discussed earlier.)

Certain additions to the melt, called inoculants, can also provide a finer grain structure. This occurs because the inoculant provides many more nucleation sites to start the solidification process. In general, the more nucleation sites, the finer the grain structure will be (17). It has been shown that magnesium alloys can be made with an extremely fine grain structure by the addition of hexachloroethane (C_2Cl_6) to the melt, which decomposes to Cl_2 and carbon inoculant (18).

Magnesium alloys also exhibit a poorly understood, but effective means of grain refinement by superheating. When molten magnesium is held at 900°C for 15 minutes and then brought back down to the pouring temperature of 760°C, the casting shows a high degree of grain refinement even without the addition of an inoculant. Interestingly, this effect tends to withstand subsequent

melting and recasting operations, even if the superheat step is not repeated (19). This technique was widely used before suitable inoculants such as C_2Cl_6 were found for magnesium. This practice has largely been abandoned due to detrimental effects on crucible life and melt contamination.

2.5 Porosity

Porosity is a major hindrance to the magnesium casting industry. The presence of porosity reduces the tensile and elongation performance of these alloys greatly. It has been shown that porosity can almost completely counter the strengthening effects of grain refinement in magnesium alloy castings (18). Porosity in castings comes from two sources: gas porosity and shrinkage porosity.

Gas porosity in castings is caused by dissolved gases in the melt coming out of the solution during the solidification process and forming bubbles or voids. This is due to the fact that gas solubility is proportional to temperature. Thus as the temperature falls during solidification, the gas is forced out of solution and into gaseous form. If this gas becomes trapped in the casting, the result is gas porosity. It can be inferred from this that high concentration of dissolved gases is a major factor in producing gas porosity.

Hydrogen gas is very soluble in molten aluminum at 1 cm^3 H_2 per 100g of metal at T_m, and more so in molten magnesium at 25 cm^3 per 100g of metal at T_m. This would lead one to believe that hydrogen gas porosity would be a major problem for these metals. While this is certainly true for aluminum, gas porosity is a fairly minor problem in magnesium castings. The reason for this apparent contradiction lies in the difference between the solubility of hydrogen in the liquid state versus the solid state for these metals (20). The decrease in solubility upon solidification is only 28% in magnesium versus 96% in aluminum. This means that even at much higher hydrogen concentrations than aluminum, the magnesium castings will be free of gas porosity. The majority of dissolved hydrogen remains dissolved in magnesium even after solidification. Therefore if magnesium melts are properly degassed prior to casting, gas porosity should be minimal.

Degassing of magnesium alloys can be accomplished in a variety of ways. In the past, chlorine gas was bubbled through the melt. This removed dissolved hydrogen and reacted with the melt somewhat to form liquid $MgCl_2$. Magnesium chloride is a fluxing agent as explained earlier, so this process had the added advantage of in situ flux creation. This practice has largely been abandoned due to obvious safety and environmental risks due to the toxic nature of chlorine gas.

Modern practice in the die casting industry is the addition of hexachloroethane (C_2Cl_6) to the melt in the form of compressed tablets. When immersed into the molten magnesium, the C_2Cl_6 decays into carbon and chlorine. The chlorine gas rises through the melt, picking up hydrogen as well as reacting with the magnesium to form $MgCl_2$. Both of these mechanisms operate concurrently. The beneficial effect is twofold: first, the chlorine gas degasses the melt and generates a fluxing agent ($MgCl_2$) in the process. Second, the carbon acts as an inoculant, providing

many nucleation sites and thus grain refining. This process eliminates the need to store hazardous compressed chlorine gas, replacing it with easy to handle and safe C_2Cl_6 tablets. The gas released from the melt surface should still be ventilated in a safe manner as they are still dangerous.

The second source of porosity in magnesium castings is shrinkage porosity. Shrinkage porosity occurs when the solidification front loses contact with a ready supply of melt. When this occurs, as the solidifying metal shrinks, no melt is available to fill in the gap and thus a pore is formed. By its nature, shrinkage porosity is predominantly found in the center of the cross section of a casting. This is due to the fact that the center of the cross section is the last to solidify. In order to understand and correct this situation, it is necessary to analyze how the alloy solidifies. Magnesium castings solidify through a nucleation and growth process. After nucleation, primary dendrites begin to grow as well as form secondary and tertiary dendrite arms. There is an area just ahead of the solidification front known as the 'mushy zone'. In this area the alloy is in a semisolid condition consisting of α -phase dendrites with slightly aluminum-rich liquid in between. As long as liquid metal can penetrate through the inter-dendrite spaces, the solidified are behind the solidification front will be sound (nonporous). However if the liquid cannot flow between the dendrites, the remainder of the liquid present will be consumed as the dendrite grows, leaving the spaces between the dendrites empty. The result is a dendrite formation separated by porosity.

It has been shown that the availability of liquid to the solidifying areas can be maintained by setting up steep thermal gradients in the direction of the risers. In the studied magnesium alloys this gradient needs to be established before the metal cools to 50 degrees below the liquidus. Factors that affect this gradient include gating, risers, chills, mold material, filling speed, and of course casting geometry. Since casting geometry and gating are not generally easily changed, risers, chills, and filling speed are the preferred engineering controls to establish this gradient.

2.6 Feeding Distance

In casting, feeding is defined as providing molten metal to a region undergoing solidification at a rate sufficient to offset solidification shrinkage. Feeding distance is a measure of the ability of an alloy to feed solidifying areas, expressed a distance from a ready supply of molten alloy (riser). It is expressed in units of length (7). The actual feeding distance for a simple bar casting with a riser on one end is the sum of the length of sound casting on the far end (end effect zone) and the length of sound casting adjacent to the riser (riser effect zone). If the feeding distance for a given alloy and casting condition is known, this information can be used to efficiently place risers and chills to produce a sound casting. Feeding distance varies with the thermal properties of the metal and mold, as well as the casting geometry. Mold thermal properties are the only factors that can be modified to any great extent. Mold thermal properties are altered by placing chills or exothermic risers strategically in the mold.

2.7 Minimum Thermal Gradient

It has been shown that there exists a critical minimum thermal gradient for a given alloy system that will produce porosity-free castings in magnesium alloys (21). The thermal gradient in a casting is an indicator of the heat transfer from the solidifying metal to the mold. In the solidification of a casting, it is desirable that solidification occur directionally towards risers. This means by definition heat will be transferred from the riser to the cold end of a casting. The result of this effect is that a thermal gradient will be generated with increasing temperature towards the riser. The presence of this gradient provides an uninterrupted supply of molten metal from the solidification front to the riser. The result is good feeding and a sound casting.

During casting, solidification proceeds from any cold surface (i.e. every mold surface the melt contacts). In order to ensure directional solidification towards the riser, and thus a sufficiently steep gradient, the far point away from the riser (cold end) must dominate heat transfer. This means that directional solidification from the cold end must proceed faster than that from the other mold surfaces (known as transverse or progressive solidification).

If the gradient is too shallow (small), the transverse solidification will proceed faster than that from the cold end. As this occurs, solidification fronts from opposite transverse mold walls meet in the center, effectively cutting off small pools of liquid from the main front. These pools will solidify without any compensation for shrinkage and centerline porosity will result. Figure 2 below shows the features of progressive and directional solidification.

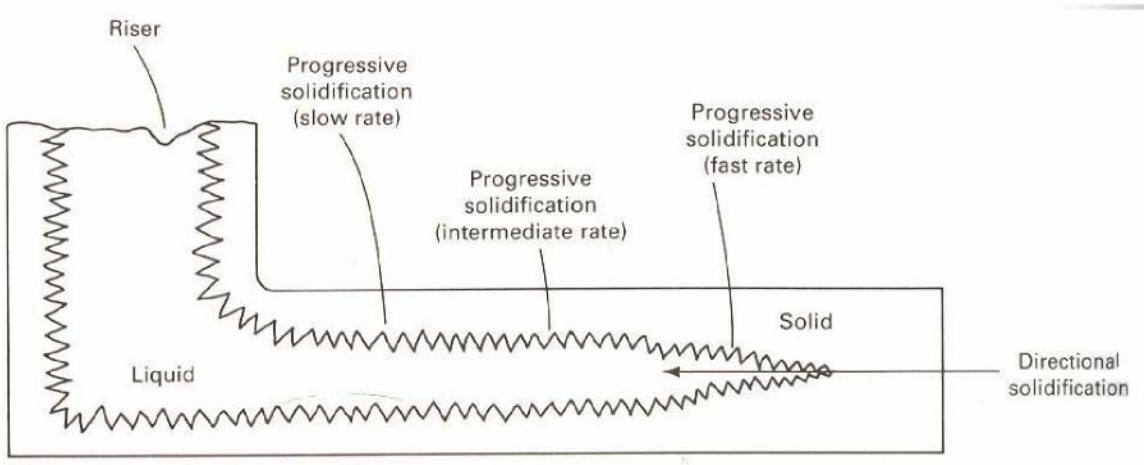

Figure 2 Directional versus progressive solidification (7)

This critical temperature gradient can be expressed by equation 2.2 below:

$$G_x = \frac{T_l - T_s}{2\sqrt{\pi k_M}} \sqrt{k_m \rho_m c_m} \tan\Theta_C \frac{1}{\sqrt{t_f}} = \frac{A}{\sqrt{t_f}} \qquad \text{(Equation 2.2)}$$

Where G_x is the critical temperature gradient, T_l is the liquidus temperature, T_s is the solidus temperature, k_M is the thermal conductivity of the metal, k_m is the thermal conductivity of the

mold, ρ_m is the density of the mold, c_m is the specific heat of the mold, Θ is the critical liquid pool angle (the angle of the solidification front with the mold wall), and t_f is the total solidification time (22). Equation 2.2 shows that the critical thermal gradient is a function of mold wall thermal properties, metal liquidus-solidus range ($T_l - T_s$) and thermal conductivity, and solidification temperature. The only one of these factors that is adjustable to any degree is the mold wall thermal properties, as casting temperature is often dictated by processing requirements. This equation can be used to calculate the critical thermal gradient for a given mold-casting system. It is also used to calculate the angle of the solidification front with a measured thermal gradient.

3 Objectives

This task will investigate the origins of porosity, known to cause lower than optimum mechanical properties in grain refined magnesium die casting alloys AM50A, AM60A, and AZ91D. Once these causes are determined, methods will be developed to avoid porosity. These methods will be tested through casting trials of each of these alloys in no-bake sand molds.

The critical minimum thermal gradient required for sound castings will be found for each of the alloys. These gradients can be used in conjunction with current finite element casting simulation software to predict the presence of porosity. These simulations will allow the magnesium casting industry to help optimize their casting processes and thus the mechanical properties of their castings before the dies are manufactured.

The mechanical properties of these alloys cast with good gating and risering practices are of interest as a base-line and target for production castings.

Any modern foundry is now equipped with casting and solidification computer simulation tools to validate the effectiveness of gates, runners and risers size and location in preventing hot spots and shrinkage porosity. Such software will be used and predictions confirmed by cutting the casting and conducting metallographic studies.

4 Experimental Procedure

4.1 Melt Preparation

All metal used in this study started in the form of new commercial grade 26 lb ingots. No recycled magnesium was used for any of the tests. The metal was melted in a commercial Lindberg electric resistance furnace with a 100 lb capacity steel crucible. The crucible in this furnace was not removable so all pouring was done by tilting the furnace. The furnace had a maximum operating temperature of 732°C with a sealed cover and the capability to deliver cover gas mix to the melt surface. With the availability of cover gas to the melting furnace, the fluxless method was used for all melting operations in this study. The furnace is shown in Figure 3.

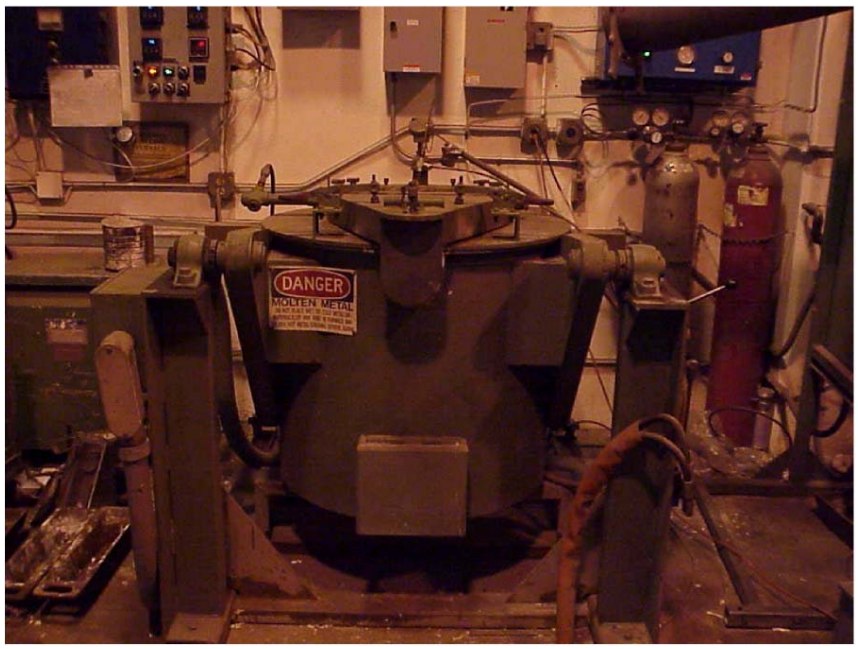

Figure 3 The Lindberg commercial magnesium alloy melting furnace.

The cover gas itself was mixed with a commercial SF_6 blending station made by Striko Dynarad. The cover gas used was a well regulated mixture of dry air, carbon dioxide, and sulfur hexafluoride. Table 4.1 below shows the cover gas mixture and flow rates used during all melting operations. All gases used were the same commercially available gases as used in industry practice. Incoming compressed air was first passed through a dessicator to ensure it was moisture free. Figure 4 shows the cover gas blending station used for all heats.

Table 5 Cover gas mixture and flow rates (expressed in Standard Cubic Feet per Hour).

Constituent	**Flow Rate (SCFH)**
Air (Dry)	7.5
CO2	3.1
SF6	0.075
Total	10.68

Figure 4 Cover gas blending station.

All ingots were cut into thirds on a large commercial hack saw to allow them to fit into the melting furnace. The ingots were checked to ensure that they were dry and uncontaminated. Two of these ingot pieces were initially loaded into a clean crucible and the cover gas was turned on. The power to the furnace was then turned on, and the metal was allowed to melt. The average time from cold start to initial melt was about 2 hours. The remaining ingot pieces for the heat (depending on heat size, usually 60 lbs.) were added one at a time due to space constraints within the furnace and allowed to melt. Once the entire heat was molten, the temperature was allowed to rise to 732°C. The melt was then skimmed to remove excess oxide film on the surface. This process was repeated for all heats in the study.

4.2 Degassing and Grain Refining

All degassing and grain refining treatments were carried out in a heated bottom-tapping steel holding ladle (shown below in Figure 5). The holding ladle had a 20 lb. capacity and was heated from the bottom with a propane burner. A type sheathed K thermocouple was placed inside the ladle, allowing real-time control of the melt temperature. Once the 20 lb. metal charge was transferred to the holding ladle, it was immediately covered with magnesium cover flux to protect the metal from oxidation. The temperature was brought up to 787°C using the propane burner. Once the melt reached this temperature, a dry, aluminum-wrapped, tablet of hexachloroethane was immersed into the melt and allowed to fully decompose. This step both introduced the inoculant (carbon) and degassed the melt. A carbon content of 0.05 wt% was achieved using one hexachloroethane tablet per 20 lb. ladle charge.

Once the hexachloroethane treatment was completed the flux was completely skimmed from the surface of the melt and replaced with fresh flux. The melt was cooled to the 760°C casting temperature and held until the molds were filled (usually no more than a few minutes).

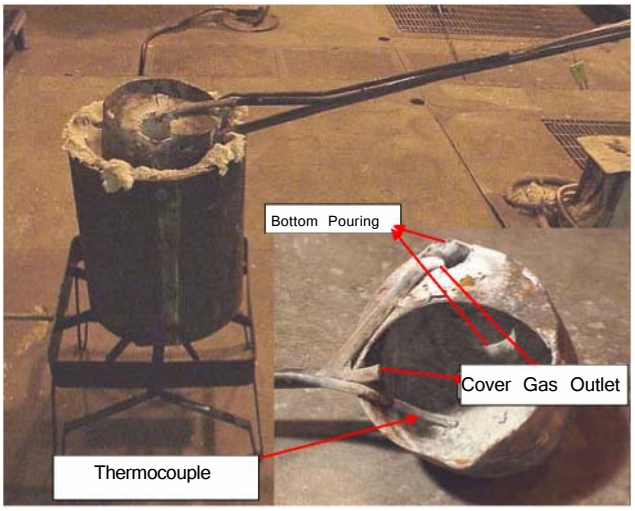

Figure 5 Bottom-tapping steel holding ladle (inset) and propane fired heater.

4.3 Mold Preparation

All sand molds used in this study were of the no-bake variety. New, clean, 60- mesh silica sand was mixed with an organic binding agent. To prevent the magnesium from reacting with any trapped moisture or oxygen, potassium fluoborate (KBF_4) was added to the sand. The final sand mixture consisted of 1.5% Linocure binder, 0.3% accelerator/hardener, 2.0% potassium fluoborate, and the remainder silica. The entire mixture was mixed in a commercial sand muller for 6 minutes to assure homogeneity.

Wooden patterns of the desired shape were attached to a wooden board and coated with a release agent. Removable flasks were then set on the boards to set the outer shape of the mold. All thermocouples and chills were cleaned of any debris or oxide to prevent reaction with the molten magnesium. All extra pieces such as risers, sprues, chills, and/or thermocouples were then added to the pattern. The sand mixture was then carefully put in the mold and compacted to ensure all voids were filled. The top of the flask was then leveled and the entire assembly was allowed to cure for at least 1 hour at room temperature.

After curing, the pattern boards and riser/sprue patterns were carefully removed. The mold cavity was then inspected and trimmed as necessary. If thermocouples were present, their position was adjusted as needed. The completed mold half was then moved to another area where the flask was removed. The mold was allowed to cure for at least 24 hours before casting.

The above process was repeated for all castings to be made in the heat. Flask size was varied depending on the casting geometry, as to use the minimum sand required for the task. While the molds were prepared, pouring basins were made as needed with any leftover sand mix. On the day of casting, the molds were set together with Foseco Corfix 19 adhesive and added weight on top to prevent break outs. Pouring basins were used to aid consistent filling of the mold. A metal mesh filter was placed over the mold filling hole and the pouring basin on top. This provided a filter to trap any large particles of entrained oxide or flux and prevent it from traveling into the casting.

4.4 Tensile Tests

All tensile tests were performed in accordance with ASTM E8 with dimensions as specified in the small-size specimens proportional to standard. The small-size specimens were used because in many cases the area to be tested was just too small to cut a full size tensile specimen. Figure 6 shows the tensile bar geometry used, with dimensions as shown in Table 6.

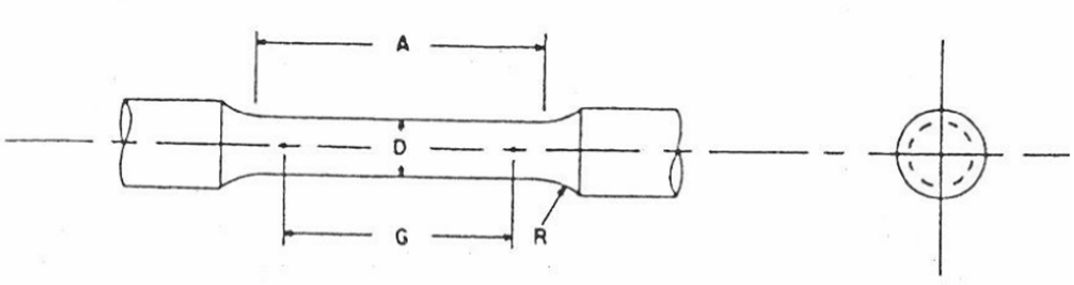

Figure 6 ATSM E8 Tensile bar schematic. (23)

Table 6 ASTM E8 Tensile bar dimensions (22)

	Specimen Type I (inches)	Specimen Type II (inches)
Nominal Diameter	0.250	0.160
G – Gauge Length	1.000 ± 0.005	0.640 ± 0.005
D – Diameter	0.250 ± 0.005	0.160 ± 0.005
R – Radius of Fillet	3/16	5/32
A – Length of Reduced Section	1 1/4	3/4

The gauge length was marked prior to testing to allow measurement of elongation at break. All bars were pulled in tension until breaking, with ultimate tensile strength and elongation at break recorded. Fracture surfaces were carefully removed from the bars to facilitate viewing with a scanning electron microscope.

4.5 Low Pressure Tests

To study the effect of hydrogen gas presence on the porosity of magnesium, several small castings were allowed to solidify under reduced pressure. For comparison, several aluminum samples were also cast. The magnesium alloys were melted as stated in section 4.1. Once molten, the magnesium was thoroughly gassed by careful addition of moist contaminants. This saturated the melt with hydrogen. The gassed melt and a melt degassed with hexachloroethane were allowed to solidify in a small steel crucible in a vacuum chamber evacuated to 650 mm Hg vacuum. Aluminum alloy A356 was melted in an induction furnace and allowed to solidify in the same manner as the magnesium alloys. The samples were then sectioned to reveal any gas porosity.

4.6 Round Plate and Tapered Bar Castings

The first goal of this study was to experimentally determine the feeding distance for the three magnesium alloys. To accomplish this task, a variety of plate and bar castings were made with varying dimensions. All of these castings were risered, and one of each dimension had a cast iron

chill in the mold. Some of the plates and bars were made with a taper to study the effect of the taper on the soundness of the casting. Figures 7 and 8 below show the casting shape while Table 7 gives the exact dimensions.

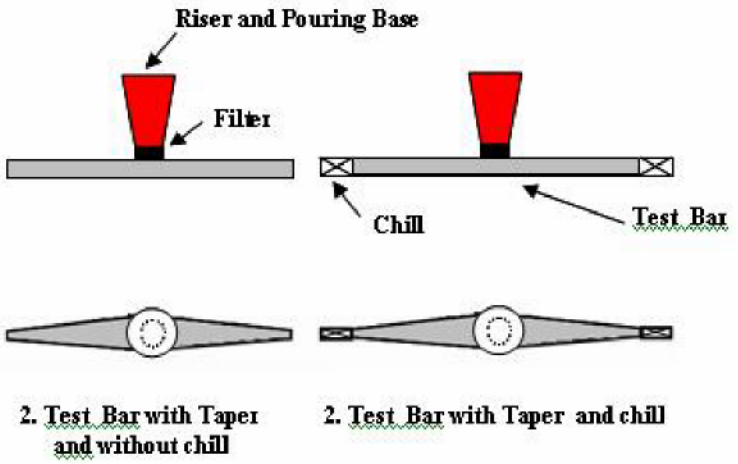

Figure 7 Tapered bar castings with riser and chill positions indicated.

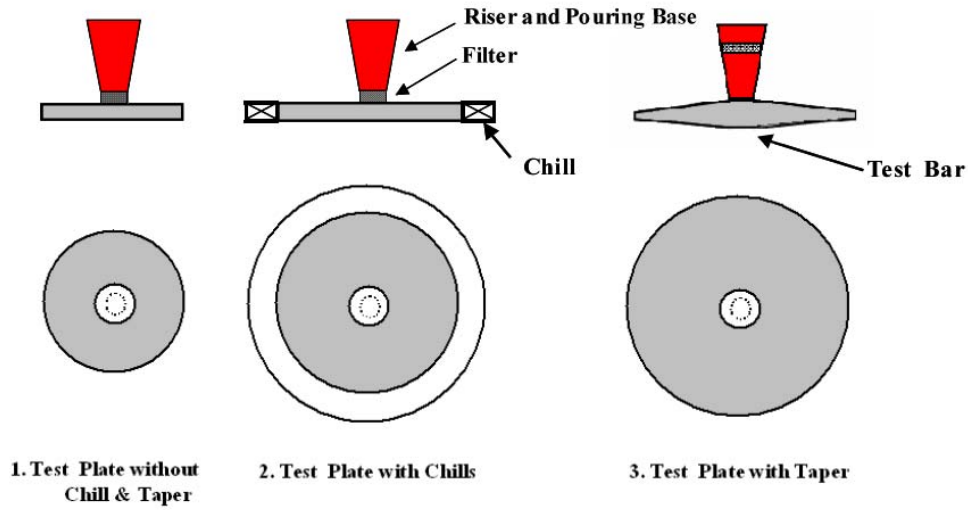

Figure 8 Plate castings with riser and chill positions indicated.

Table 7 Plate and tapered bar casting dimensions.

Plate Name	Dia.	Thickness	Taper	Riser location	Riser Size
Small Plate-1	6″	3/8″	None	Center	Ø 3″ x4.5″
Small Plate-2	6″	%″	None	Center	Ø 3″ x4.5″
Large Plate	15″	3/4″ (center)	3/4″ to 1/3″	Center	Ø 3″ x5.5″
Bar Name	**Length**	**Thickness**	**Taper**		
Small Tapered	13″	11/8″	3/4″ to 3/8″	Center	Ø 3″ x4.5″
Large Tapered	15″	11/8″	9/8″ to 3/4″	Center	Ø 3″ x4.5″
Not Tapered	15″	11/8″	None	Filling Plug only	None

One of each of these castings was produced for each of the three alloys. The castings were shaken out 24 hours after they were cast, and then cleaned. Each of the plates was x-rayed at a commercial x-ray testing lab. Cross sections were also taken and polished to determine the extent of any porosity and to confirm the radiographic analysis results.

4.7 15-inch Bar Castings and MAGMA Simulation

To better understand the feeding distance and micro-shrinkage phenomena, 15 inch bar castings were made. These bars were cast with and without risers and chills to give a wide variation in the extent of microshrinkage. The bars were of square cross section, 9/8 inch by 9/8 inch and 15 inches in length. Whether or not riser was used a pouring basin and filter setup as described earlier was used. Figure 9 below shows a drawing of the 15 inch bar casting with riser and chill placement.

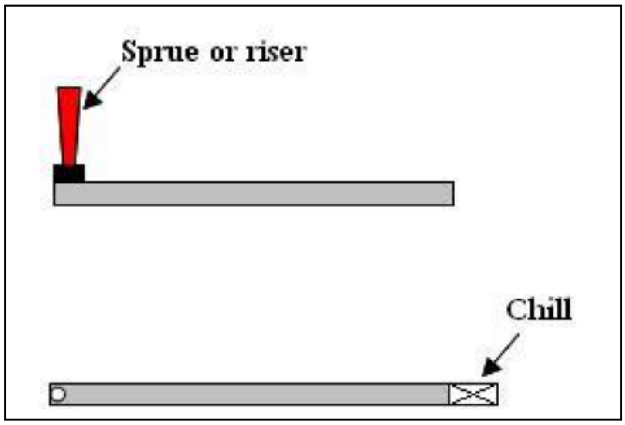

Figure 9 Drawing of 15" bar casting indicating riser and chill placement.

Two of each of these castings were made for each of the three alloys studied. One was cast without a riser or chill and one was cast with both a riser and chill. Each of these bars was then x-rayed to determine the extent of porosity.

In addition to the casting trials, this bad geometry was modeled in a casting modeling software package called MAGMAsoft. MAGMA is widely used in industry for mold and casting design modeling and optimization. This software uses finite element analysis to model the pouring and solidification of castings. The goal of this step was to determine with what accuracy the software could predict the presence of micro-porosity in magnesium castings. The bar, riser, and pouring basin assembly was first rendered in AutoCAD 2000 computer aided design software. This rendering was converted to a three-dimensional representation of the assembly and exported to the MAGMA program.

4.8 Thermal Gradient Castings

To experimentally determine the critical minimum thermal gradient discussed in section 2.7, more of the 15 inch bar and large tapered plate castings were made. The main difference this time being the addition of 5 sheathed type K thermocouples to the molds. The arrangement of the thermocouples is as shown below in Figures 10 and 11. The limit of five thermocouples was imposed by the limits of the data acquisition system used for the experiment.

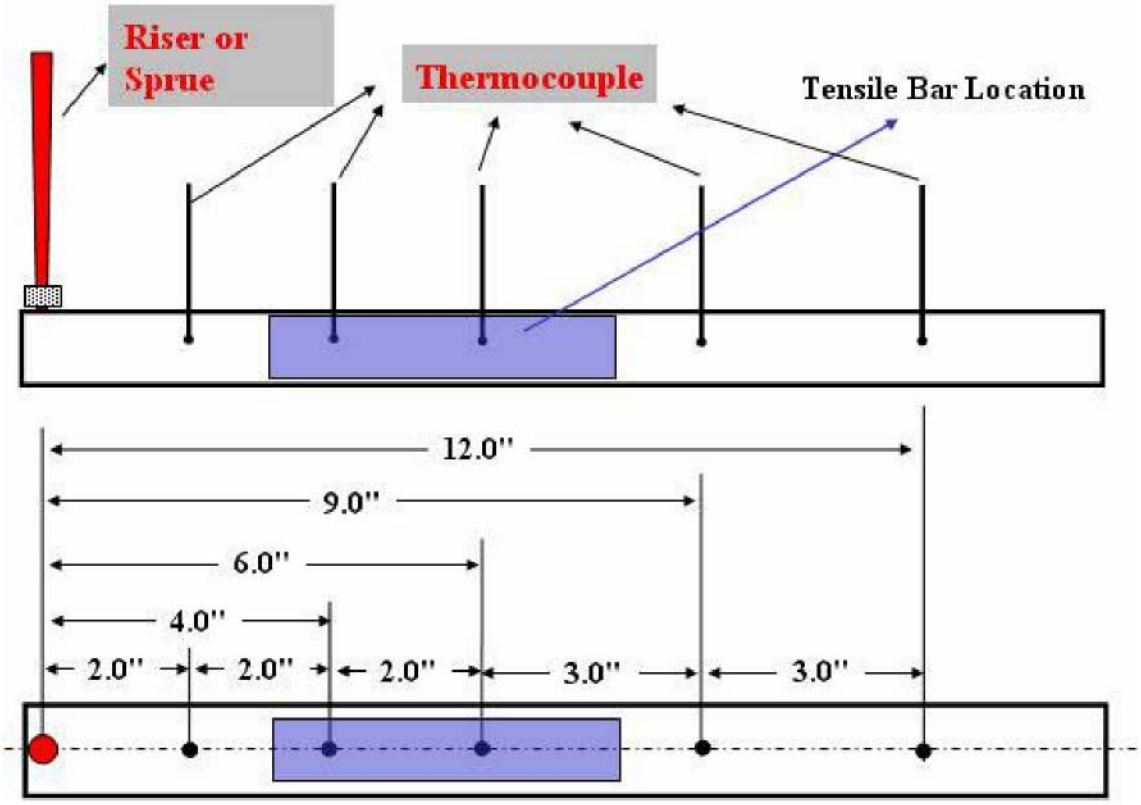

Figure 10 Thermocouple locations in the 15-inch bar castings

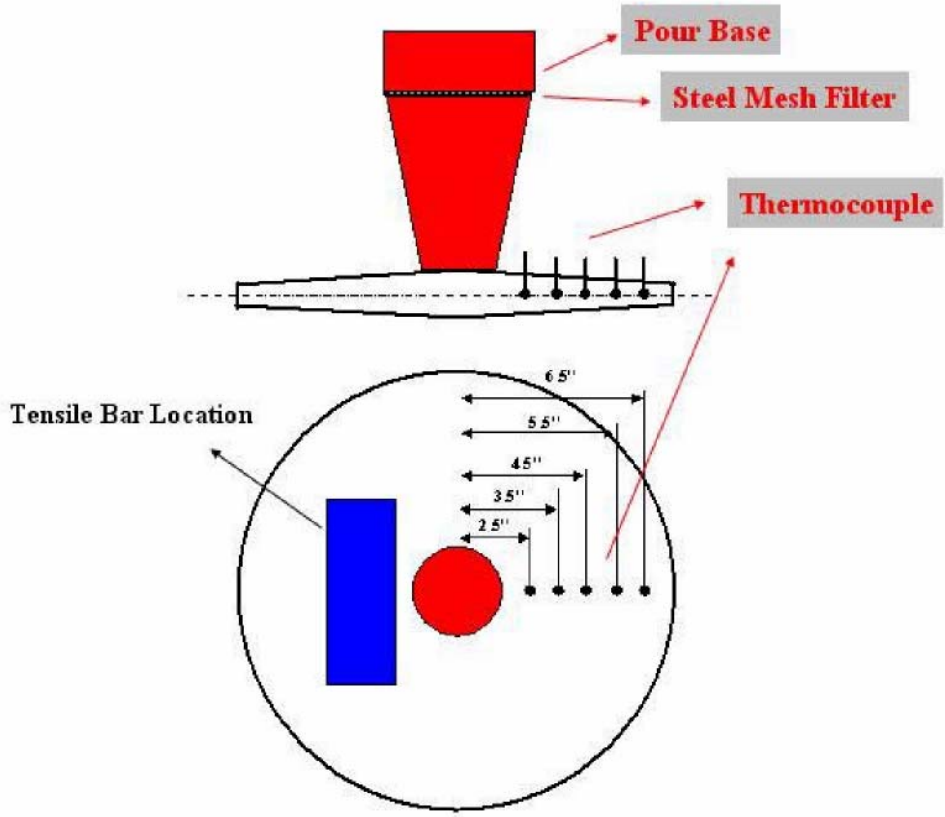

Figure 11 Thermocouple locations in the large tapered plate castings

To ensure proper placement of the thermocouples in the molds, equal-depth holes were drilled into the wooden pattern where the thermocouples were set during mold preparation. The leads were bent so that the sand would lock them into position and prevent slippage during mold assembly and casting. All of the thermocouple junctions were placed in the exact center of the casting cross section, as this is where the temperature gradient is most critical in avoiding microshrinkage. Each of the thermocouples was tested prior to mold preparation to ensure functionality.

Once the molds were ready for casting, the thermocouple leads were attached to an IOtech USB data acquisition system which was attached to a laptop computer. Data was taken at a rate of 1.5 samples per second per thermocouple. Using these five temperature readings and their positions in the casting, the temperature gradients across the long axis of the casting could be calculated. To correlate this data with porosity extent, tensile test bars were cut from areas that were predicted to be most likely to contain porosity. These areas are indicated in Figures 10 and 11.

5 Results and Discussion

5.1 Low Pressure Tests

Figure 12 shows the cross section of the low pressure samples. The aluminum sample, as expected has many large voids that resulted from the hydrogen coming out of solution during solidification. It is obvious to see why degassing is so critical to aluminum casting. The AZ91D magnesium sample, however, shows very little porosity. This was also expected due to the small 28 % difference between liquid and solid state solubility of hydrogen in magnesium. This test shows that with sufficient degassing, such as that provided by hexachloroethane inoculation, gas porosity is a very minor contributor to overall porosity in magnesium castings. With this knowledge, it is within reason to assume that porosity in magnesium alloy castings will be the result of shrinkage. Thus if shrinkage porosity can be minimized or eliminated, sound castings will result.

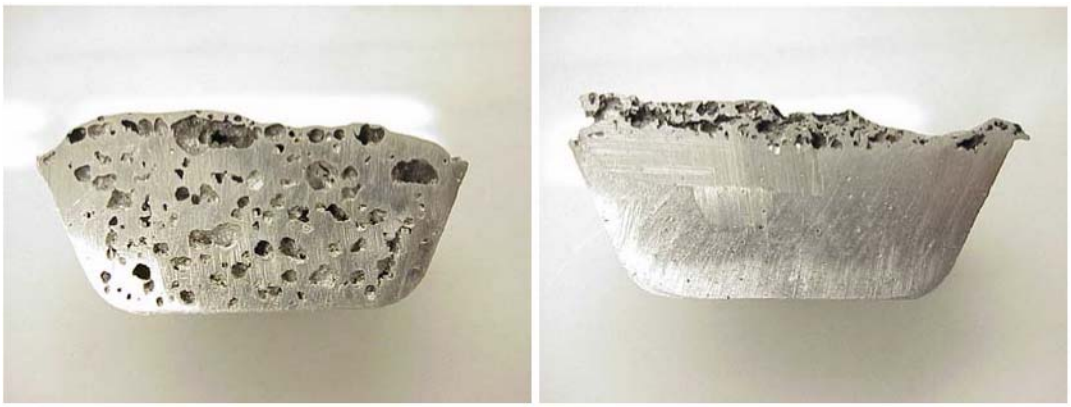

Figure 12 Cross sections of aluminum (l) and magnesium (r) castings with high hydrogen content, solidified under reduced pressure.

5.2 Round Plate and Tapered Bar Castings

After shake out, the castings for each alloy were x-rayed and sectioned to determine the extent of porosity. Bars were cut along their long axis, while plates had wedge shaped sections taken radially. Table 8 below shows the results of the analysis of the sections and x-rays.

Table 8 Plate and bar porosity results.

Sample	Porosity
Thin Plate w/chill	None
Thin Plate w/o chill	None
Thick Plate w/chill	None
Thick Plate w/o chill	None
Large Plate w/chill	None, (AM50A some dross)
Large Plate w/o chill	None, (AM50A some dross)
Tapered Bar w/chill	None
Tapered Bar w/o chill	None
Straight Bar	None

Figure 13 shows examples of the castings after sectioning with the riser still attached to the plate. The metallography and x-rays both showed fully dense castings, with little to no oxide or flux inclusions. This means that for the given casting geometries and riser sizes, the feeding distance was equal to the length of the bar or radius of the plate. Therefore the chills, risers, and/or tapers were sufficient to create the necessary gradients and allow full feeding. While these results were positive, it was clear that the casting geometry was too small to find the limit of feeding. Longer distances between the riser and chill were needed to induce porosity. Additionally, the next set of castings would be made without taper to further emphasize this effect.

Figure 13 Sectioned small plate castings (left) and tapered bar castings (right) 5.3 15 Inch Bar Castings and MAGMA Simulation

The fifteen inch bar castings showed a varying amount of centerline porosity depending on the presence of risers and chills. A major problem developed in the interpretation of the x-ray films for the castings. While the literature suggested that microporosity would be very visible, despite the low density of magnesium alloys, our films showed very little (24). It was known beyond a reasonable doubt that the unrisered and unchilled bars would exhibit a great deal of porosity, the films showed sound castings on first inspection.

Upon detailed inspection with a very bright lamp, fine, feathery porosity contrast was seen through the castings. With the apparent unreliability of radiograph interpretation, a more definitive test for porosity was sought. It was finally decided that tensile bars should be taken from known problem areas, as these would by definition break at the weakest point in an area. This all but

guaranteed finding the points of maximum porosity, assuming no macroscopic defect such as a crack, inclusion, etc. was in the fracture surface. This technique was employed exclusively in the final set of tests involving the plate and bar thermal gradient tests with great success.

As expected, the unrisered and unchilled castings were filled with centerline shrinkage porosity from one end to the other. This was due to the absence of a sufficient thermal gradient, and thus the proper heat transfer profile for directional solidification to dominate. Transverse or progressive solidification dominated in every case with no riser or chill.

As risers and chills were added to the bars, the sound fraction of the total length of the bar increased proportionally. When a large riser and chill were employed, the porous zone was limited to an area between 4 inches and 9 inches from the center of the riser. Figure 14 shows a schematic of the areas in the bar castings.

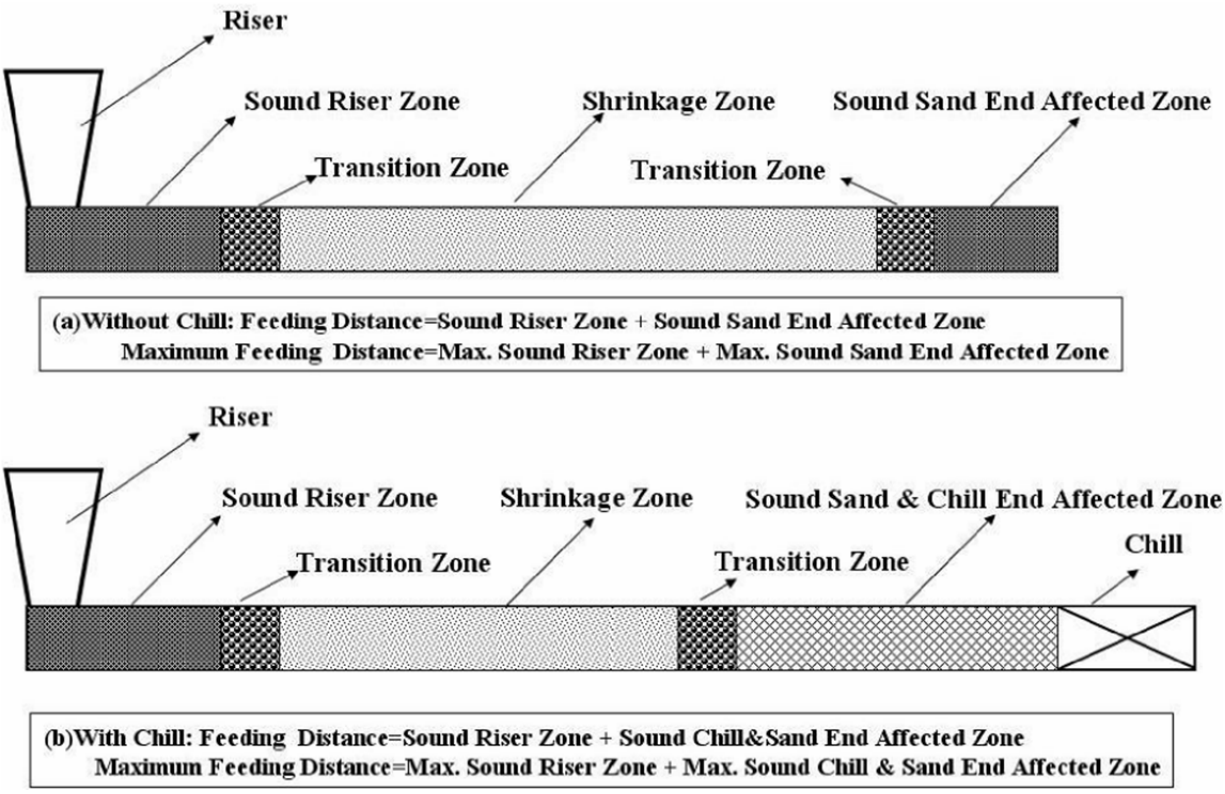

Figure 14 (a) and (b) Zone schematic for the 15 inch bar castings.

As shown in Figure 14a, the riser and sand end both create a length of sound casting. A larger riser will increase this "sound riser zone" while a smaller one will have the opposite effect. The addition of a chill at the sand end, greatly improves the ability of the mold to extract heat in that direction. This greatly increases the length of the end sound zone. At the periphery of these sound zones, an area of increasing porosity occurs due to the diminishing ability of the riser or chill to establish a sufficient gradient. Larger chills and risers will increase this effect up to a critical point at which the thermal conductivity of the metal begins to limit their effectiveness at longer distance. This is shown in Figure 14b.

In between these transitions is an area of high centerline porosity and thus the weakest part of the casting. Due to the inability of radiography to show these zones and their borders with any regularity, an improved method of measuring them was sought.

Metallography became impractical as well due to the large size of the specimens and inability to obtain consistent polishing along such a large length.

At this point it was decided to determine if MAGMA could predict the presence of porosity in magnesium alloy castings. The software has shown this ability with other more common alloy systems. With the bar, riser, pour basin, and mold modeled in MAGMA, a series of simulations were run to predict porosity in the bars. Figure 15 shows a MAGMA rendering of an AM50A bar casting with predicted porosity levels and location shown. Figure 16 shows the same plot for an AZ91D simulation.

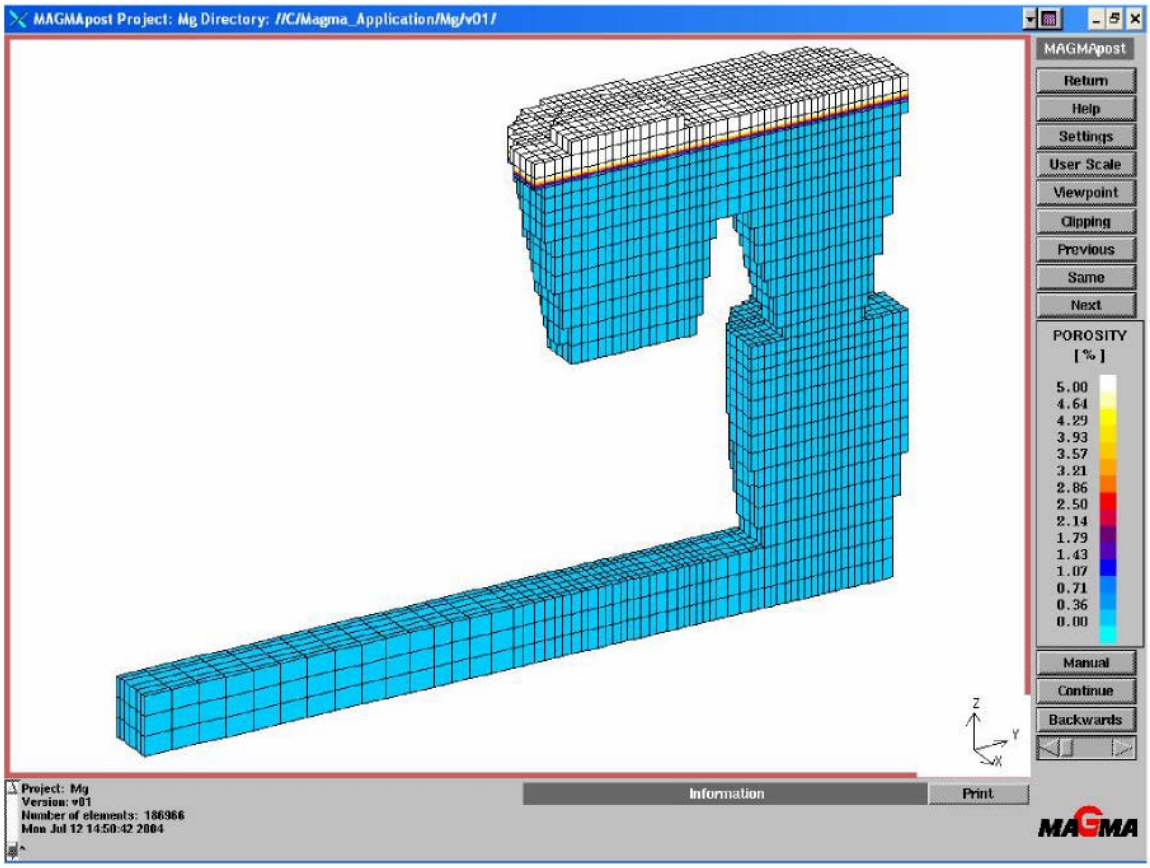

Figure 15 Cross section of MAGMA simulation of bar casting with pour basin showing porosity prediction for AM50A.

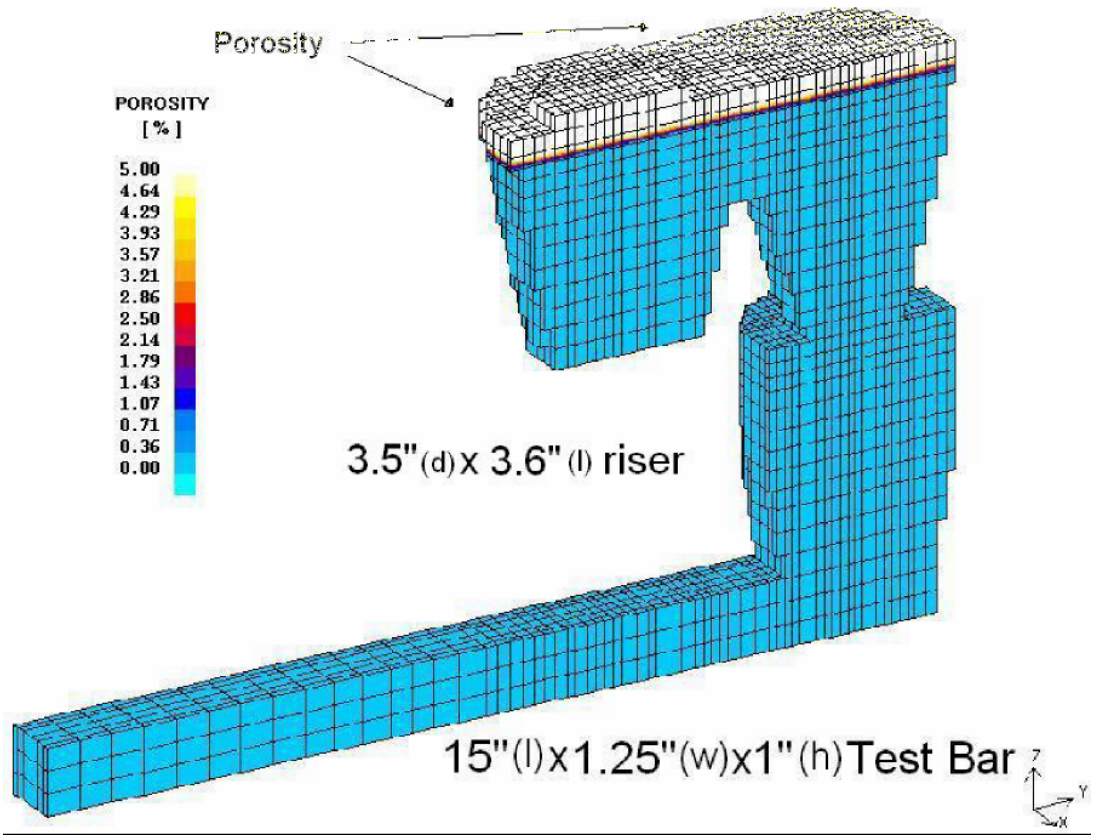

Figure 16 Cross section of MAGMA simulation of bar casting with pour basin showing porosity prediction for AZ91D.

At first inspection of these plots, the software predicted no porosity to be formed except at the very surface of the pour basin. Obviously, having found porosity in the actual casting trials, the software seemed to be in error. Since any shrinkage porosity would be in the center of the bar, the plots in the figures above are of a cross section to clearly show the center line of the bars. This confirmed that our revision of MAGMA was incapable of accurately predicting shrinkage porosity in magnesium alloys with these castings. It was then decided to model an extreme case scenario, with a much longer bar with larger cross section and no riser or chill to see if the software would predict any porosity at all in the casting. Figure 17 below shows the results of the simulation.

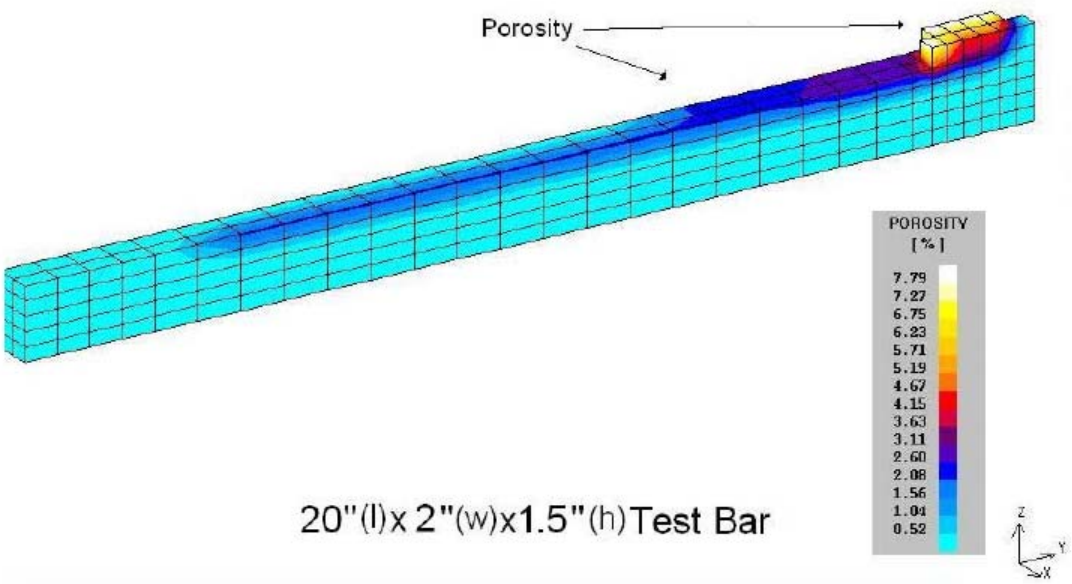

Figure 17 Cross section of MAGMA simulation of a hypothetical 20 inch bar and no riser showing predicted porosity for AZ91D.

As can be seen in the figure, MAGMA finally predicted porosity, but along the top surface instead of along the centerline as seen experimentally. Notice how it failed to predict the riser effect sound zone at all. These results led to the conclusion that MAGMA in its current form was unsuited to simulate shrinkage porosity in magnesium alloys. This showed a need for a tool that could be used in conjunction with these modeling programs to accurately predict soundness, and help optimize castings. This is incredibly important for die casting due to the extreme cost involved in die manufacture. Trial and error is completely unfeasible in this case, so the dies must be made correctly the first time.

5.4 Thermal Gradient Castings

Figure 18 shows a sample temperature profile during casting of an AM60A thermal gradient bar with no riser or chill. The thermocouples in the predicted porous zone (2-9 inches from riser) are following the same curve, indicating a very low thermal gradient. Only the end thermocouples (9 and 12 inches from sprue) show any deviation from the others, and thus an appreciable gradient. Figure 19 shows the same plot and alloy with the addition of riser and chill, as well as the liquidus and solidus temperatures indicated. Notice the larger spread in the data with the riser and chill. This is indicates a much higher thermal gradient. Figure 20 shows a plot of the thermal gradient versus time for the AM60A bar with riser and chill. From this plot it is easily seen that the 4- to 6-inch areas has the lowest gradient, and thus the greatest possibility for porosity. This corresponds well to the predicted porosity profile with a riser and a chill as shown in Figure 14b. Appendix 2 contains the temperature vs. time and thermal gradient versus time plots for the full set of castings.

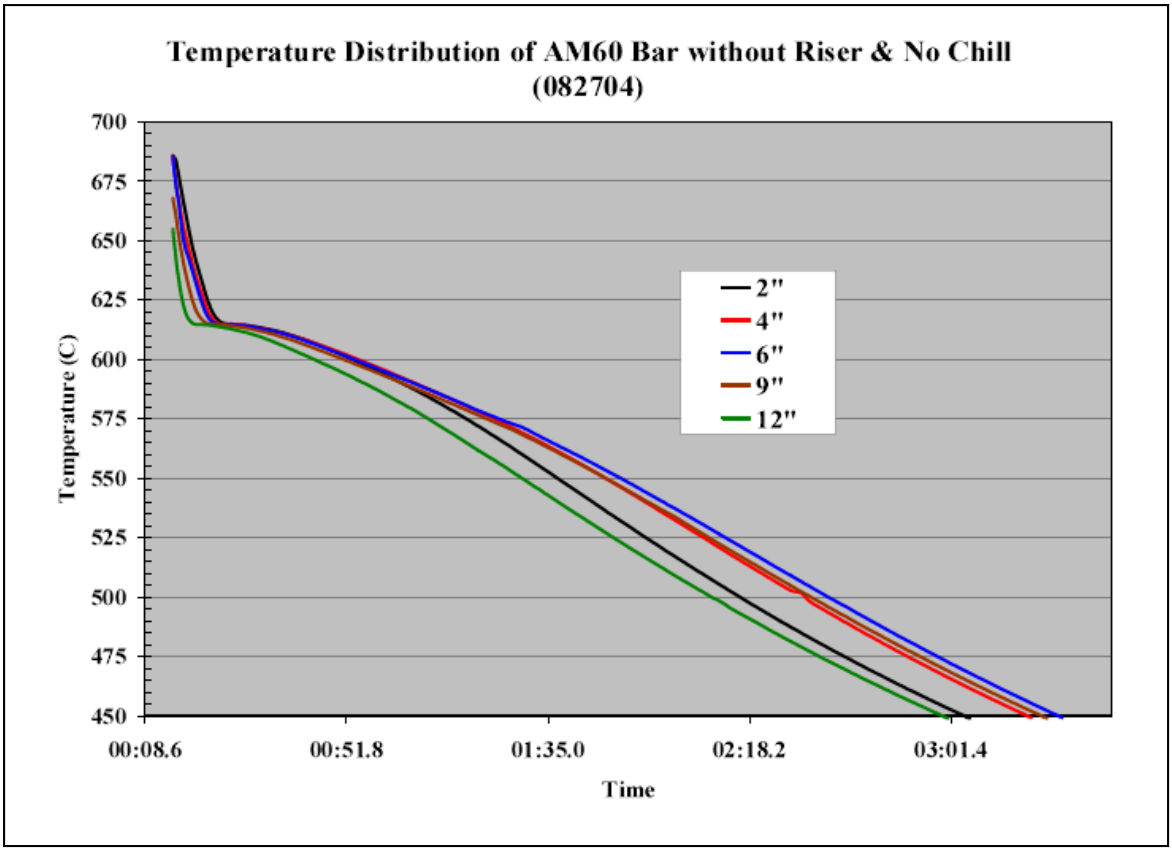

Figure 18 Temperature versus time plot for an AM60A bar with no riser or chill.

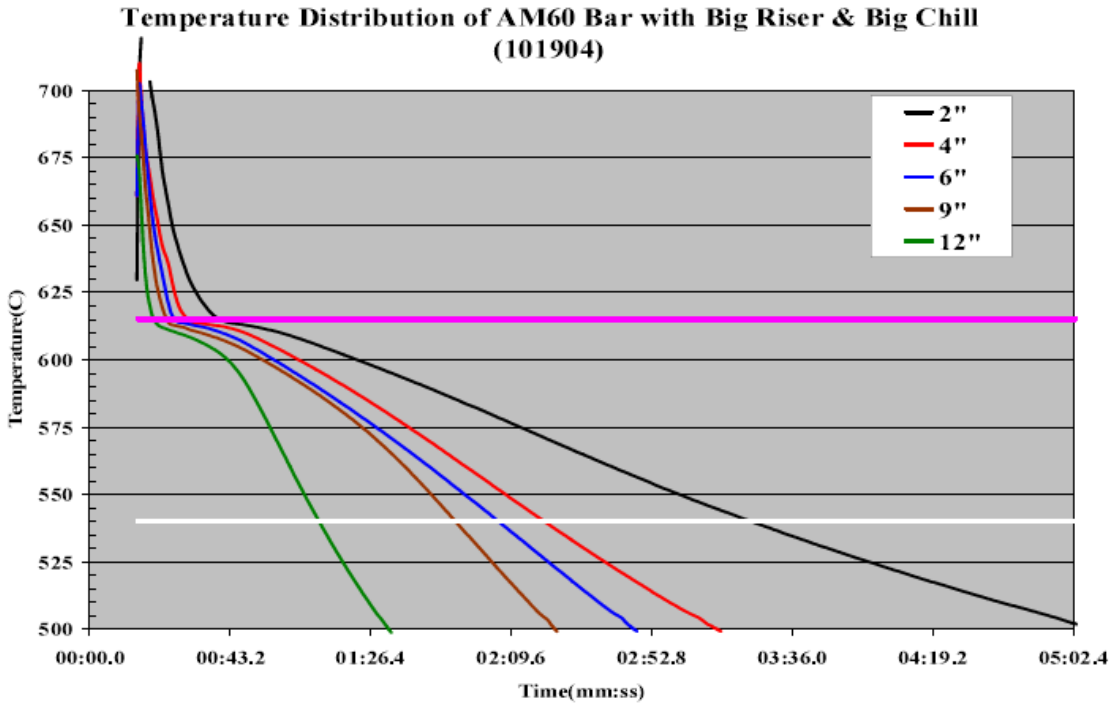

Figure 19 Temperature versus time plot for an AM60A bar with riser and chill.

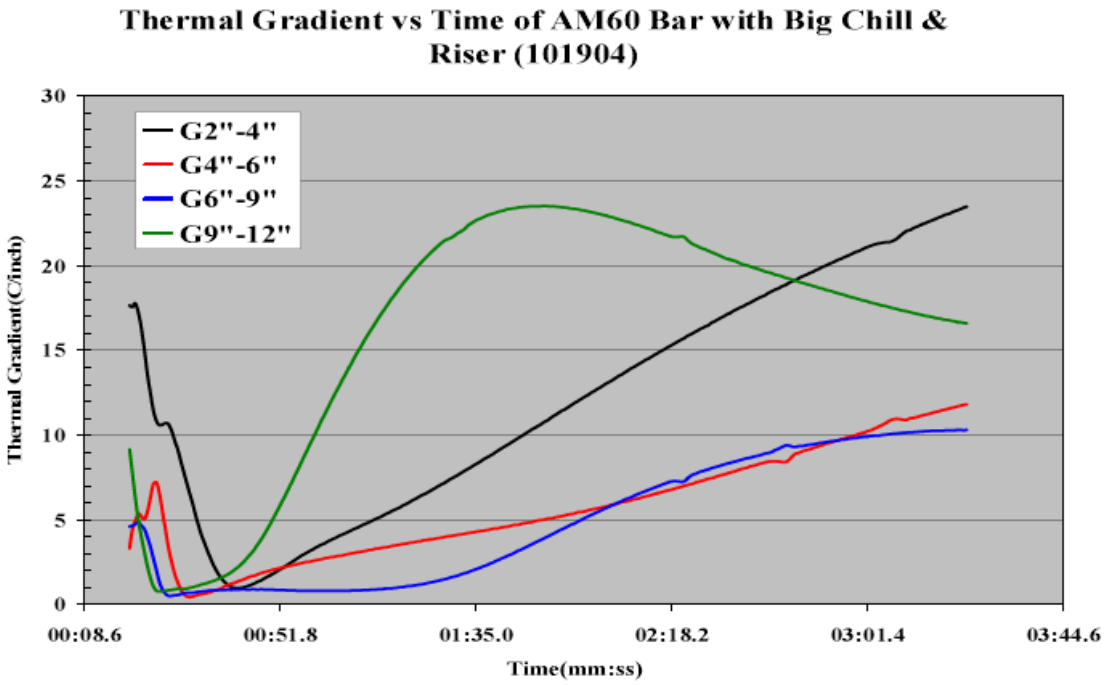

Figure 20 Thermal Gradient versus time plot for an AM60A bar with riser and chill.

Figure 21 shows the same temperature versus time plot for AM60A, but this time for the 15 inch tapered plate. The effect of the large riser and taper is very well pronounced, as shown by the large difference between the thermocouples, and thus a large gradient. This is shown in the temperature gradient versus time plot in Figure 22.

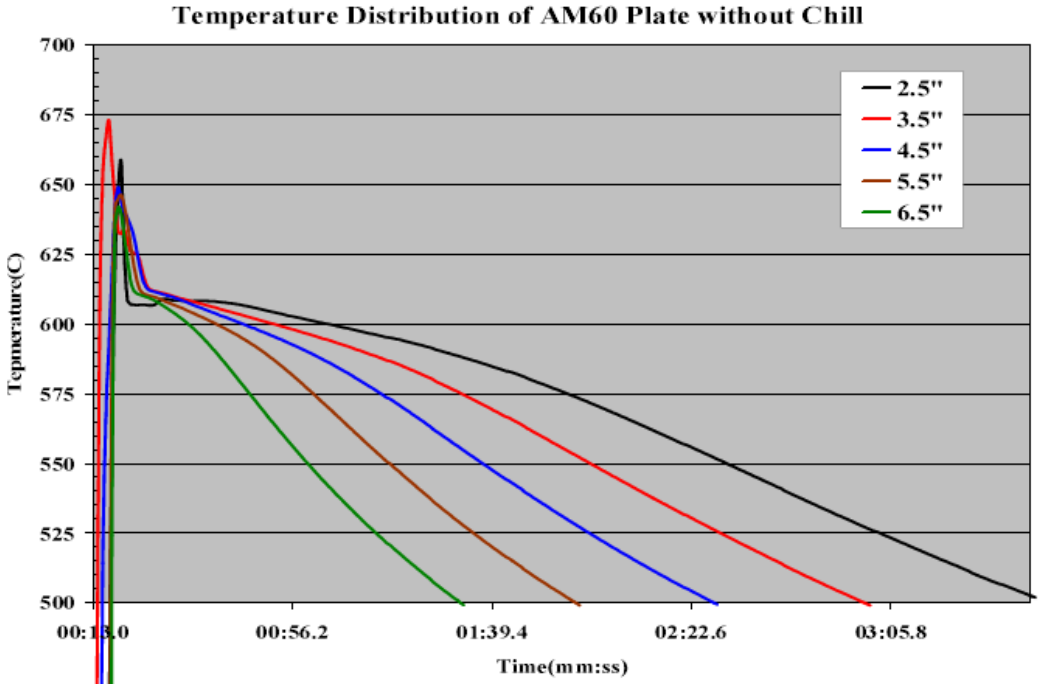

Figure 21 Temperature versus time plot for an AM60A plate without chill.

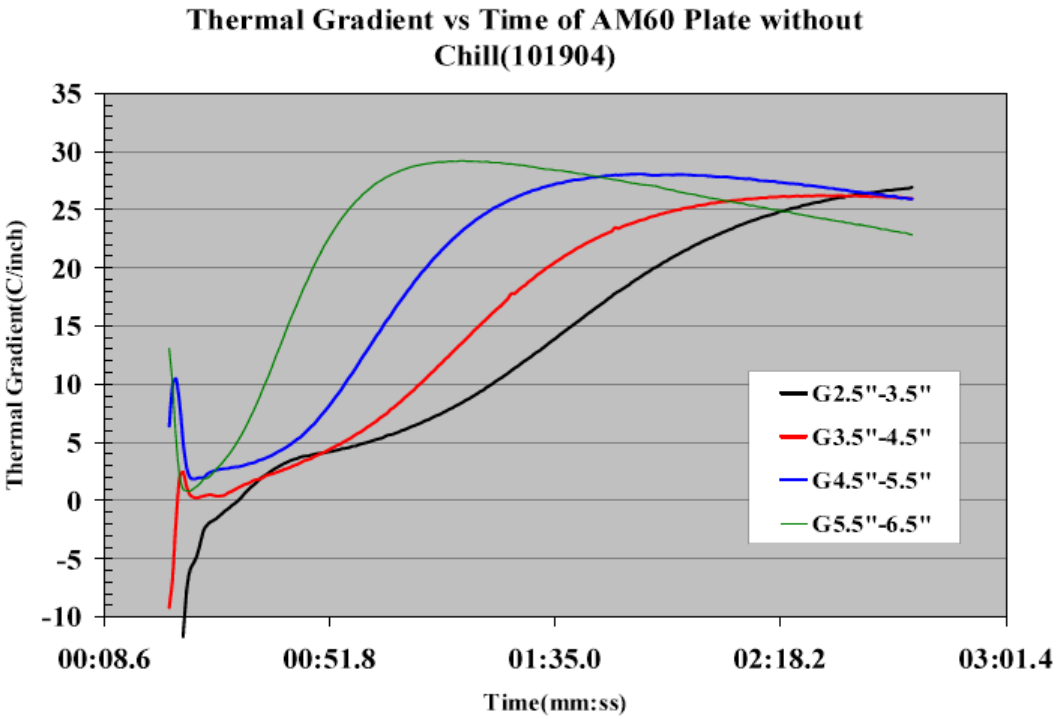

Figure 22 Thermal gradient versus time plot for an AM60A plate without chill.

The thermal gradient is most critical at about 50°C below the liquidus. At this point, the casting is partially solidified (mushy) and feeding becomes critical to preventing porosity. For all of the plate and bar castings, a set of tensile bars was cut from the areas indicated in Figures 10 and 11. Figure 23 below shows SEM micrographs of the fracture surfaces low gradient castings for each alloy (i.e. those without risers or chills).

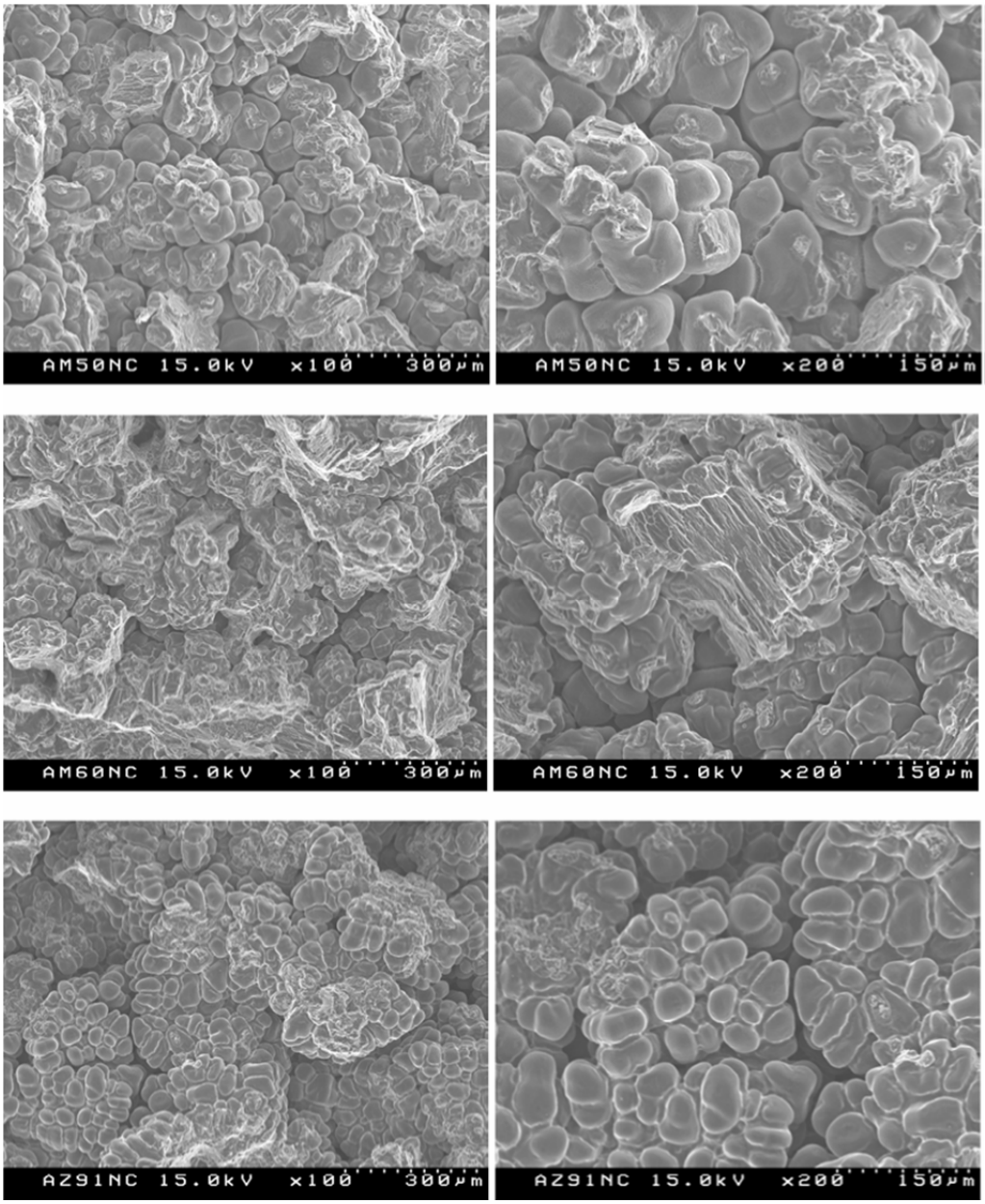

Figure 23 SEM micrographs of tensile bar fracture surfaces for each alloy showing porosity. 100x magnification on left, 200x magnification on right. (High resolution images are available in appendix I)

Figure 24 shows SEM micrographs of the fracture surfaces from fully sound castings. The differences between these sets of pictures are remarkable. In the porous samples, the inter-dendrite voids are very visible and take up the majority of the fracture surface. This is shown by the grape-bundle like features of the surface. It is clear that these areas were not connected at all to the opposite face of the fracture surface. The fully dense fracture surfaces show none of these inter-dendrite voids. The entire area shows evidence of fracture, and thus connection to the opposing surface.

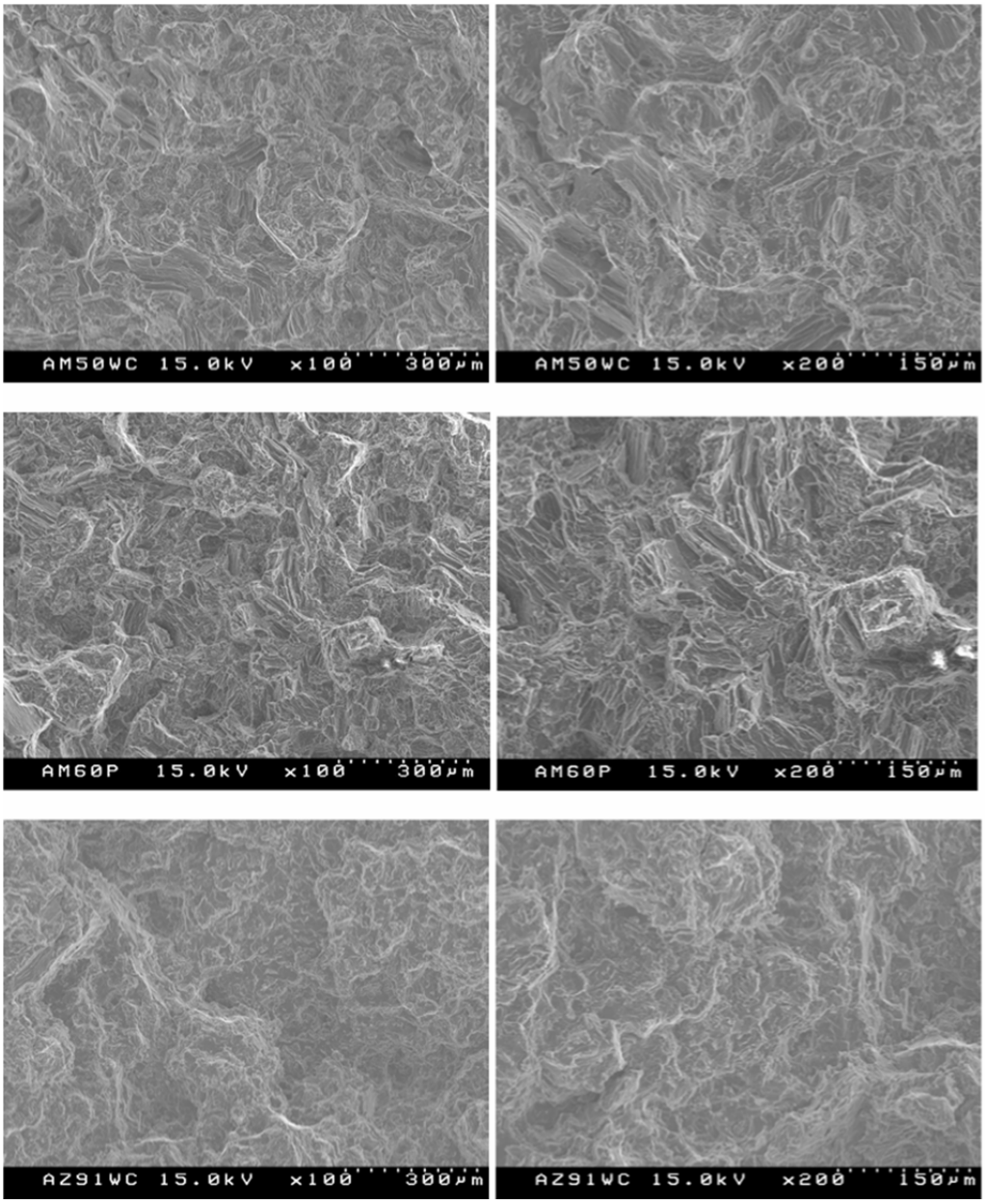

Figure 24 SEM micrographs of tensile bar fracture surfaces for each alloy showing fully dense fracture. 100x magnification on left, 200x magnification on right. (High resolution images are available in appendix I)

The tensile strength and elongation data from all of these bars correlates very well to the fracture surfaces. As expected, the porous samples failed at relatively low load, while the fully dense samples failed at near-optimum ultimate tensile strength for the as cast (F) condition. The elongation is also near-optimum for the fully dense samples, while it is very low for the porous samples. Table 9 below shows the mechanical data for the tensile bars.

Table 9 Tensile test results for each alloy and casting condition.

Casting Condition		UTS (MPa/ksi)	Elongation (%)
With shrinkage sampled from untapered and unchilled bars	AM50A	110 / 16	4
	AM60A	96.5 / 14	5
	AZ91D	55.2 / 8	3
Without shrinkage from risered and chilled bars	AM50A	179 / 26	9
	AM60A	186 / 27	13
	AZ91D	172 / 25	7
Without shrinkage sampled from tapered and chilled large plate	AM50A	207 / 30	14
	AM60A	200 / 29	15
	AZ91D	193 / 28	8

It is clear that the tapered and risered plates have the best overall mechanical properties, as expected. This indicates that they are indeed fully dense, and gradients found will be more than the critical value. The bars, however, despite the fully dense appearance of the fracture surfaces, have tensile and elongation values which are slightly less than optimal. This was most likely due to the increased thickness in these castings. This led to a slightly increased grain size in the center. The small size of the tensile specimens made them more sensitive to grain size at the center than the casting as a whole.

The calculated minimum thermal gradients to achieve sound castings for each of the three alloys are shown in Table 10 below:

Table 10 Observed minimum thermal gradients in sound plate and bar castings at 50°C below the liquidus for each alloy.

Alloy	Thermal Gradient Observed in Sound Plate Castings (°C/cm)	Thermal Gradient Observed in Sound Bar Castings (°C/cm)
AM50A	3.15	2.02
AM60A	3.16	1.99
AZ91D	2.15	1.97

Given the fracture surfaces and mechanical properties in conjunction with these gradients, it is possible to predict that as long as a casting maintains these minimum gradients at 50°C below the liquidus, the casting will be sound. It is definitely possible that there are smaller gradients for these alloys that will yield sound castings, but further experimentation would be needed to further narrow down these numbers. It is likely that the 2°C/cm gradients found in the bars are closer to the true value of this minimum gradient. Obviously, any number greater than this value will produce shrinkage-free and porosity-free castings.

5.5 The Effect of Cooling Rate

Two alloys, AZ91E and AM50A were selected for this part of the study. The grain refiner, C_2Cl_6 is widely used in industrial practice. About hundred pounds of virgin alloy ingot was melted in a resistance electrical furnace at 135º0F under the protection of dry air+CO_2+SF_6. The melted Mg alloy was tapped out into a preheated ladle and 0.2% of the C_2Cl_6 grain refiner was plunged to the bottom of the ladle with a bell plunger. The molten metal was then overheated to 1450ºF, held for six minutes then fast cooled to 1350ºF. During the entire time the molten metal was protected by a 310 flux. The alloy was then cast into a preheated vertical

permanent mold. The dimensions of the step casting are shown in Figure 25(a). The mold was coated with Hill & Griffith Concote^{TM} Mag 669, a wash that prevents reaction and sticking of the casting to the mold. The mold was pre-heated to 400^{o}F using an electrical die heater. In order to measure the local cooling rate, a thermocouple was embedded in the center of each step as shown in Figure 25(b). Tensile test bars were machined from the center of each step as shown in Figure 26. These samples are designated 1, 2 and 3 respectively, like the steps they originate from. Metallographic samples for optical microscopy were cut from the grip part of the tensile bars, solution treated and etched. The solution treatment and etchants used to reveal the grains are listed in Table 11.

Table 11 Solution treatment and etching reagent for AZ91E and AM50A

Alloy	AM50A	AZ91E
Heat treatment process	785^{o} F × 20 hour Air cooling	775^{o}F × 16 hour Air cooling
Etching reagent	5 ml glacial acetic acid 6 gram picric acid 100 ml ethanol 10 ml water	60 ml ethylene glycol 20 ml glacial acetic acid 19 ml water 1 ml nitric acid

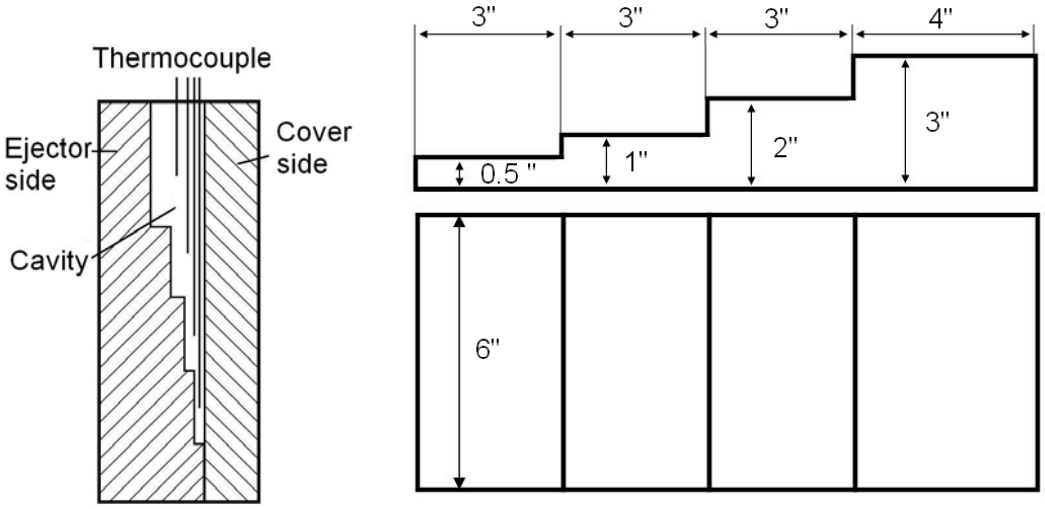

Figure 25 (a) Dimensions of the step casting and (b) Illustration of the set-up for cooling rate measurement.

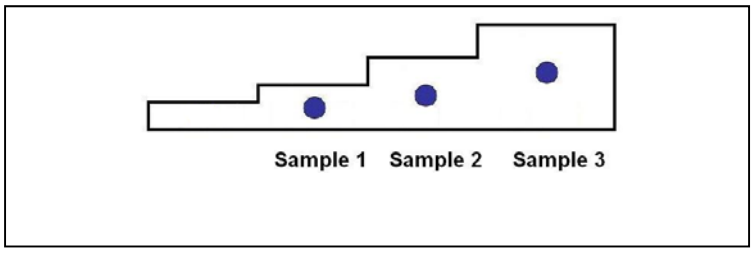

(a)

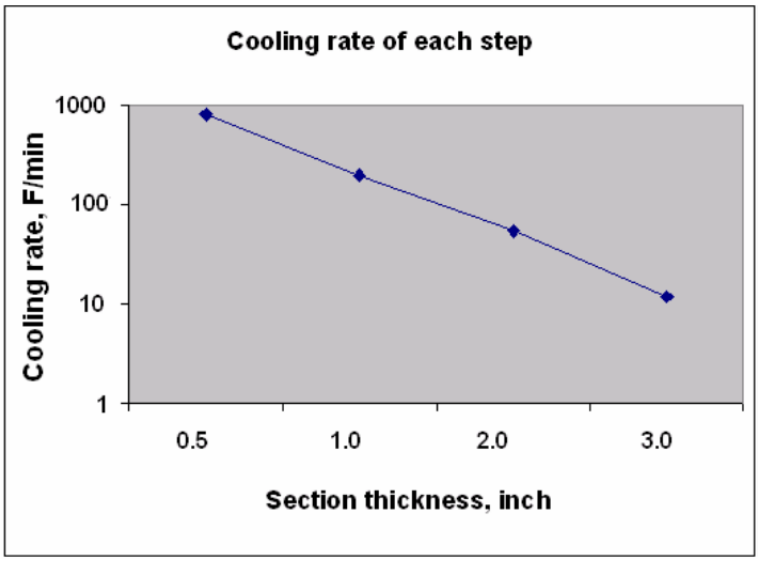

(b)

Figure 26 (a) Tensile sample location and (b) respective cooling rates.

The average tensile testing results of the two alloys are shown in Figures 27 and 28 and summarized in Table 12. The ultimate tensile stress, yield stress and elongation of the grain refined samples are higher than the untreated samples. Faster cooling rates also improve the mechanical properties. The highest cooling rate is obtained in the thinnest step. The cooling rate gradually decreases toward the heaviest section. The effect of the cooling rate is more obvious for the grain refined samples. The results show that sample 1, taken from the 1 inch step, had the highest UTS, yield strength and elongation. On the other hand, sample 3 taken from the 3 inches step had the lowest UTS, yield stress and elongation. Typical room temperature properties AZ91E are ultimate strength of 40 ksi and elongation of 6%. For die cast AM60A the ultimate strength is 30ksi and elongation is 6%[25]. Elongations as high as 23% have been reported for AM60B die cast under optimized conditions [26].

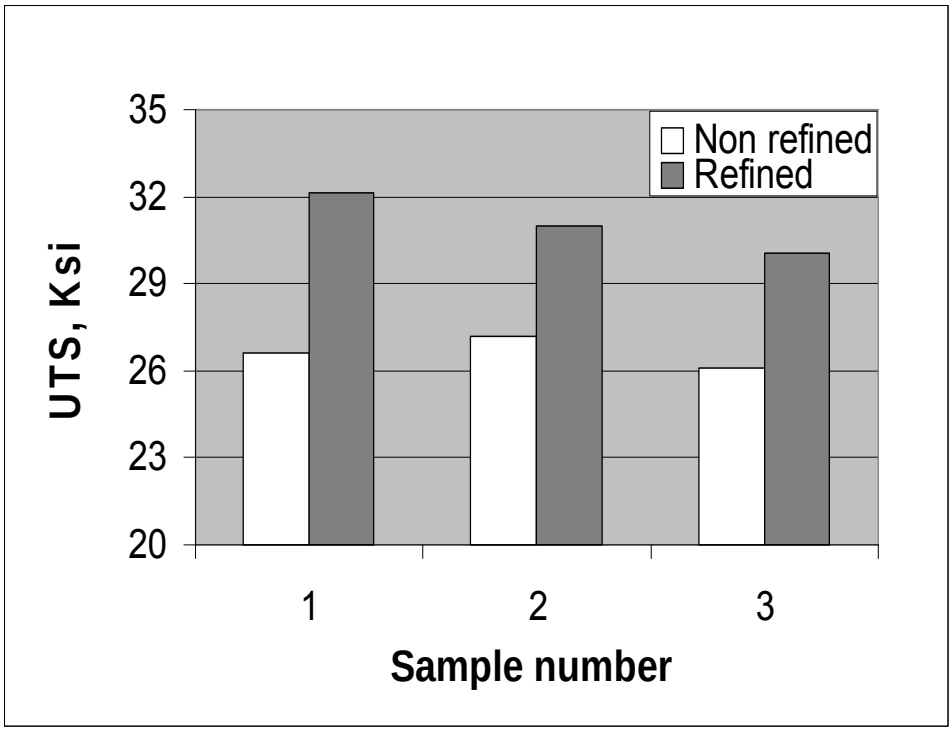

Figure 27(a) UTS of permanent mold cast AM50A (1, 2 and 3 indicates the samples were obtained from 1", 2" and 3" steps respectively)

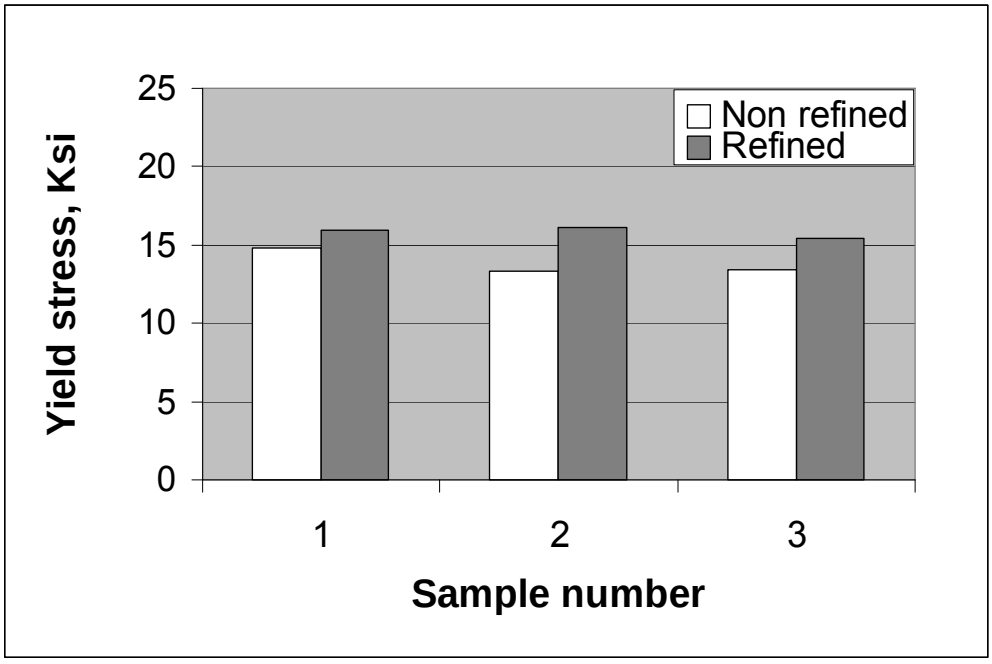

(b)

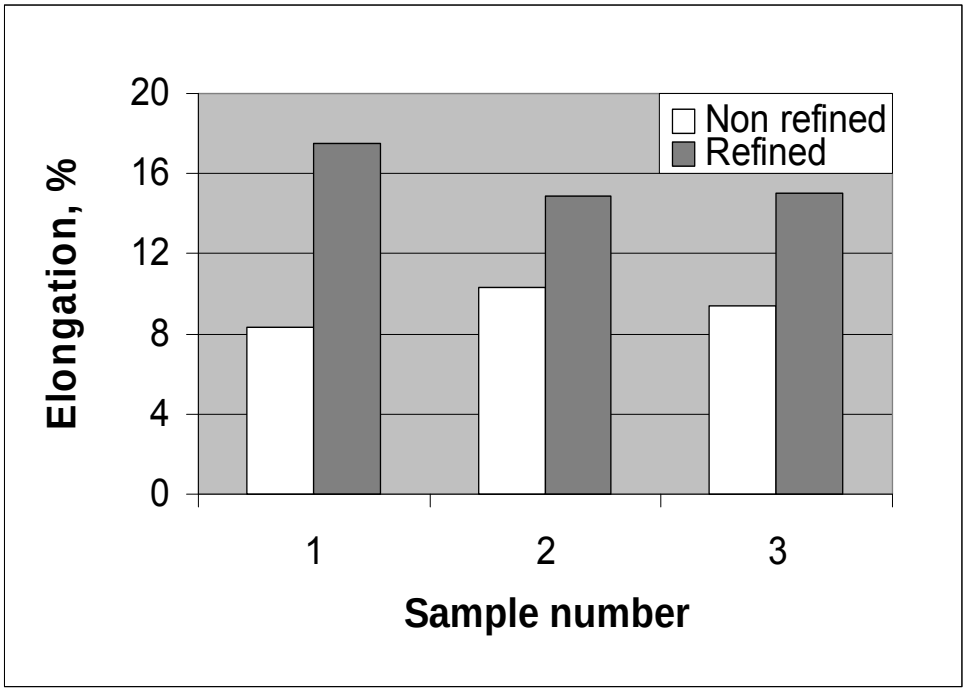

(c)

Figure 27(b)(c) Yield strength and elongation of permanent mold cast AM50A (1, 2 and 3 indicates the samples were obtained from 1", 2" and 3" steps)

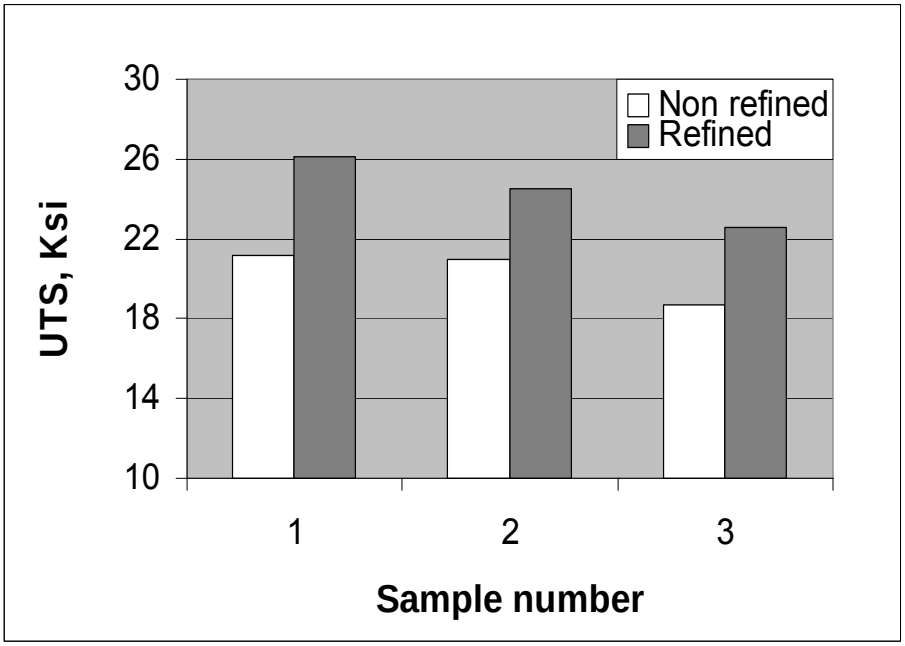

(a)

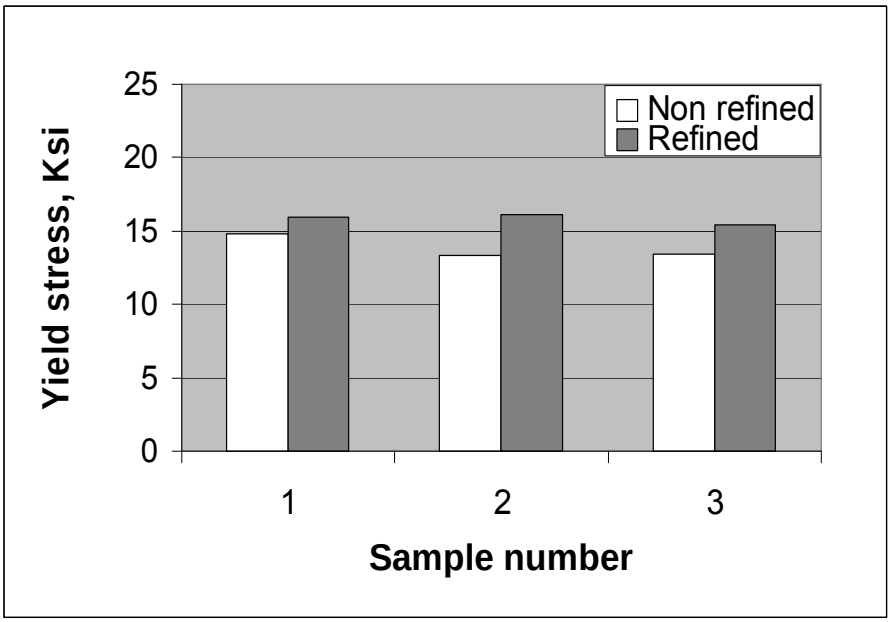

(b)

Figure 28(a)(b) UTS and Yield Strength of permanent mold cast AZ91E (1, 2 and 3 indicates the samples were obtained from 1", 2" and 3" steps respectively)

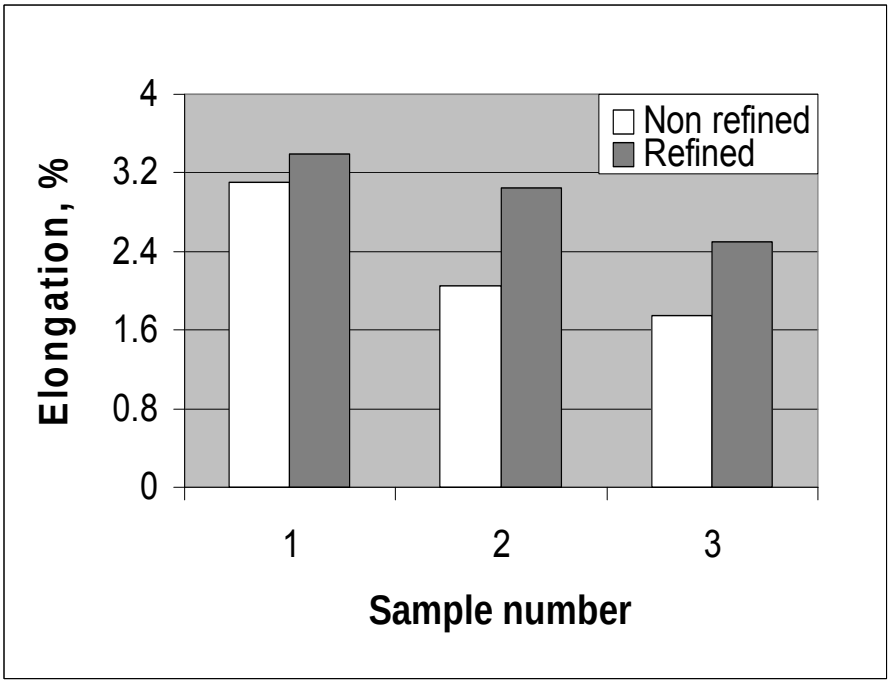

(c)

Figure 28(c) Elongation of permanent mold cast AZ91E (1, 2 and 3 indicates the samples were obtained from 1", 2" and 3" steps respectively)

Table 12 Average tensile properties of grain refined vs. non-grain refined alloys

	Sample number	UTS (Ksi)	Yield stress (Ksi)	Elongation (%)
Non Refined AM50A	1	26.60	18.60	8.30
	2	27.20	9.60	10.30
	3	26.10	9.55	9.40
Refined AM50A	1	32.15	22.55	17.50
	2	31.00	10.60	14.90
	3	30.05	10.05	15.00
Non refined AZ91E	1	21.20	14.85	3.15
	2	20.95	13.30	2.05
	3	18.75	13.45	1.75
Refined AZ91E	1	26.05	15.94	3.40
	2	24.50	16.10	3.05
	3	21.55	15.45	2.50

*1, 2 and 3 indicates the samples were obtained from 1, 2 and 3 inches step respectively.

Figures 29 and 30 show typical microstructures of the refined and non-refined samples taken from the 1 inch step. It is noted the grain size of the refined sample are smaller than that of the non-refined sample. This is more obvious in the AZ91E alloy than in the AM50A alloy.

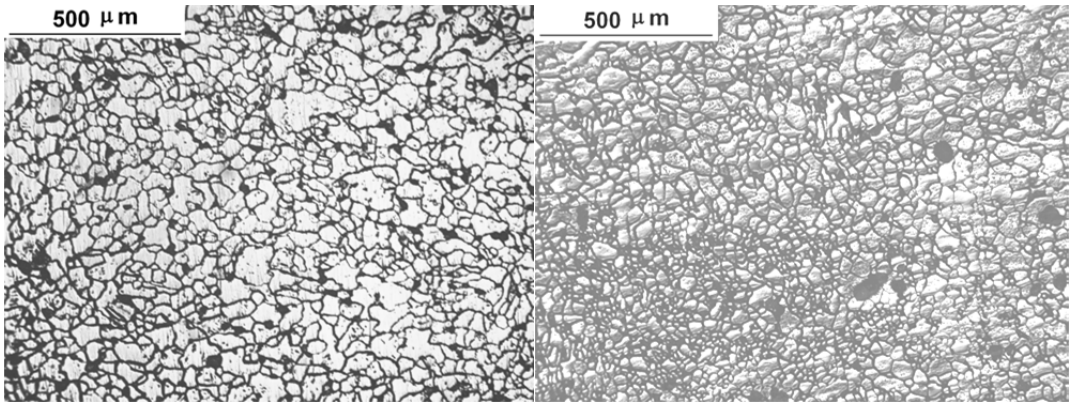

Figure 29 Optical microstructure of non- refined (left) and refined AM50A (right)

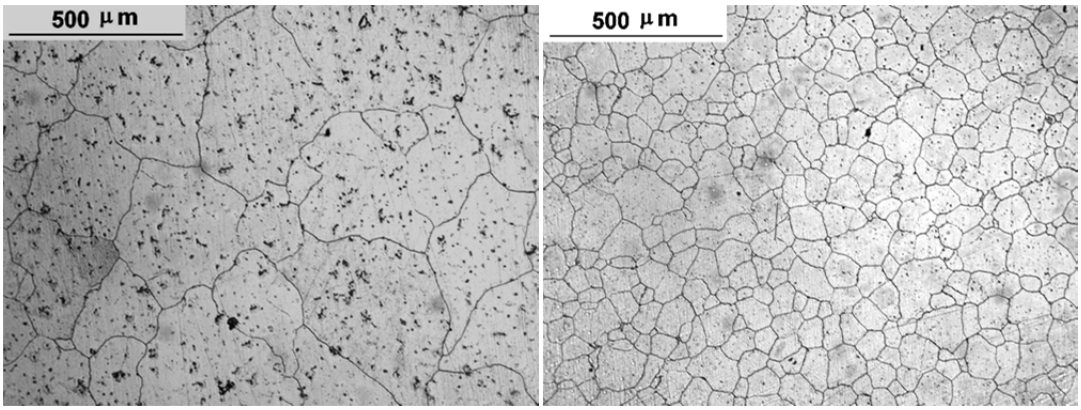

Figure 30 Optical microstructure of non-refined (left) and refined AZ91E (right)

In order to investigate effect of cooling rate and the grain refiner on the grain size of the casting, samples were taken from the center of each step. The ASTM 112 Intercept Method was used to determine the grain size. Figure 31 shows the variation of the grain size of the two alloys against

the cooling rate. Evidently, as the cooling rate increases, the average grain size decreases. However, the reduction in grain size caused by increasing the cooling rate from 12°F/min to 200°F/min is not very large. The effect of grain refining with C_2Cl_6 on grain size is much more pronounced, especially in AZ91E. Generally speaking, finer grains mean higher mechanical properties regardless of the mechanism that produced them. This explains why the grain refined samples have higher mechanical properties. The higher cooling rates lead to finer grain size hence the highest mechanical properties.

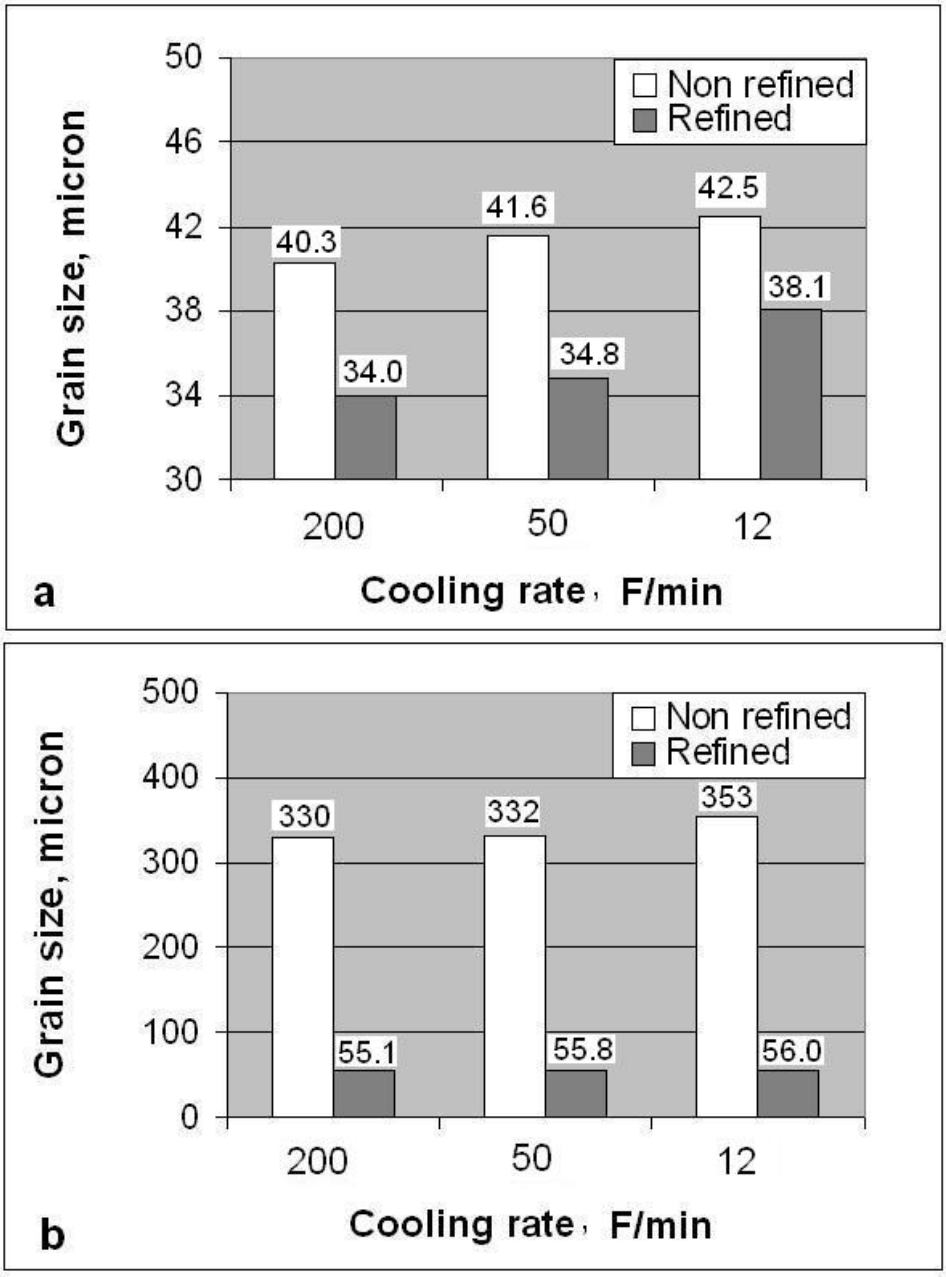

Figure 31 Relationship between average grain size and cooling rate (a) AM50A (b): AZ91E. (200°F/min , 50°F/min and 12°F/min in steps 1, 2 and 3.)

The grain refining mechanisms involved with carbon inoculation are not yet fully understood. According to Wang *et al.* [27], when the C_2Cl_6 is added into the molten Mg-Al alloys at high temperature, the following reactions will occur:

$$\text{(eq. 5.1)} \qquad C_2Cl_6 = 2C + 3Cl_2$$

$$\text{(eq. 5.2)} \qquad 3C + 4Al = Al_4C_3$$

Al_4C_3 is a very effective nucleant for magnesium alloys containing Al [27]-[29]. It is an active heterogeneous nucleating phase for α-Mg, since both Al_4C_3 and α-Mg have a hexagonal lattice structure [27]. This implies a very low lattice mismatch between them that makes it a preferred nucleation site. As soon as the primary Mg grains are nucleated on the Al_4C_3 particles in the melt, they start grow radially, in a uniform fashion. As a result, effective nucleating particles are often expected in the central regions of the primary Mg grains [28]. Figure 32 shows the microstructure of a grain refined sample. A multitude of opened pores were observed in the center of each grain. This feature was not present in non-grain refined samples. Such pores are believed to have been originally occupied by Al_4C_3 particles. Al_4C_3 particles are extremely reactive to water according to the following equation:

$$\text{(eq. 5.3)} \qquad Al_4C_3 + H_2O = Al(OH)_3 + 3CH_4$$

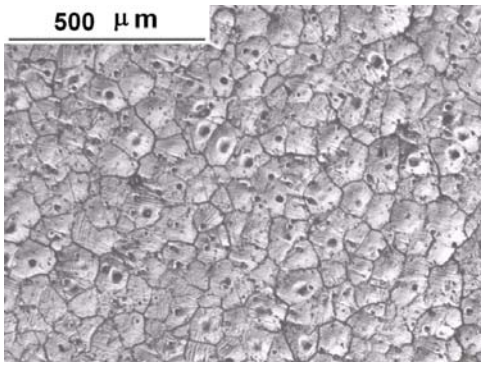

Figure 32 Optical microstructure of refined AZ91E alloy

Consequently, in most cases, Al_4C_3 cannot be found in the optical microstructure samples. However, in some areas, Al_4C_3 can still be detected by SEM and EDS analysis. Figure 33 shows the SEM picture of a particle and the EDS analysis. The Mg peak in the EDS originates from the matrix. Presumably the particle consists of Al, C and O. STEM diffraction of the particle would be required to positively confirm the structure of the particle. Some researchers have pointed out that Al_2OC is also suitable as the nucleant for magnesium alloys. Al_2OC can form by the following reaction [29]-[30]:

$$\text{(4)} \qquad Al_4C_3 + Al_2O_3 = 3Al_2OC$$

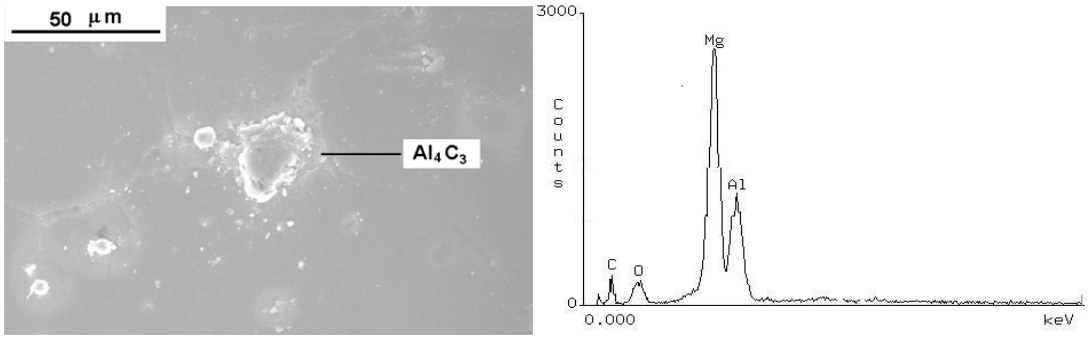

Figure 33 SEM (left) and EDS (right) analysis of the particle

However, according to Jin *et al.* the formation of Al_2OC in magnesium alloys containing less than 10% Al is impossible [39]. In the case of the alloys studied here, both AZ91E and AM50A have less than 10% Al. It is therefore more likely that the particles are Al_4C_3. The oxygen could be introduced during the casting and sample preparation.

5.6 Industrial Case Study

A major goal of this project was to suggest best practices for obtaining porosity free magnesium castings. Current best practices in metal casting apply preliminary computer simulation to optimize the gating design of the casting. This approach is even more critical in porosity-sensitive alloys such as magnesium. To demonstrate this approach, a detailed Magma simulation of a magnesium commercial casting was carried out. The objective was to determine the sections in the casting prone to develop porosity. As a parallel effort, the casting was sectioned, and tensile testing specimens were excised and tested. The following Figures 34 and 35 show the CAD model and a top view of the cast magnesium wheel selected for the study.

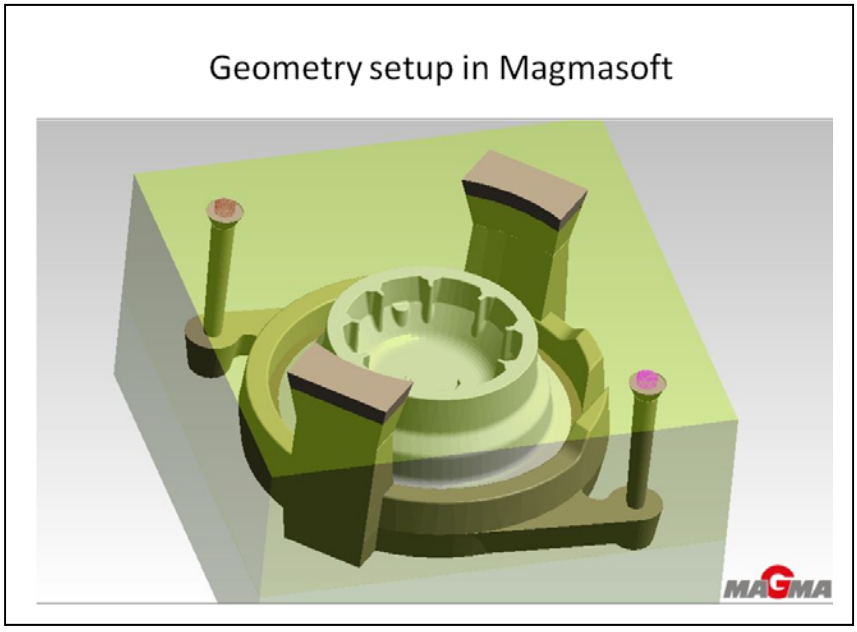

Figure 34 CAD model of the magnesium wheel

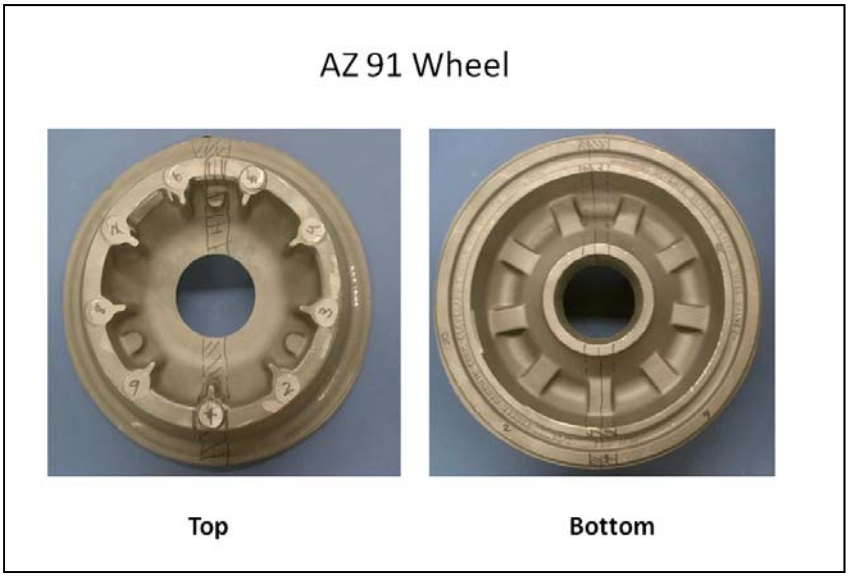

Figure 35 Top and bottom views of the magnesium wheel

The circular geometry of the casting favors a round runner, with a continuous ingate feeding the casting simultaneously, all around the circumference. This is the most important decision made in the casting process. By selecting a gating design that is well-customized to the cylindrical configuration of the casting, hot spots and problems with feeding the casting are minimized. This experienced magnesium foundry then decided to use not one, but two sprues to feed the molten metal. This allows using a smaller, tapered cross-section for each sprue, creating less air aspiration and turbulence and shortening the distance molten metal has to flow before filling the mold. Since magnesium has a low heat content, it is imperative to fill the cavity fast, before the molten metal cools excessively. Avoiding air aspiration is critical, since magnesium reacts with oxygen instantaneously, forming detrimental oxides. Two generous risers top this well-designed gating system, providing a large reservoir of hot molten metal to feed the casting during directional solidification and avoid shrinkage.

The next step was to run the simulation. Figure 36 shows the Magma output for the porosity prediction. The model predicts extremely low levels of porosity, mostly in the heavier hubs of the casting as shown in the Z-section shown in Figure 37.

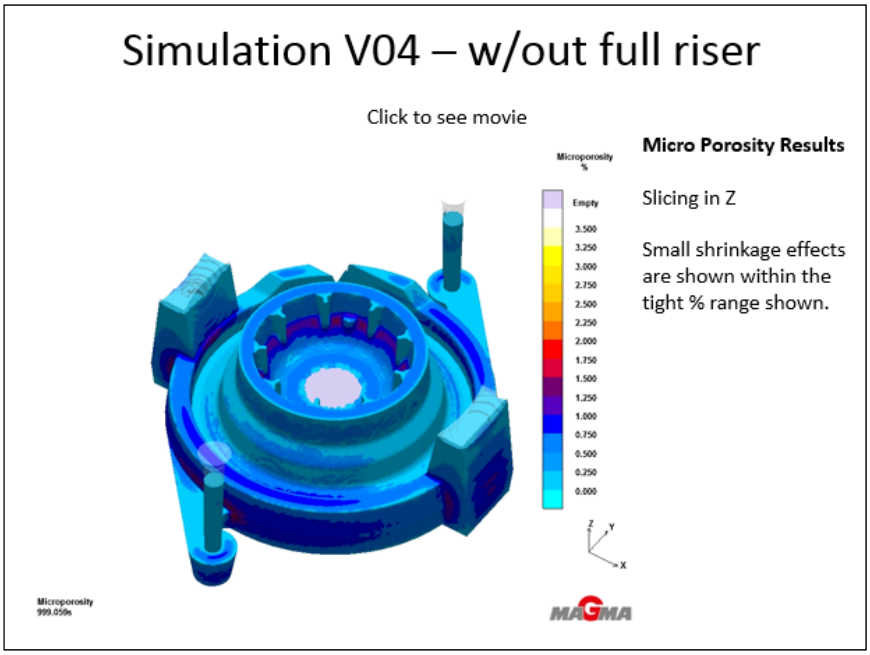

Figure 36 Magma model for the porosity prediction.

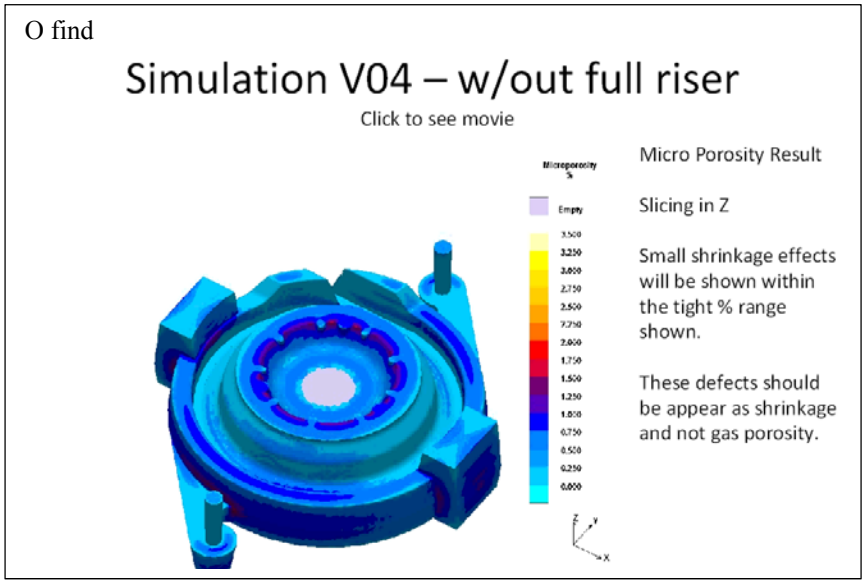

Figure 37 Low level porosity predicted by Magma in the casting (see in red at the top ID)

To find out if the predictions of the simulation are indeed valid, the wheel was sectioned in the hub areas, polished and examined, as shown in Figures 38-40. The micrographs show minimal micro-porosity in only a few of the micrographs, confirming the low porosity level prediction of the computer simulation. To further validate this result, tensile testing bars were machined from the hubs of the wheel and tested in tension. The results are shown in Figure 41. The mechanical properties of the wheel are well in line with the requirement, and similar to those obtained for the 2" step of the step casting shown in Figure 38.

Figure 38 Sections in the wheel

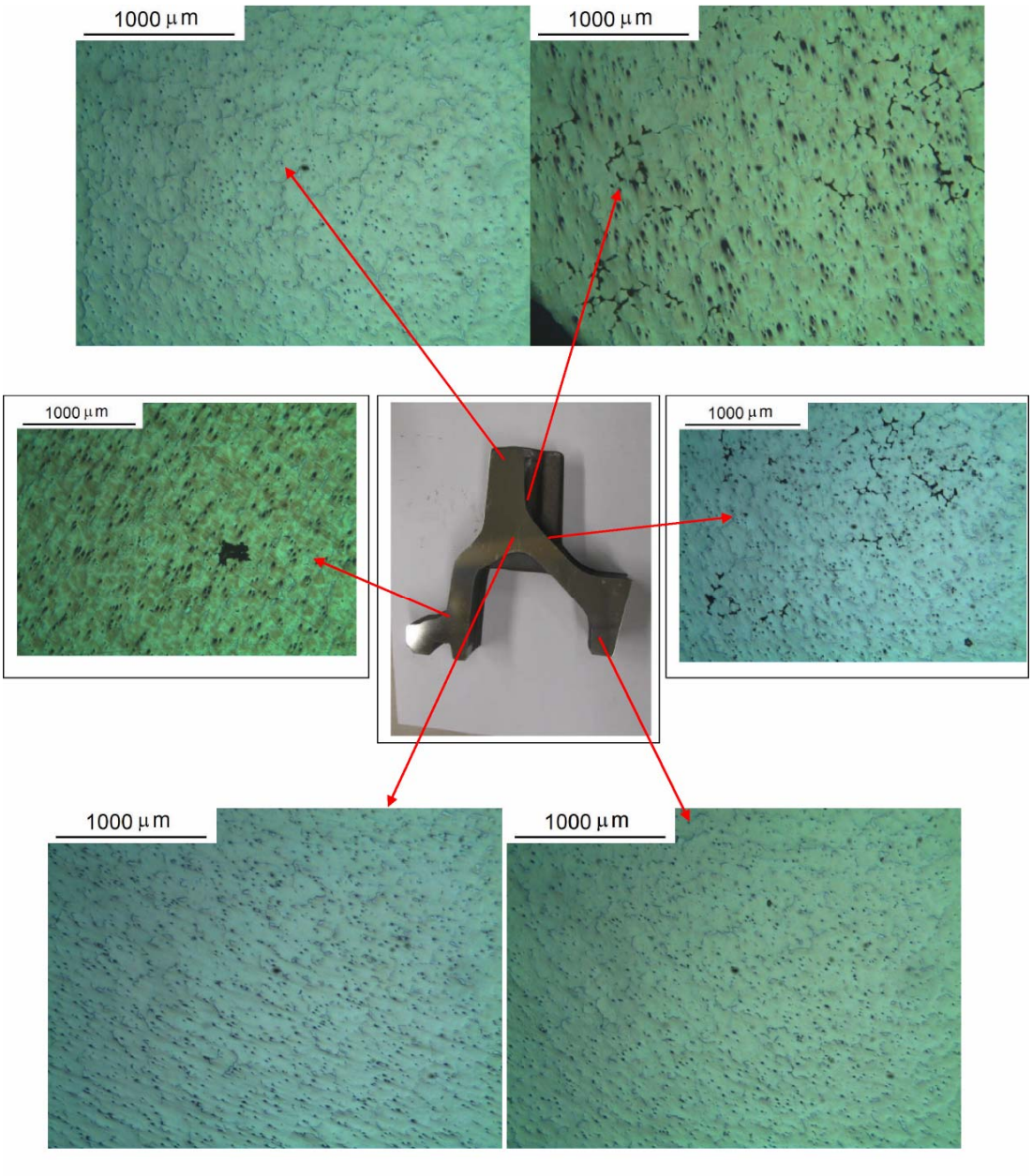

Figure 39 Optical micrographs from sample 1A

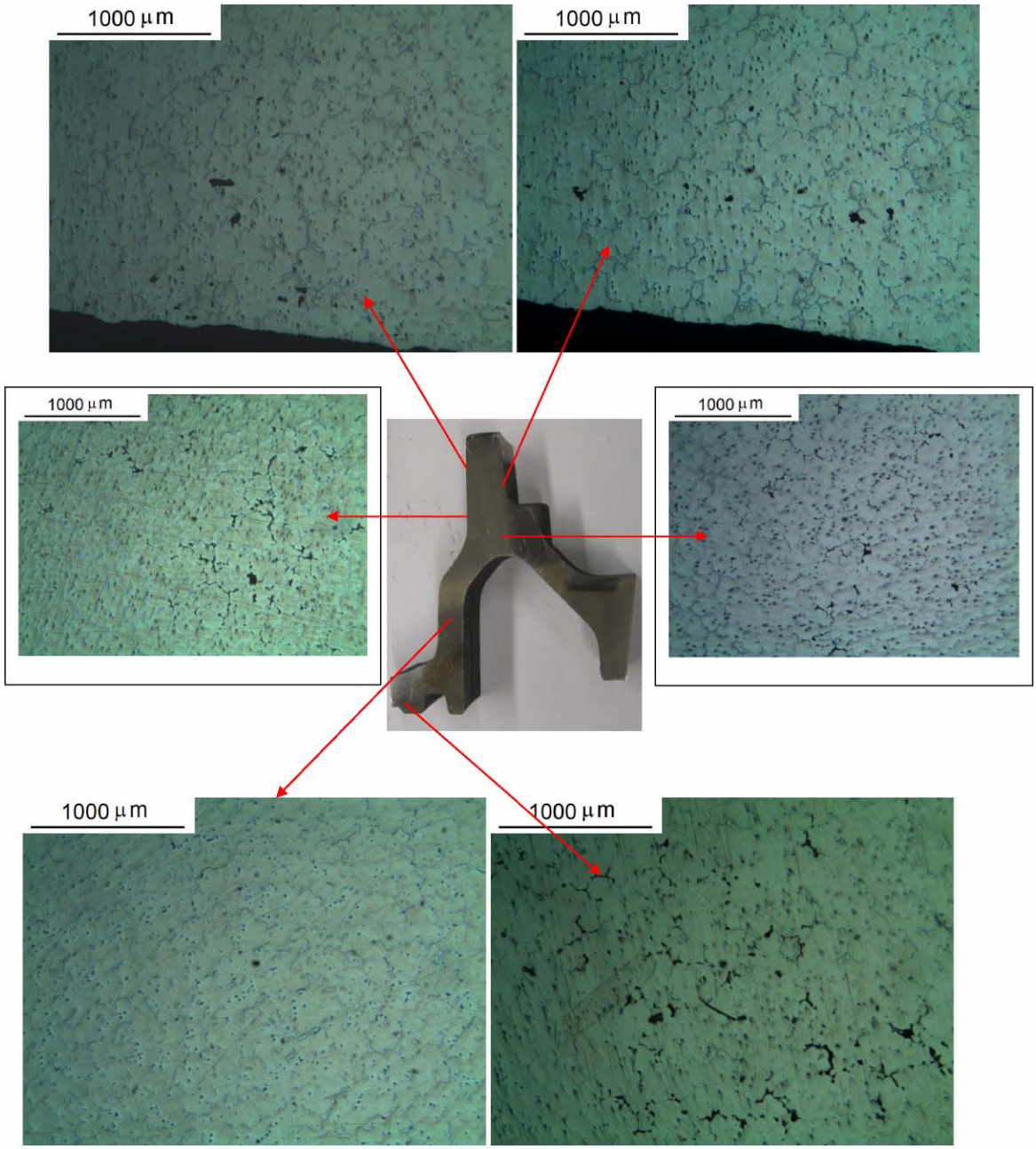

Figure 40 Optical micrographs taken from sample 5.25 A

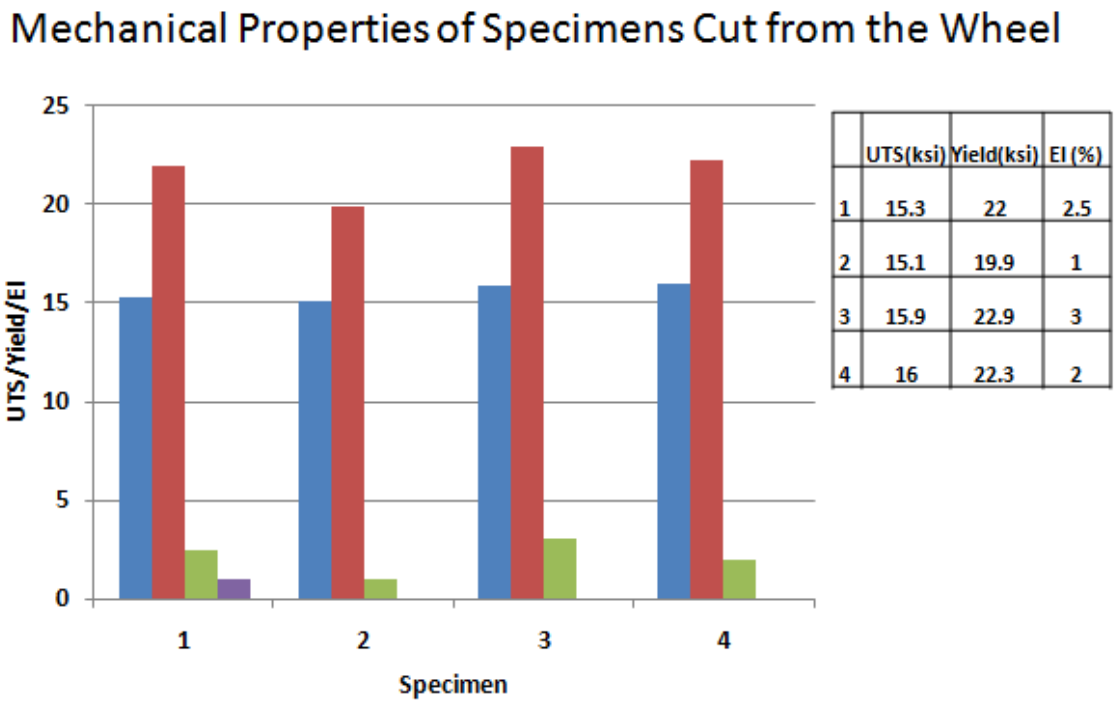

Figure 41 Tensile properties of the wheel

6 Benefits Assessment

Wider implementation of best practices in magnesium casting impact first and foremost the yield of the process. Since cast magnesium alloys are prone to excessive micro-porosity, high scrap rates are common among magnesium foundries. Often times the porosity is exposed only during machining of the castings, incurring added unnecessary cost. The energy invested in production of these castings is wasted if the parts have to be scrapped.

It is estimated application of predictive porosity computer simulation methods and best practices of gating and risering can reduce scrap by at least 2%. To translate this reduction in scrap into dollar savings we are using industry statistics provided by the American Foundry Society (32) and shown in Figure 42.

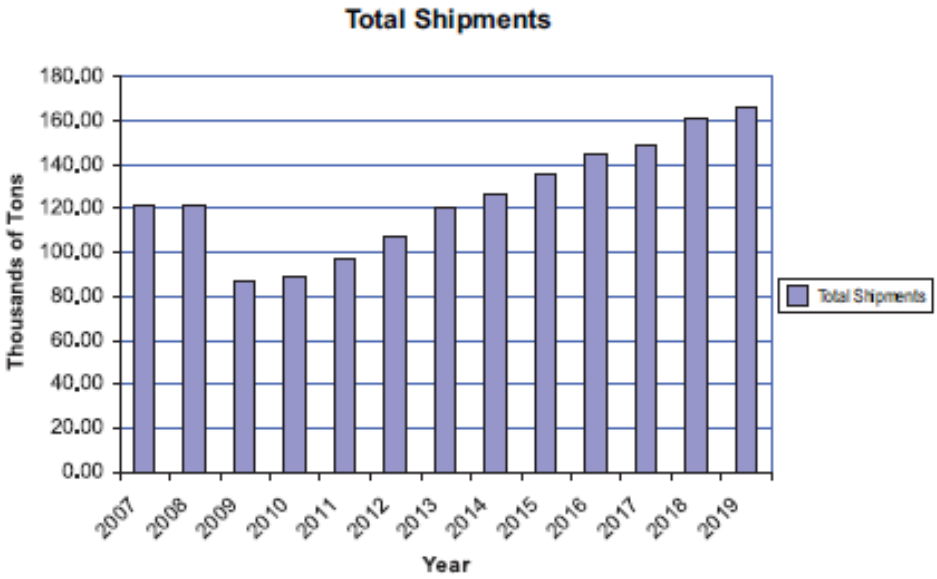

Figure 42 Total U.S. magnesium casting shipments

Using the 100 thousands of tons of magnesium casings produced in the US as a base-line, the 2% reduction in scrap translates into 2,000 tons/year (4.41 Million pounds/year). At an average melting energy of 1,800 BTU/lb (33) the energy savings resulting from this scrap reduction are 7.93×10^9 BTUs. The cost of the energy savings assuming an average cost of $5/MMBTU is almost $39.6 Millions/year. These savings assume full penetration and commercial implementation of the suggested improvements.

Another tool to predict similar benefits for improvements in yield of castings is the Metal Casting Energy Best Practice Guidebook published by the Wisconsin Focus on Energy program. Figure 43, taken from the guidebook estimates the energy savings resulting from yield improvements of the casting process:

The Energy Impact of Scrap Reduction through Improved Mold Design and Process Optimization

				ENERGY SAVED PER CAST TON (Btus*)						
				IRON	ALUMINUM MELT**					
					REVERB WET		REV - DRY	CRUCIBLE		CORELESS INDUCT
GROSS CASTINGS*** [tons]	SCRAP REDUCTION	TOTAL MELT SAVINGS [tons]	SAVINGS / TON MELT [tons]		GAS [therms]	ELE [kWh]	GAS [therms]	GAS [therms]	ELE [kWh]	ELE [kWh]
10,000	0.50%	50	0.005	5,950	13,500	7,285	11,000	47,500	8,875	7,285
10,000	0.75%	75	0.008	8,925	20,250	10,928	16,500	71,250	13,313	10,928
10,000	1.00%	100	0.010	11,900	27,000	14,570	22,000	95,000	17,750	14,570
10,000	1.25%	125	0.013	14,875	33,750	18,213	27,500	118,750	22,188	18,213
10,000	1.50%	150	0.015	17,850	40,500	21,855	33,000	142,500	26,625	21,855
10,000	1.75%	175	0.018	20,825	47,250	25,498	38,500	166,250	31,063	25,498
10,000	2.00%	200	0.020	23,800	54,000	29,140	44,000	190,000	35,500	29,140
10,000	2.25%	225	0.023	26,775	60,750	32,783	49,500	213,750	39,938	32,783

* 3413 BTU = 1 kWh

** Energy values taken from Theoretical/Best Practice Energy Use in Metal Casting Operations Page 37 - Table 19 and Page 15 - Table 12

*** Gross tons of castings represents the gross cast tons of production before scrap

Figure 43 Table, taken from the guidebook estimating the energy savings resulting from yield improvements of the casting process.

The "*Energy and Environmental profile of the U.S. Aluminum Industry*" estimates that emissions from current aluminum melting and casting practices are ~0.9 lbs/ton for SOx, ~0.8 lbs/ton for NOx, and ~430 lbs/ton for CO2. The emissions for magnesium may be higher due to the use of SF_6 protective gas that is being slowly phased out.

7 Commercialization

The U.S. Geological Survey estimated that 110,000 tons of primary magnesium metal was produced throughout the world in 2010, which did not include the United States and China. The China Magnesium Association (CMA) reported that 654,000 tons of primary magnesium was produced in 2010. It is estimated that the U.S. produced approximately 45,000 tons of primary magnesium in 2010. Total 2010 production of primary magnesium in the world was approximately 809,000 tons (31).

Only a small but important fraction of this magnesium is used for casting. Magnesium alloy die castings produced for automotive use reached over 82,000 tons and are predicted to reach production levels of 250,000 tons by 2015 (5). In 2002, fuel savings due to lightweight aluminum and magnesium cast parts in automobiles were estimated to be over 719 million dollars (6). This energy savings has been the driving force for a renewed interest in lightweight alloy castings including magnesium. This interest is demonstrated, among other by the intent to establish 2013 a new Lightweight and Modern Metals Manufacturing Innovation (LM3I) Institute. The technical focus of the imminent LM3I includes magnesium alloys as a priority: "There are several metals manufacturing technologies that the DoD has interest in scaling up from MRL 4 to MRL 7, and into production (MRL 8-9). These include, but are not limited to, the manufacturing of low-cost and high performing metal components and assemblies for lightweight ground, aerospace, and maritime systems; applications utilizing advanced alloys (e.g., titanium-, aluminum- and **magnesium-based alloys** and processing."

The current project sets the stage for casting of porosity free, high integrity magnesium alloy castings. Activities to commercialize best magnesium casting practices have been initiated during the last phase of the project at Thompson Aluminum. Validation of computer simulation results described in this report will facilitate wider use of computer simulation software to predict the presence of porosity and modify the gating and risering system to eliminate it. The results of the project are disseminated among magnesium foundries in collaboration with the American Foundry Society to further promote the adoption of best practices.

8 Accomplishments

The results of the project have been disseminated through presentations at the regular meetings of the Magnesium Division of the American Foundry Society. Presentations on the subject matter were also made at the Annual Metalcasting Congress and published in the proceedings as "Shrinkage Behavior of AM50, AM60 and AZ91, Transactions of the American Foundry Society V 113 Paper 05-028(06) P 849 – 855.

The best practices developed as part of the project have been implemented and are used by commercial magnesium foundries involved in the project.

9 Conclusions

9.1 Conclusions

Plate and bar sand castings were made of three commonly used magnesium die casting alloys: AM50A, AM60A, and AZ91D. Various combinations of risers, chills, and tapers were added to the casting to influence the heat transfer profile and thus the formation of shrinkage porosity. It was found that gas porosity is a relatively small contributor to overall porosity in these alloys.

Risers were found to be an essential component in setting up the proper heat transfer profile, and thus the thermal gradients in magnesium alloy castings. The large size of the risers provides both a large pool of available liquid to help offset shrinkage, as well as a heat reservoir. Chills are an effective method of increasing the rate of heat transfer into the mold wall, and when placed correctly can help set up the proper gradients.

Directional solidification towards the riser should dominate over progressive solidification to ensure sound castings. The geometry of the solidification front determines which of these modes dominates. The geometry of the overall solidification front greatly depends on the thermal properties of the mold. This can be adjusted with strategically placed risers and chills. The thermal gradients in a casting will indicate the shape of the front, and thus the mode of solidification. These minimum gradients may be used in conjunction with casting simulation software such as MAGMA to predict soundness. This will help alleviate a major lack of functionality in current generation software and provide a powerful tool for mold and die design and optimization.

The minimum temperature gradients found in sound tapered plate castings was found to be 3.15°C/cm for AM50A, 3.16°C/cm for AM60A, and 2.15°C/cm for AZ91D. The minimum temperature gradients for sound bar castings were found to be 2.02°C/cm for AM50A, 1.99°C/cm for AM60A, and 1.97°C/cm for AZ91D. If these gradients are met or exceeded when an area of the casting reaches 50°C below the liquidus for the alloy, the casting will be free of shrinkage porosity in that area.

The cooling rates measured during casting magnesium alloys in a pre-heated step permanent mold ranged from 12°F/min in the three inches thick step to 200°F/min in the one inch step. The effect of the cooling rate on the grain size and the mechanical properties was noticeable but not substantial.

Grain refining with C_2Cl_6 had a marked effect on the grain size of the permanent mold step casting. It reduced it by 10-15% in AM50A and by a factor of six in AZ91E from 300 μm to around 55 μm. The mechanical properties of both permanent mold cast AZ91E and AM50A were improved by grain refinement. The most prominent increase was in the elongation of AM50A that more than doubled from 8% to 17%.

A Magma computer simulation of porosity was conducted for a commercial wheel casting. The simulation did not predict significant porosity in the wheel. The mechanical testing of tensile specimens excised from the wheel indeed confirmed good properties, in line with the specifications for this alloy. Evidence of minimal micro-porosity was detected in sections cut from the wheel and investigated under optical microscopy.

Predicting the porosity in the casting using a casting and solidification software is key in ensuring a porosity free casting. Best gating practices and modifications in the gating and risering of the casting need to be pursued until the porosity in the model is eliminated. This iterative procedure has a very good rate of success in reducing porosity.

10 Suggestions for Future Work

The most important step in any future work would be to find a bulk method for testing for porosity location. Possibilities for this include eddy current analysis or ultrasonic inspection. This ability would greatly enhance the accuracy with which porosity content could be quantified.

It would also be suggested to design experiments with the goal of further narrowing down the minimum thermal gradient required for soundness. Increasing the number of thermocouples would aid this effort greatly. Simulations and casting trials should be performed to correlate the simulations results with real foundry results.

A wider variety of casting geometries and feeding conditions should be studied to give these gradient results wider applicability. Such conditions include feeding through a reduced section, or castings with unfavorable tapers. Thin section castings should be studied to determine the applicability, if any, of these minimum gradients.

11 Appendix

11.1 Appendix I

Table 13 ASTM composition specification for AM50A. (2)

Element	Wt. %	Element	Wt. %	Element	Wt. %
Al	4.4 - 5.4	Mg	94.8	Other, each	Max 0.02
Cu	Max 0.01	Mn	0.26 - 0.6	Si	Max 0.1
Fe	Max 0.004	Ni	Max 0.002	Zn	Max 0.22

Table 14 ASTM composition specification for AM60A. (2)

Element	Wt. %
Al	5.5 - 6.5
Cu	Max 0.35
Mg	94
Mn	0.13 - 0.6
Ni	Max 0.03
Si	Max 0.5
Zn	Max 0.22

Table 15 ASTM composition specification for AZ91D. (2)

Element	Wt. %
Al	8.3 - 9.7
Cu	Max 0.03
Fe	Max 0.005
Mg	90
Mn	Min 0.13
Ni	Max 0.002
Si	Max 0.1
Zn	0.35 – 1

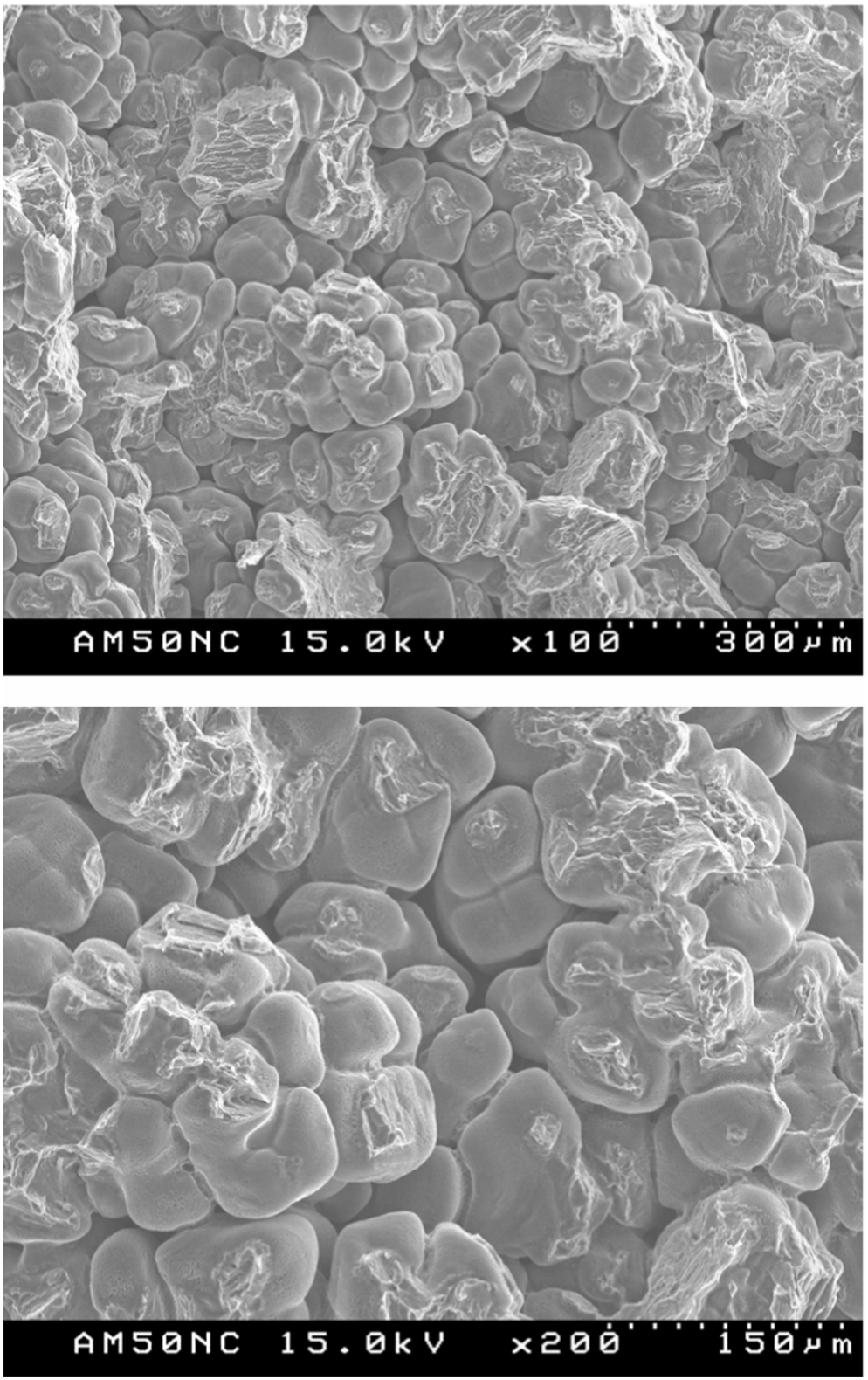

Figure 44 SEM pictures of the tensile bar fracture surface from an unchilled AM50 bar casting.

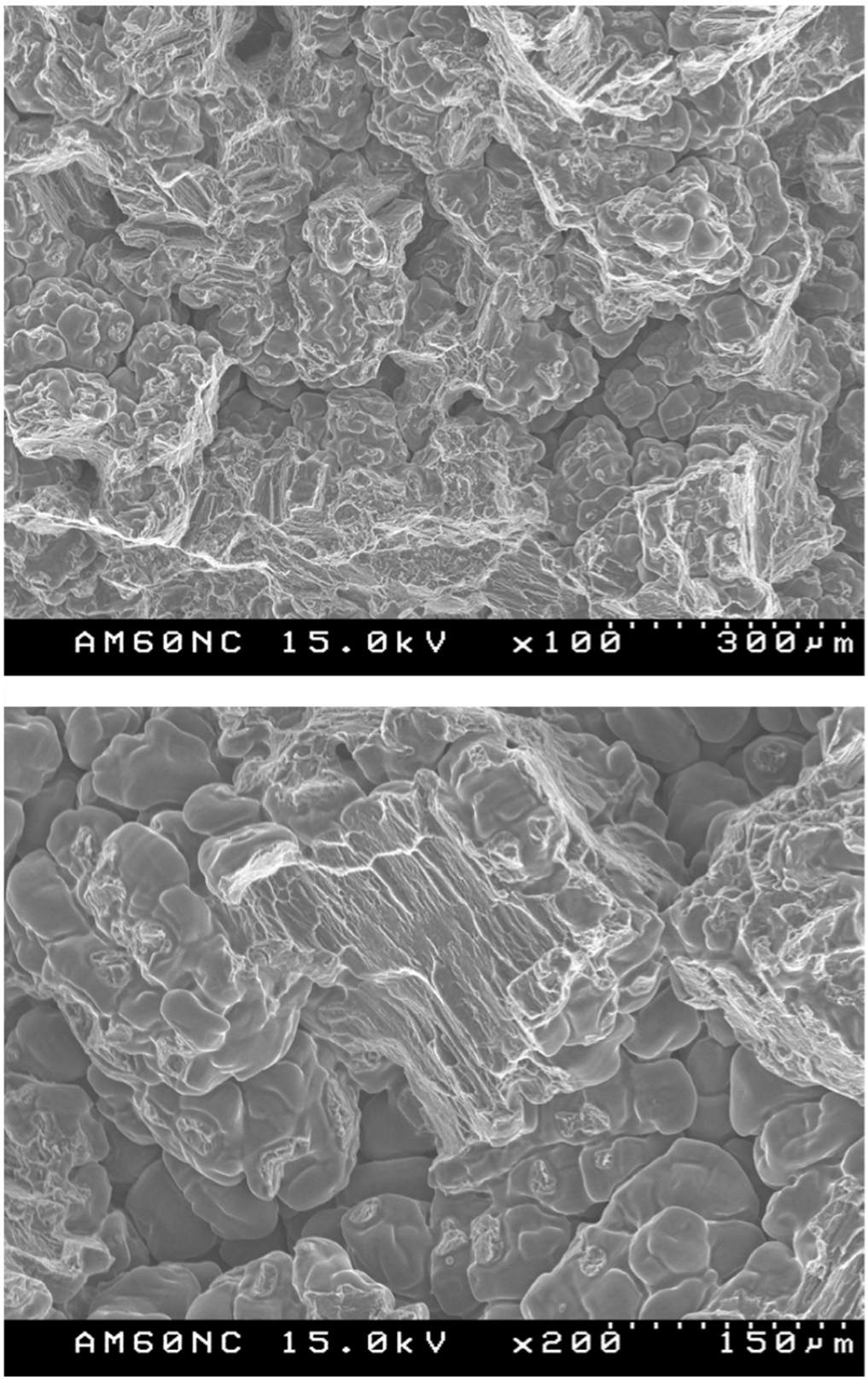

Figure 45 SEM pictures of the tensile bar fracture surface from an unchilled AM60 bar casting.

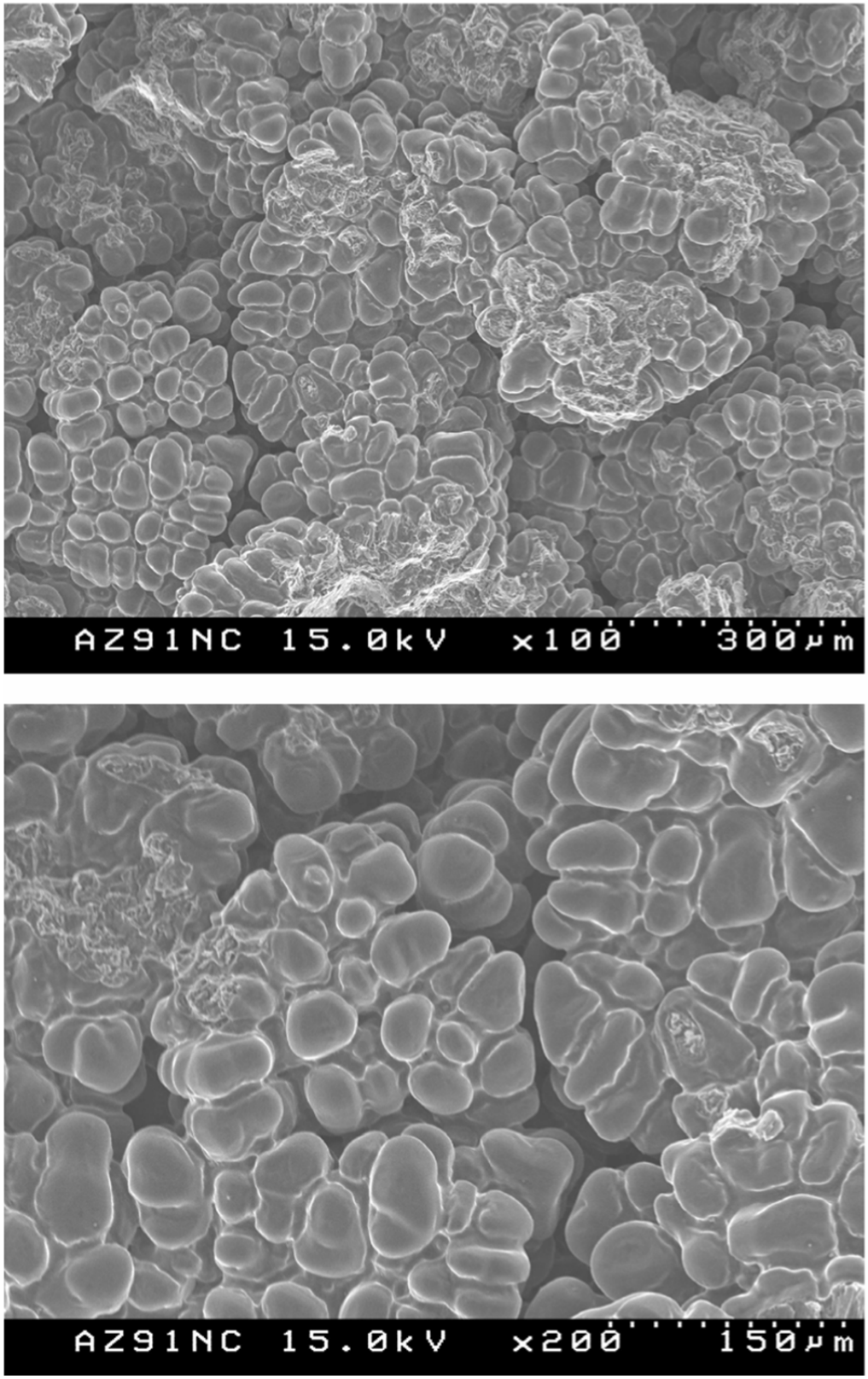

Figure 46 SEM pictures of the tensile bar fracture surface from an unchilled AZ91 bar casting.

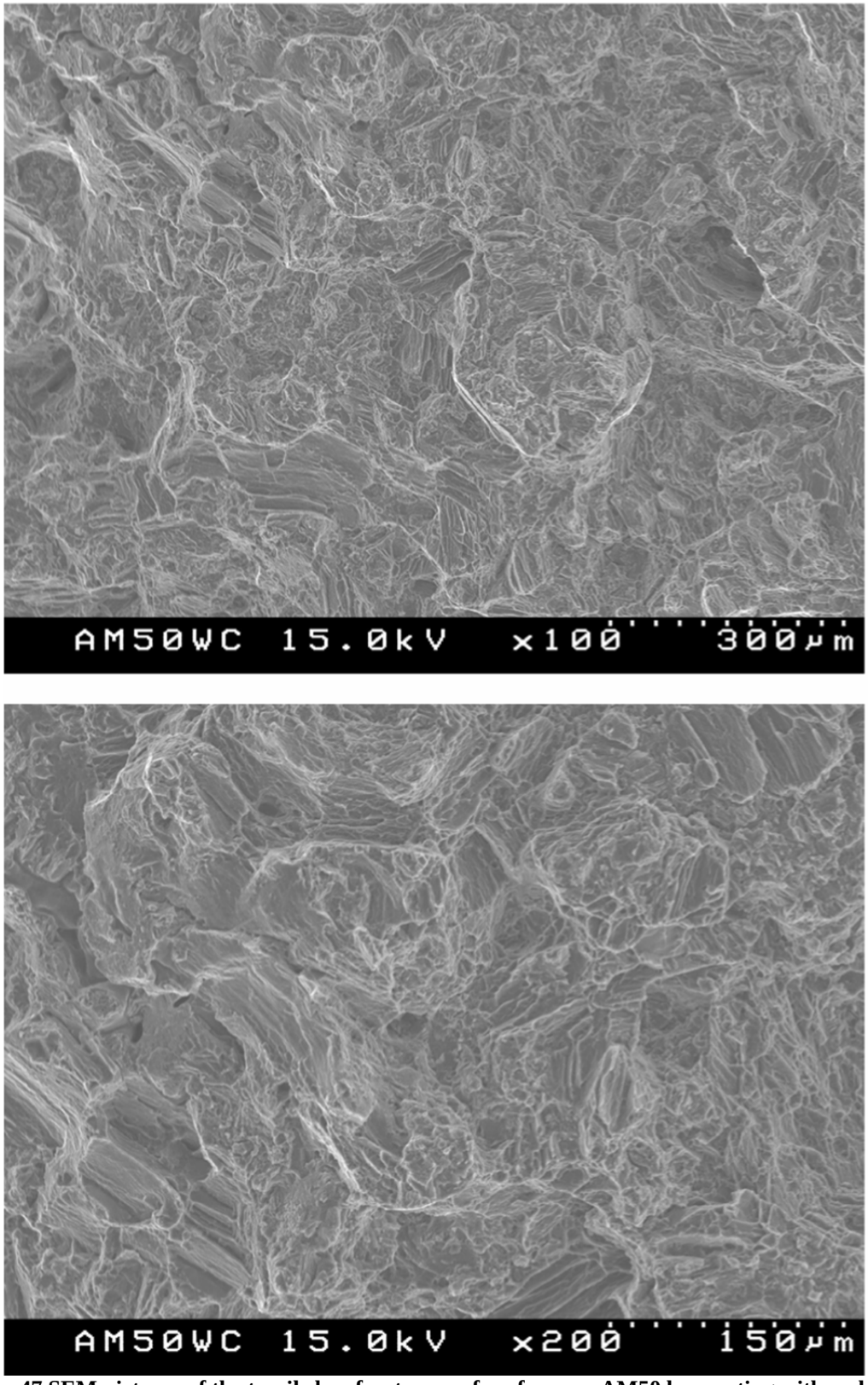

Figure 47 SEM pictures of the tensile bar fracture surface from an AM50 bar casting with end chill.

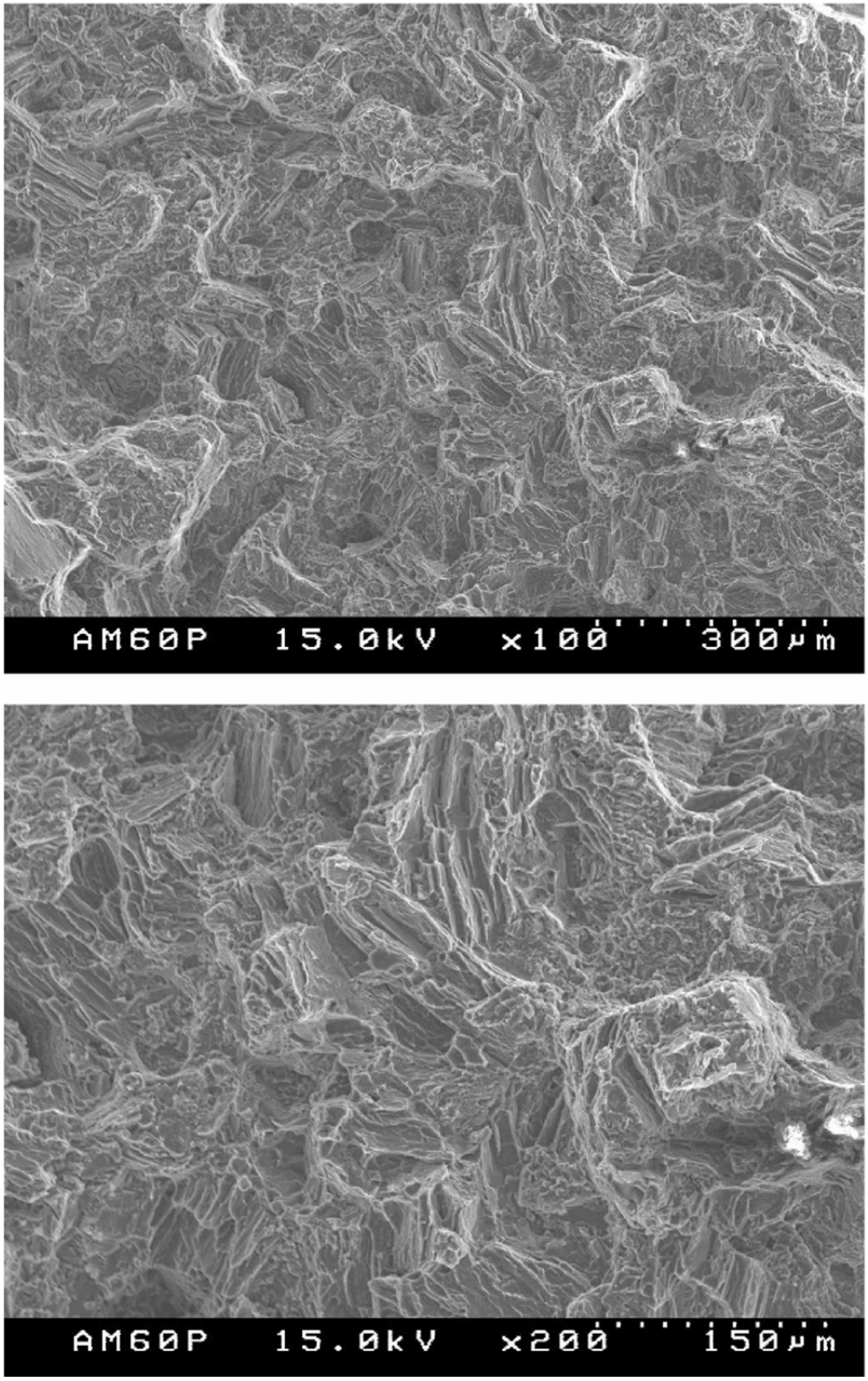

Figure 48 SEM pictures of the tensile bar fracture surface from an AM60 bar casting with end chill.

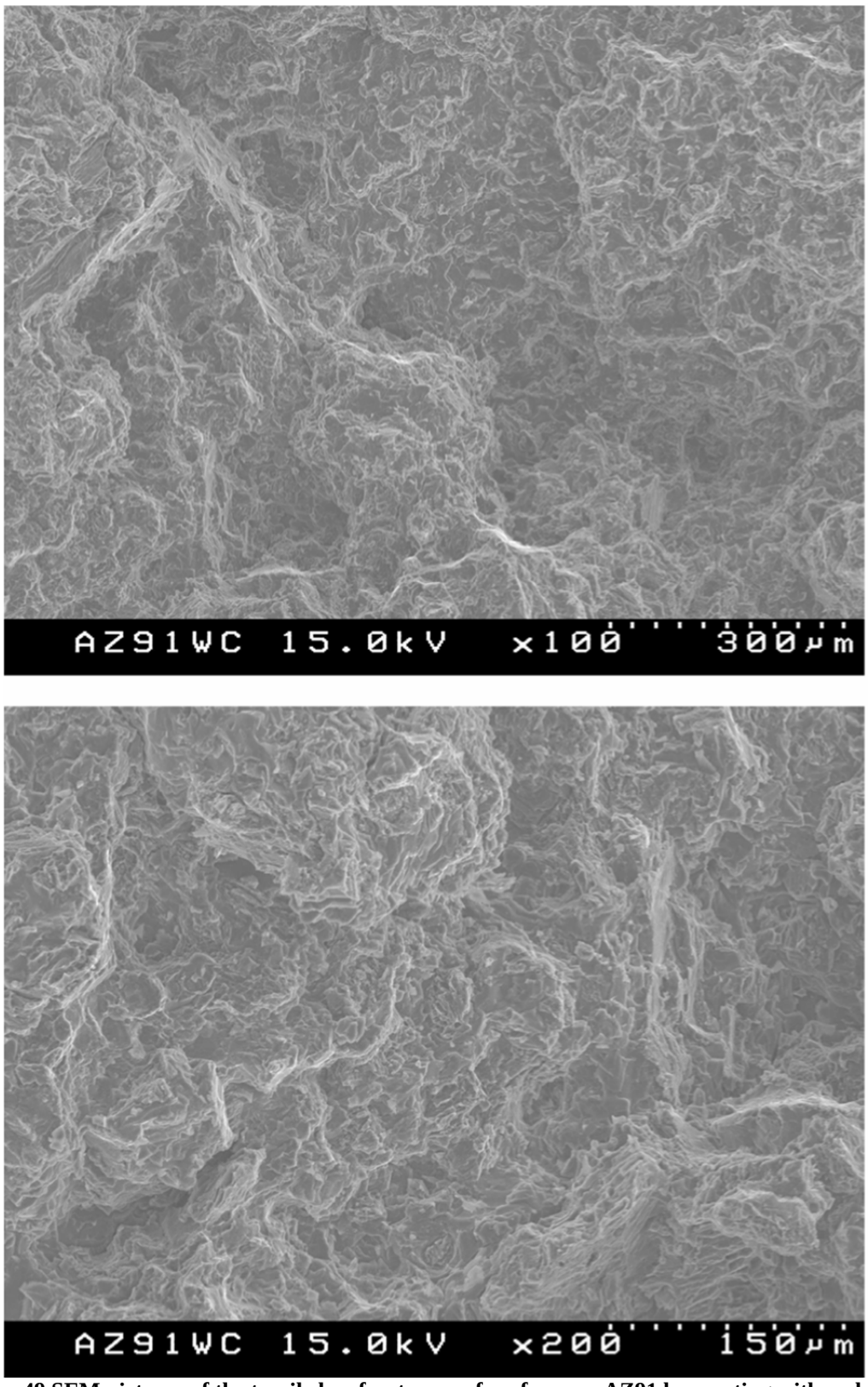

Figure 49 SEM pictures of the tensile bar fracture surface from an AZ91 bar casting with end chill.

11.2 Appendix II

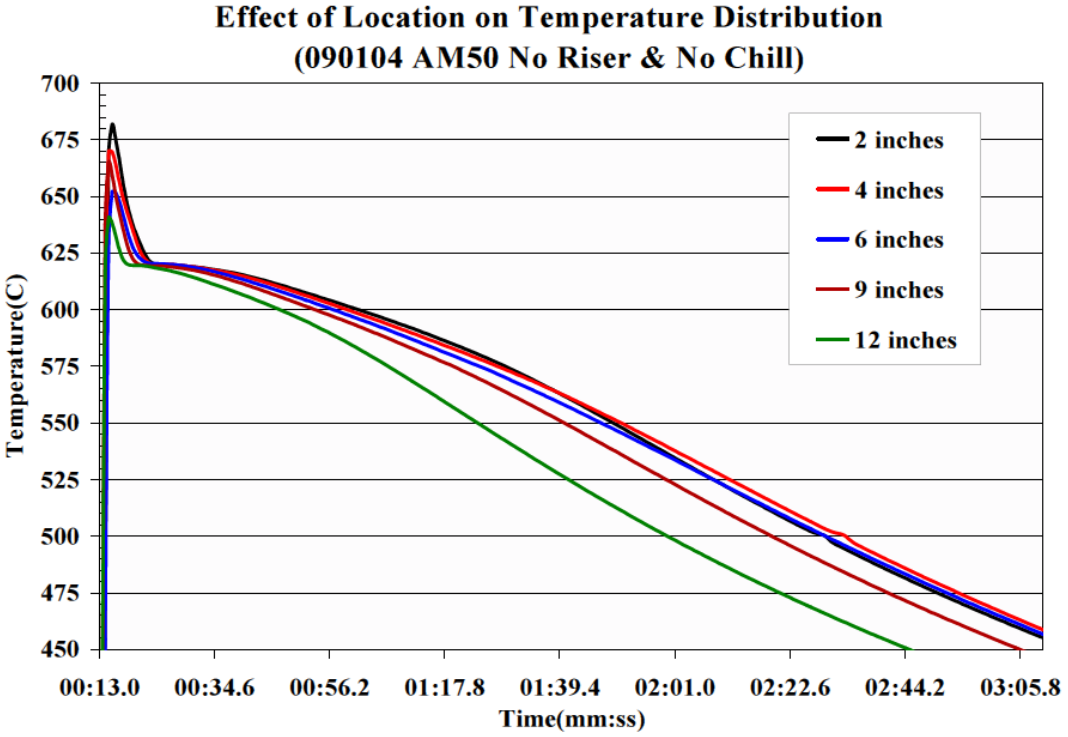

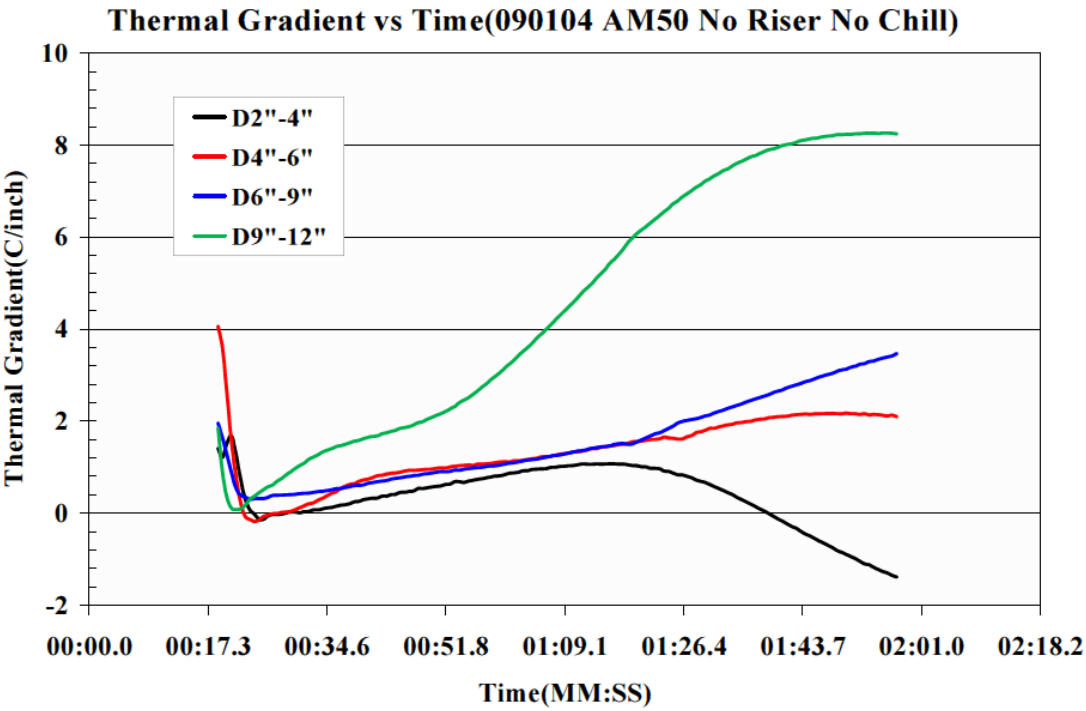

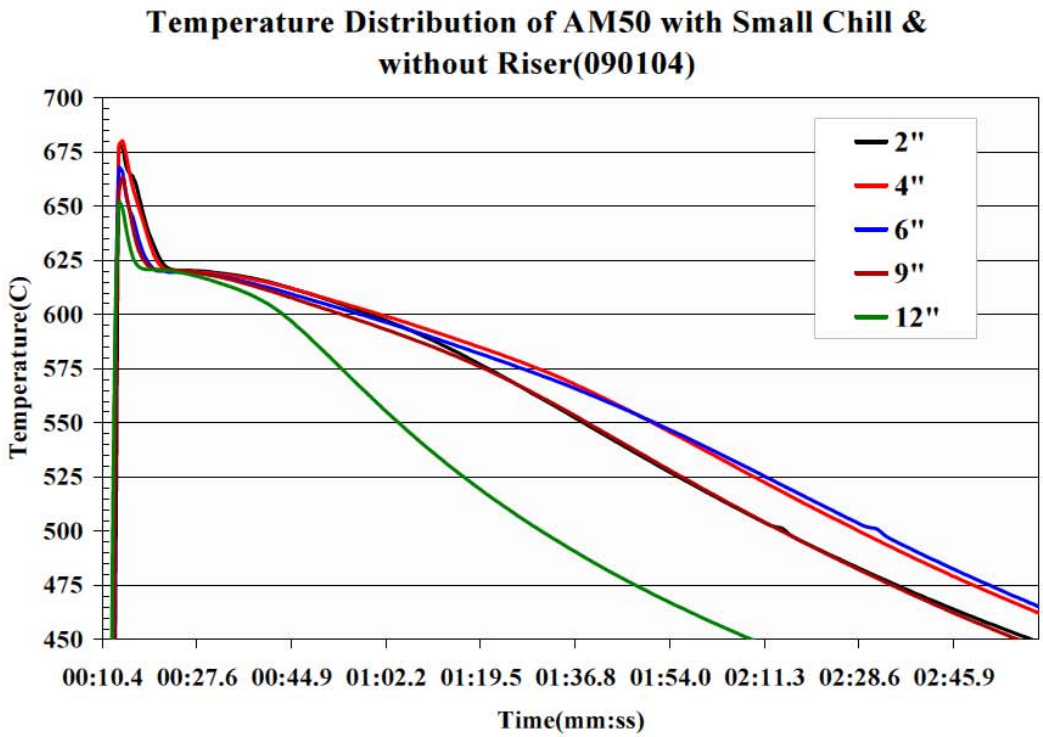
Temperature Distribution of AM50 with Small Chill & without Riser(090104)
700
675
650
625
600
575
550
525
500
475
450
Temperature(C)
2"
4"
6"
9"
12"
00:10.4 00:27.6 00:44.9 01:02.2 01:19.5 01:36.8 01:54.0 02:11.3 02:28.6 02:45.9
Time(mm:ss)

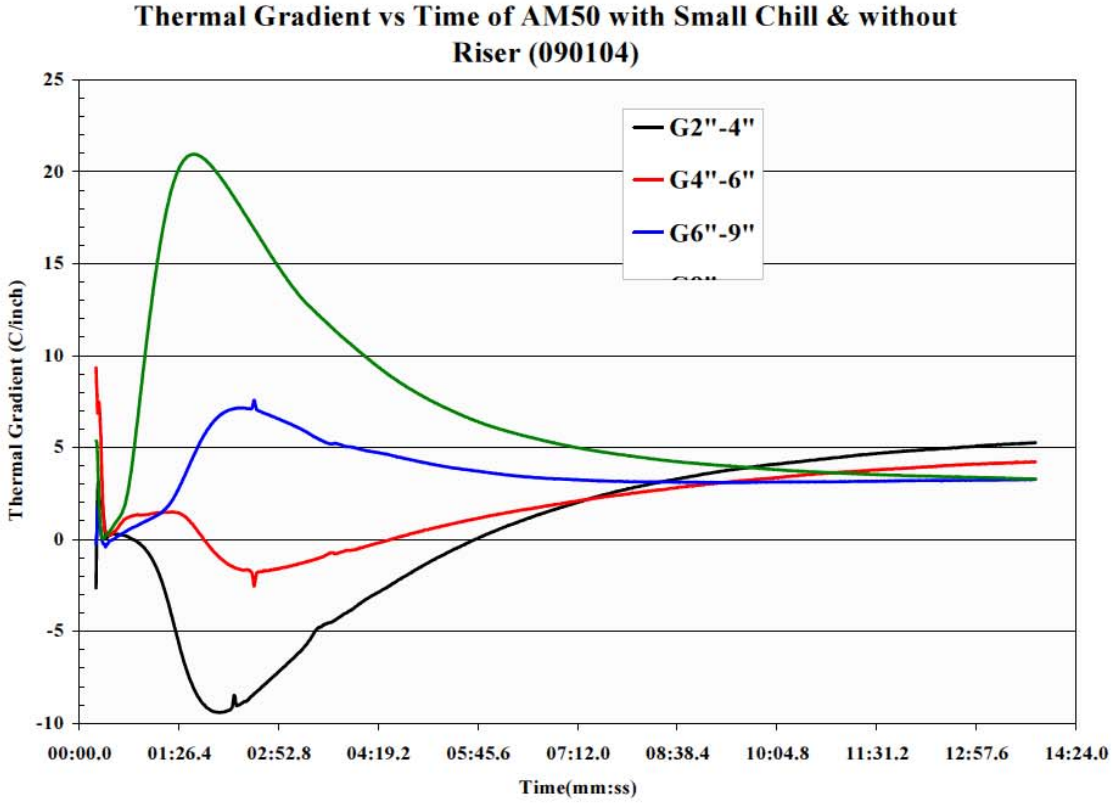
Thermal Gradient vs Time of AM50 with Small Chill & without Riser (090104)
25
20
15
10
5
0
-5
-10
Thermal Gradient (C/inch)
G2"-4"
G4"-6"
G6"-9"
00:00.0 01:26.4 02:52.8 04:19.2 05:45.6 07:12.0 08:38.4 10:04.8 11:31.2 12:57.6 14:24.0
Time(mm:ss)

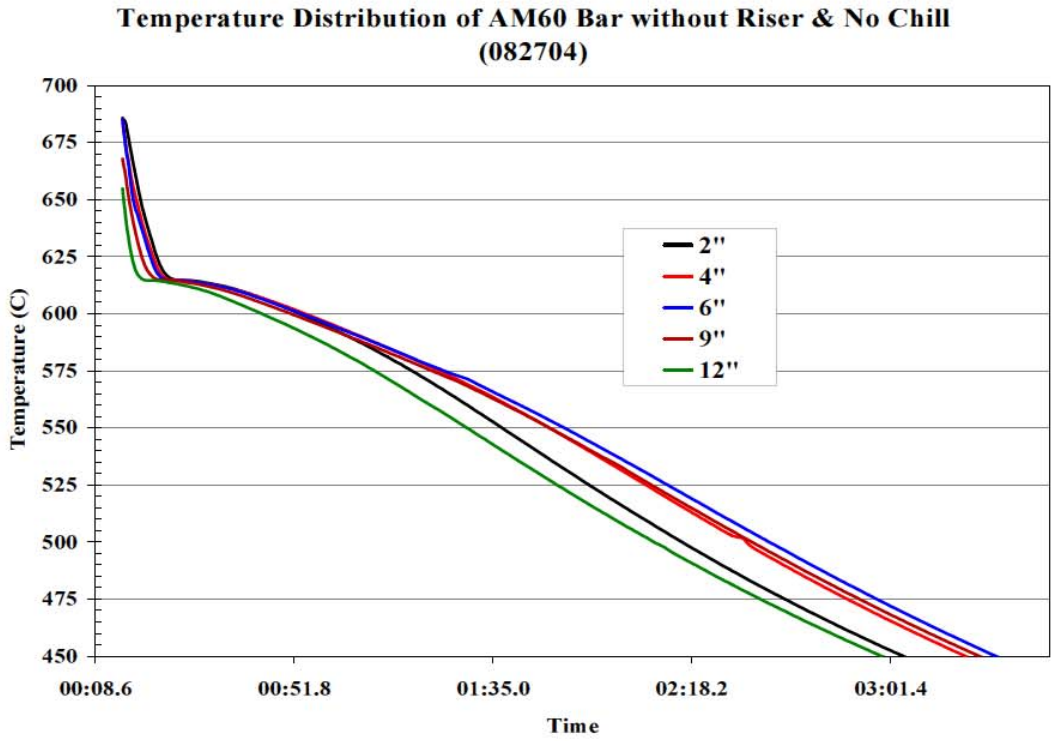
Temperature Distribution of AM60 Bar without Riser & No Chill
(082704)
Temperature (C)
700
675
650
625
600
575
550
525
500
475
450
00:08.6
00:51.8
01:35.0
02:18.2
03:01.4
Time
2"
4"
6"
9"
12"

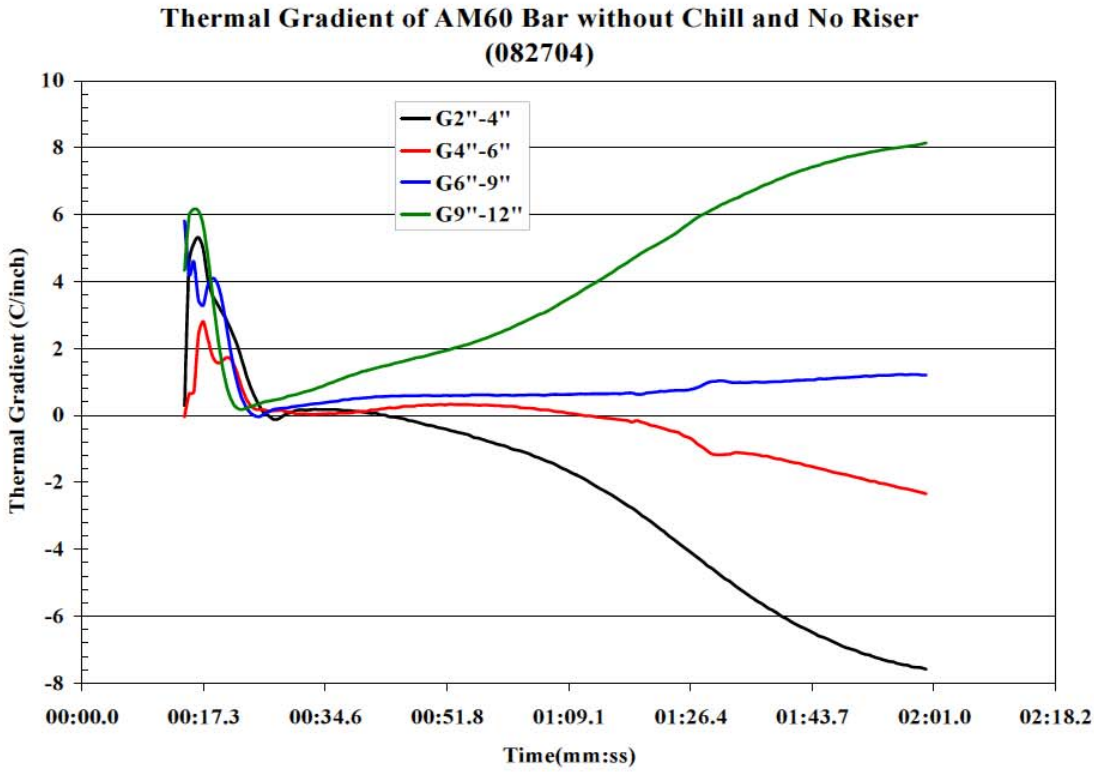
Thermal Gradient of AM60 Bar without Chill and No Riser
(082704)
Thermal Gradient (C/inch)
10
8
6
4
2
0
-2
-4
-6
-8
00:00.0
00:17.3
00:34.6
00:51.8
01:09.1
01:26.4
01:43.7
02:01.0
02:18.2
Time(mm:ss)
G2"-4"
G4"-6"
G6"-9"
G9"-12"

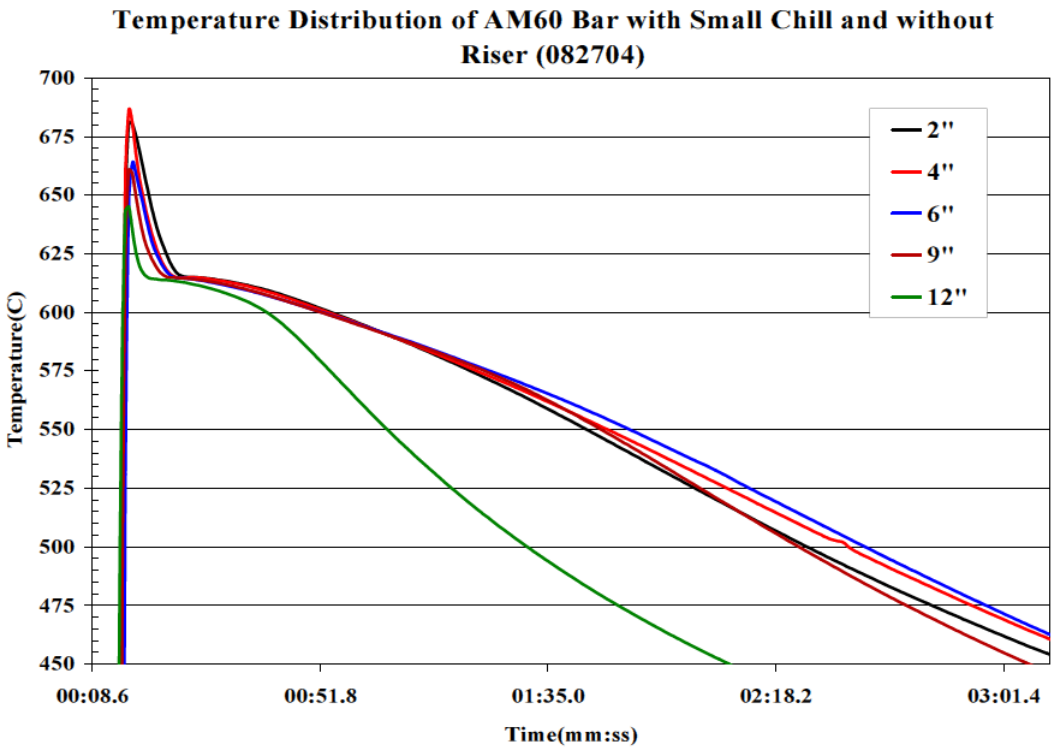
Temperature Distribution of AM60 Bar with Small Chill and without Riser (082704)
Temperature(C)
700
675
650
625
600
575
550
525
500
475
450
00:08.6
00:51.8
01:35.0
02:18.2
03:01.4
Time(mm:ss)
2"
4"
6"
9"
12"

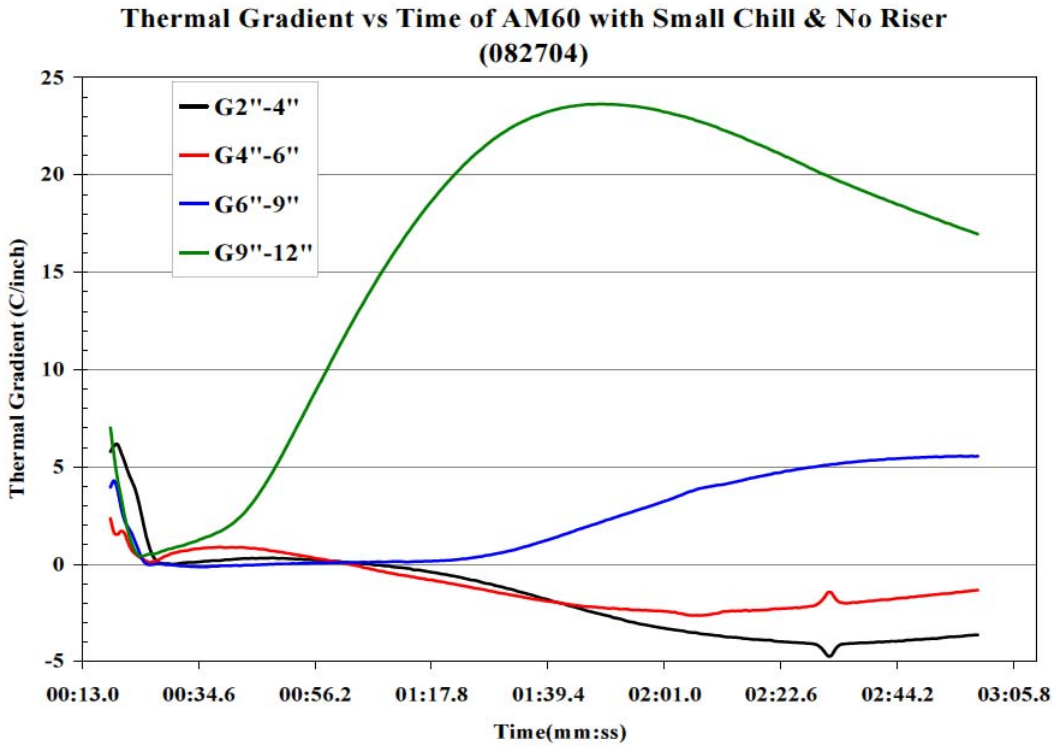
Thermal Gradient vs Time of AM60 with Small Chill & No Riser (082704)
Thermal Gradient (C/inch)
25
20
15
10
5
0
-5
00:13.0
00:34.6
00:56.2
01:17.8
01:39.4
02:01.0
02:22.6
02:44.2
03:05.8
Time(mm:ss)
G2"-4"
G4"-6"
G6"-9"
G9"-12"

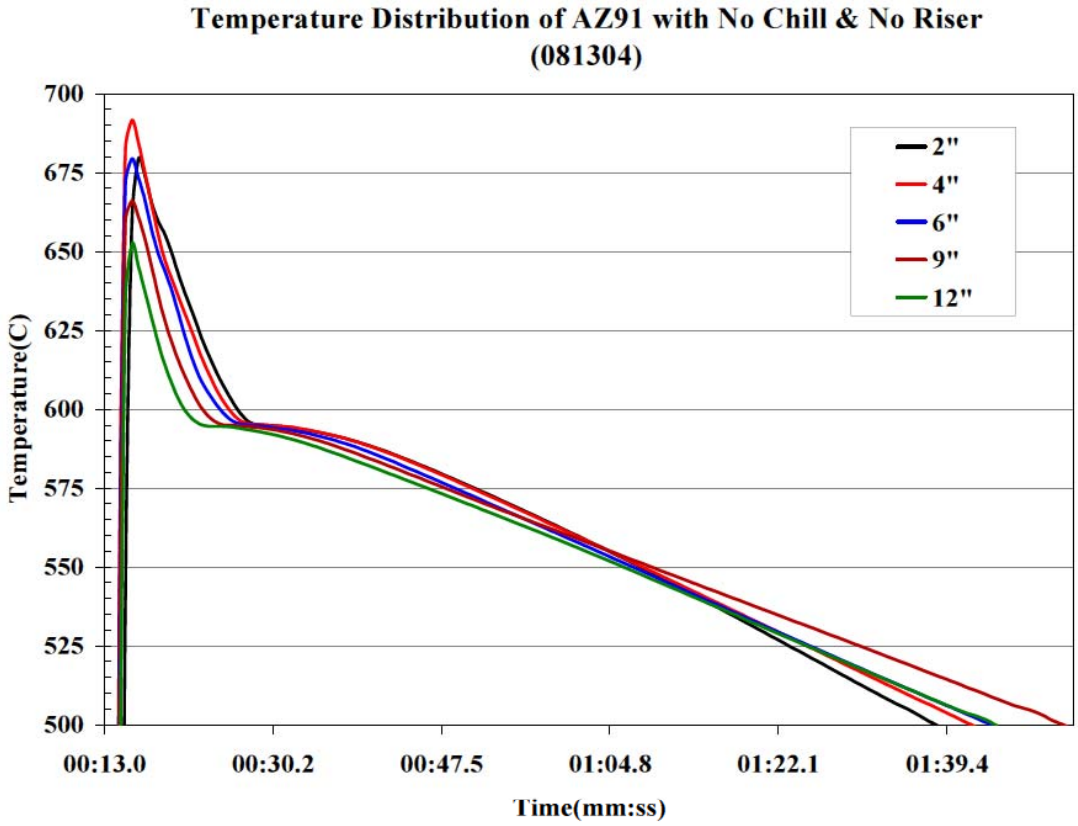
Temperature Distribution of AZ91 with No Chill & No Riser (081304)
700
675
650
625
600
575
550
525
500
Temperature(C)
2"
4"
6"
9"
12"
00:13.0
00:30.2
00:47.5
01:04.8
01:22.1
01:39.4
Time(mm:ss)

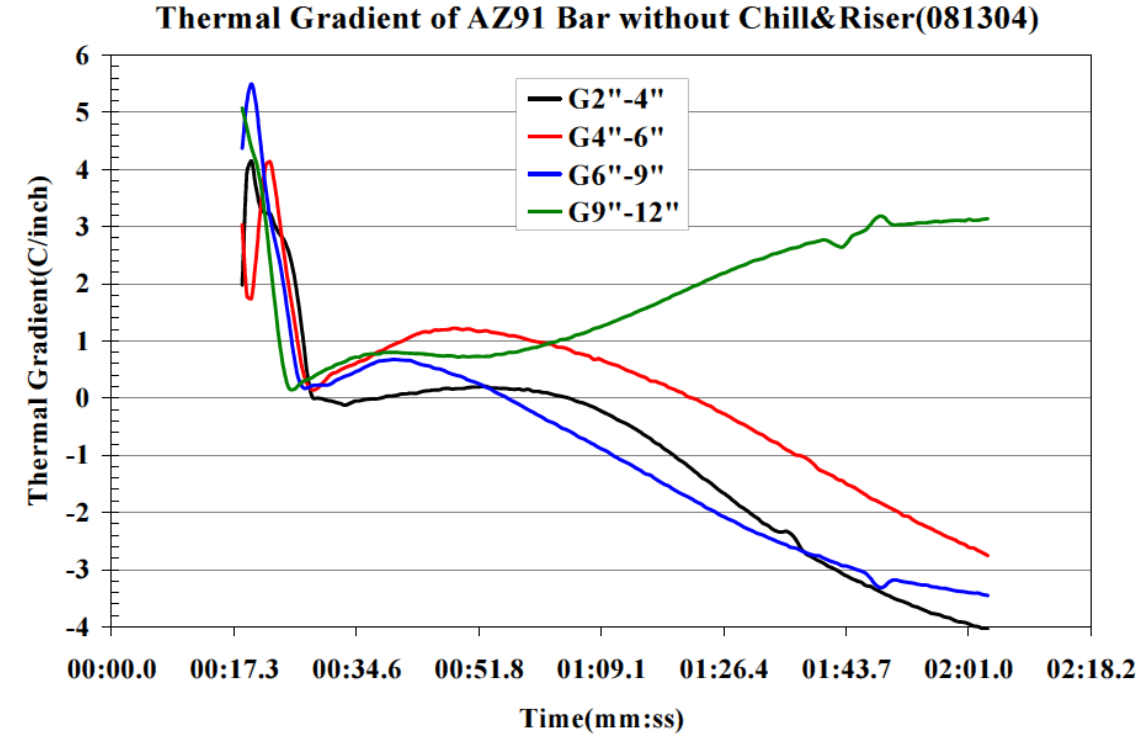
Thermal Gradient of AZ91 Bar without Chill&Riser(081304)
6
5
4
3
2
1
0
-1
-2
-3
-4
Thermal Gradient(C/inch)
G2"-4"
G4"-6"
G6"-9"
G9"-12"
00:00.0
00:17.3
00:34.6
00:51.8
01:09.1
01:26.4
01:43.7
02:01.0
02:18.2
Time(mm:ss)

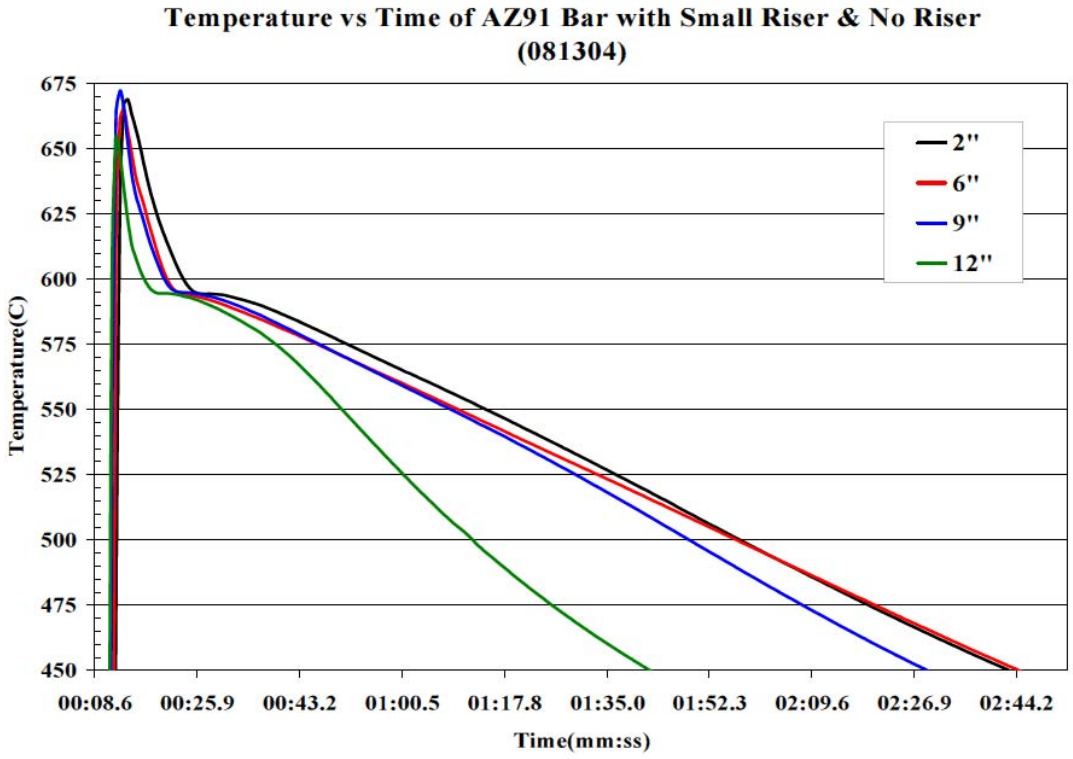
Temperature vs Time of AZ91 Bar with Small Riser & No Riser
(081304)
675
650
625
600
575
550
525
500
475
450
Temperature(C)
2"
6"
9"
12"
00:08.6
00:25.9
00:43.2
01:00.5
01:17.8
01:35.0
01:52.3
02:09.6
02:26.9
02:44.2
Time(mm:ss)

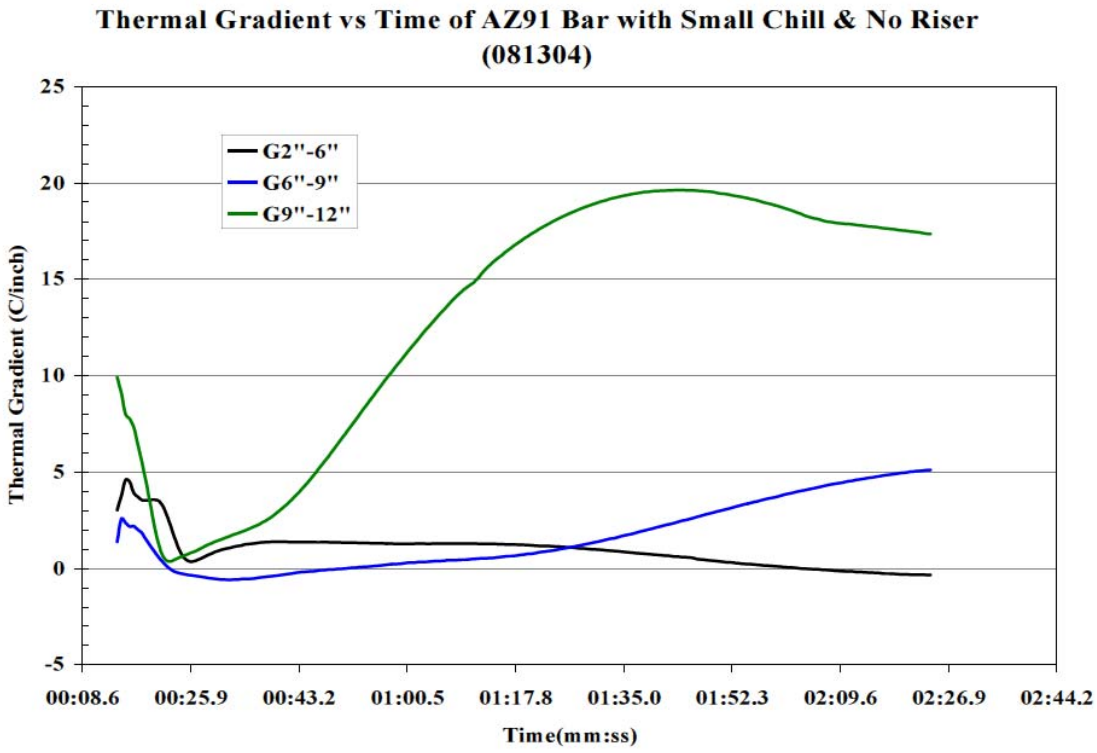
Thermal Gradient vs Time of AZ91 Bar with Small Chill & No Riser
(081304)
25
20
15
10
5
0
-5
Thermal Gradient (C/inch)
G2"-6"
G6"-9"
G9"-12"
00:08.6
00:25.9
00:43.2
01:00.5
01:17.8
01:35.0
01:52.3
02:09.6
02:26.9
02:44.2
Time(mm:ss)

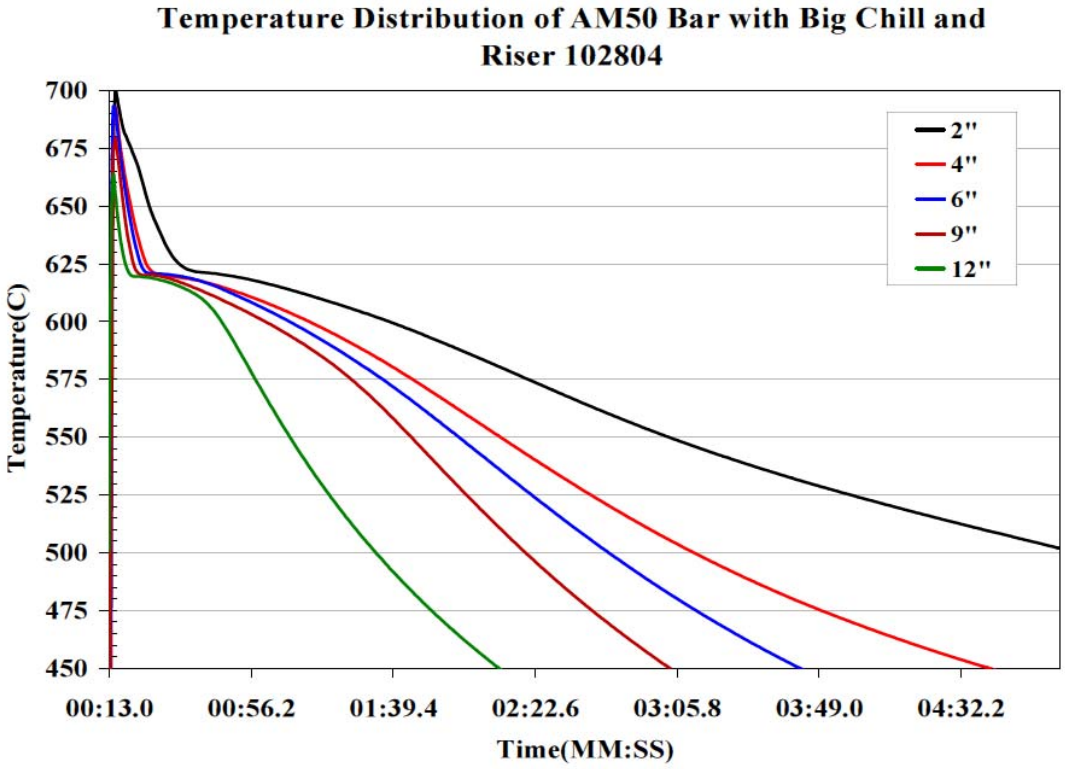
Temperature Distribution of AM50 Bar with Big Chill and Riser 102804
700
675
650
625
600
575
550
525
500
475
450
Temperature(C)
2"
4"
6"
9"
12"
00:13.0
00:56.2
01:39.4
02:22.6
03:05.8
03:49.0
04:32.2
Time(MM:SS)

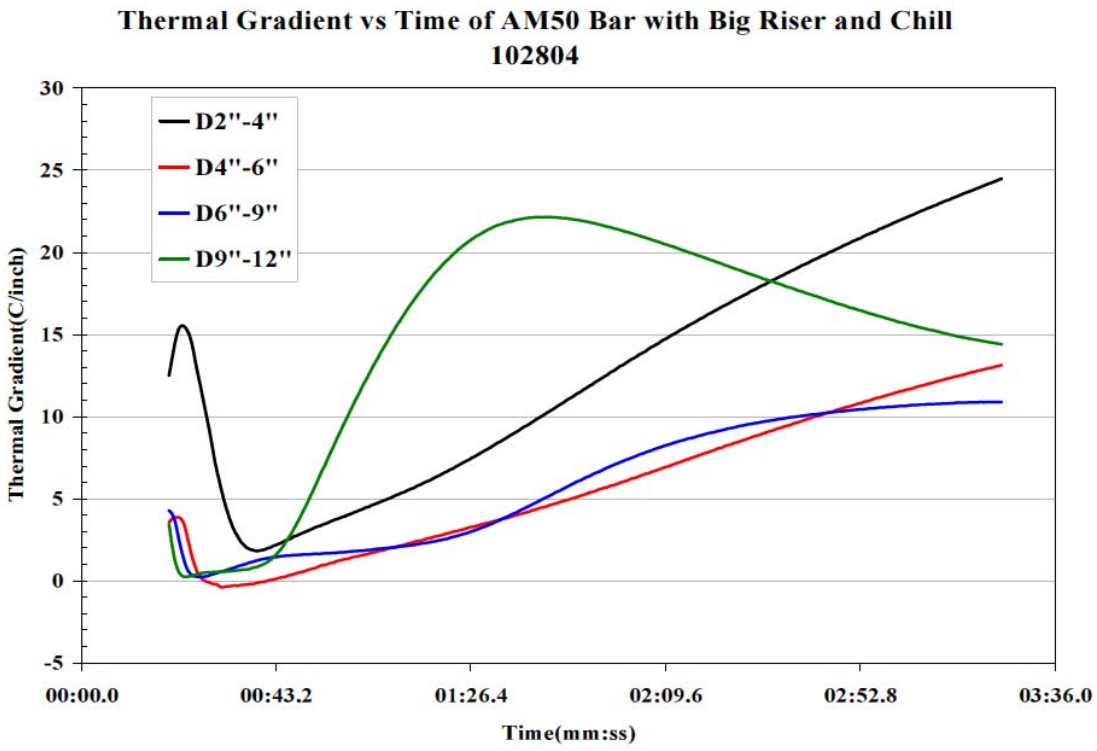
Thermal Gradient vs Time of AM50 Bar with Big Riser and Chill 102804
30
25
20
15
10
5
0
-5
Thermal Gradient(C/inch)
D2"-4"
D4"-6"
D6"-9"
D9"-12"
00:00.0
00:43.2
01:26.4
02:09.6
02:52.8
03:36.0
Time(mm:ss)

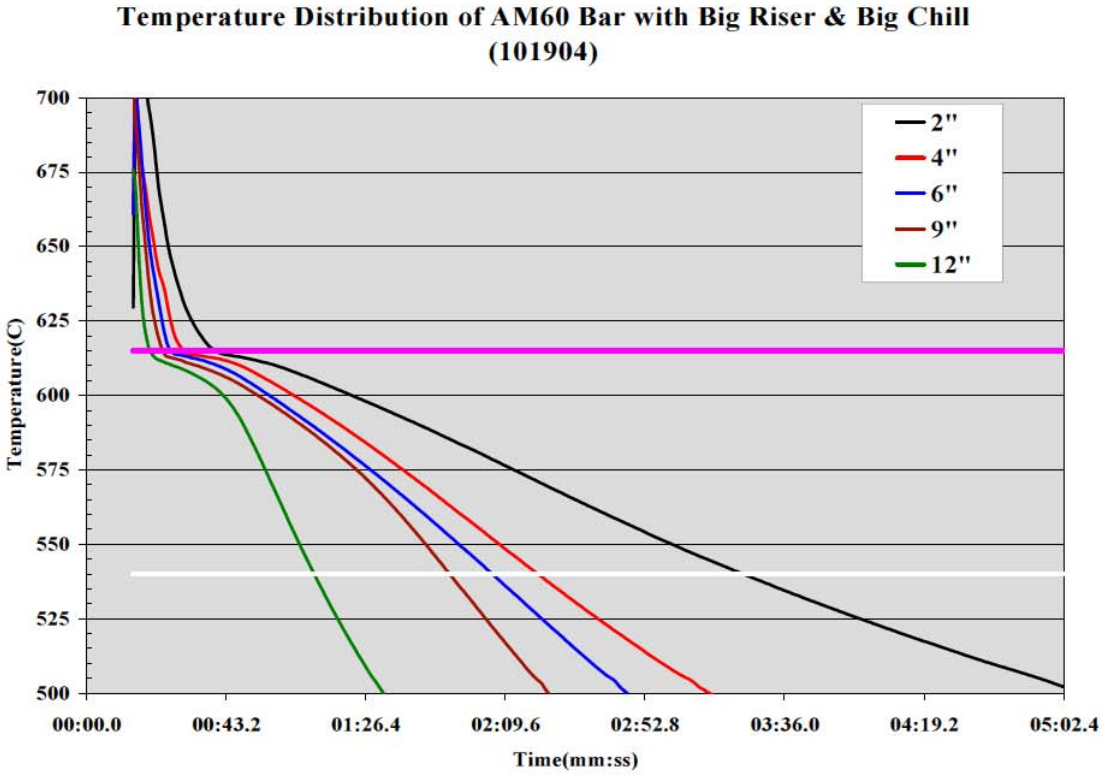
Temperature Distribution of AM60 Bar with Big Riser & Big Chill (101904)
Temperature(C)
700
675
650
625
600
575
550
525
500
00:00.0
00:43.2
01:26.4
02:09.6
02:52.8
03:36.0
04:19.2
05:02.4
Time(mm:ss)
2"
4"
6"
9"
12"

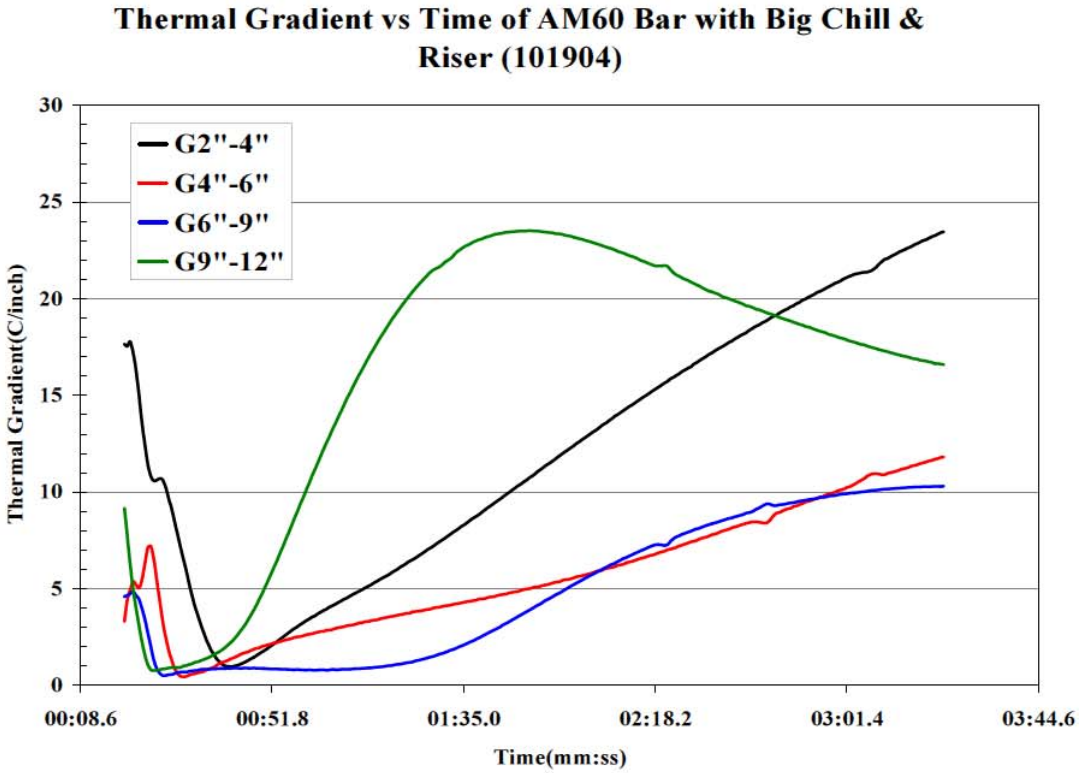
Thermal Gradient vs Time of AM60 Bar with Big Chill & Riser (101904)
Thermal Gradient(C/inch)
30
25
20
15
10
5
0
00:08.6
00:51.8
01:35.0
02:18.2
03:01.4
03:44.6
Time(mm:ss)
G2"-4"
G4"-6"
G6"-9"
G9"-12"

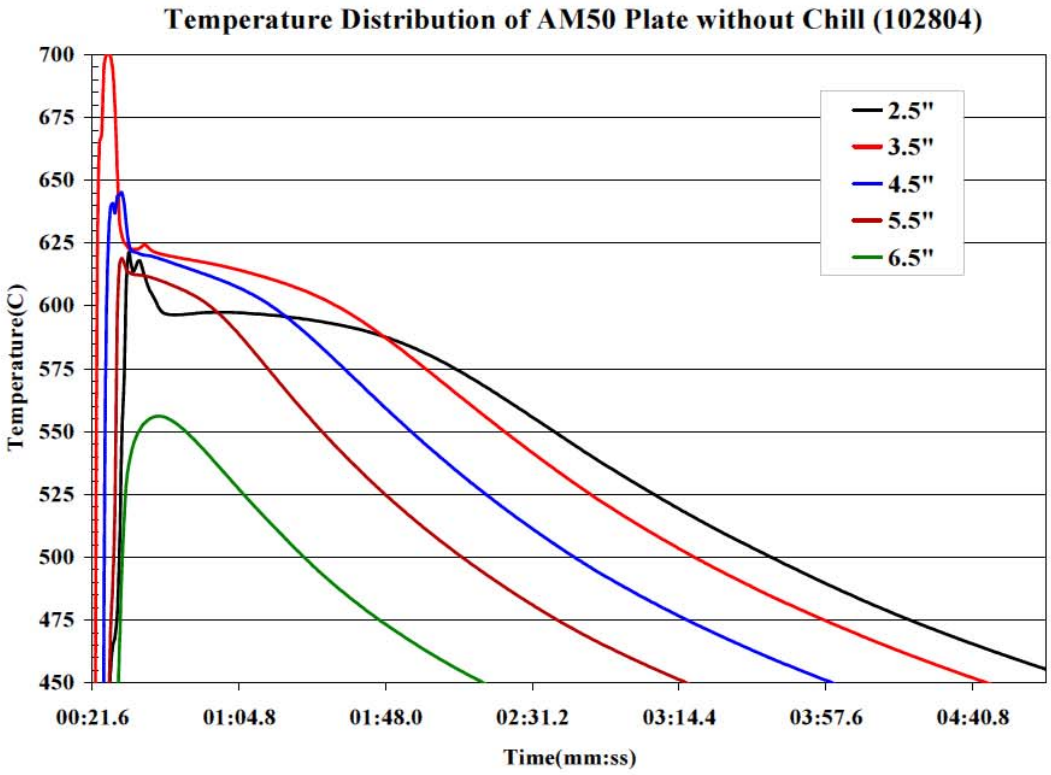
Temperature Distribution of AM50 Plate without Chill (102804)
700
675
650
625
600
575
550
525
500
475
450
Temperature(C)
2.5"
3.5"
4.5"
5.5"
6.5"
00:21.6
01:04.8
01:48.0
02:31.2
03:14.4
03:57.6
04:40.8
Time(mm:ss)

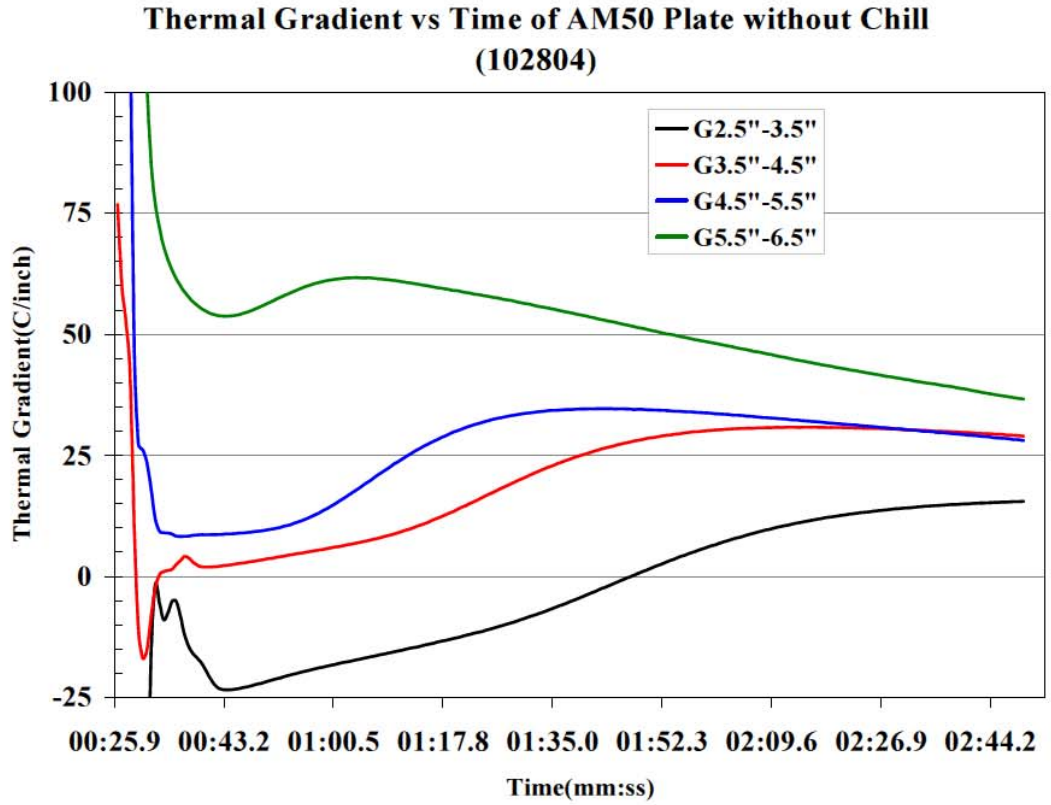
Thermal Gradient vs Time of AM50 Plate without Chill (102804)
100
75
50
25
0
-25
Thermal Gradient(C/inch)
G2.5"-3.5"
G3.5"-4.5"
G4.5"-5.5"
G5.5"-6.5"
00:25.9
00:43.2
01:00.5
01:17.8
01:35.0
01:52.3
02:09.6
02:26.9
02:44.2
Time(mm:ss)

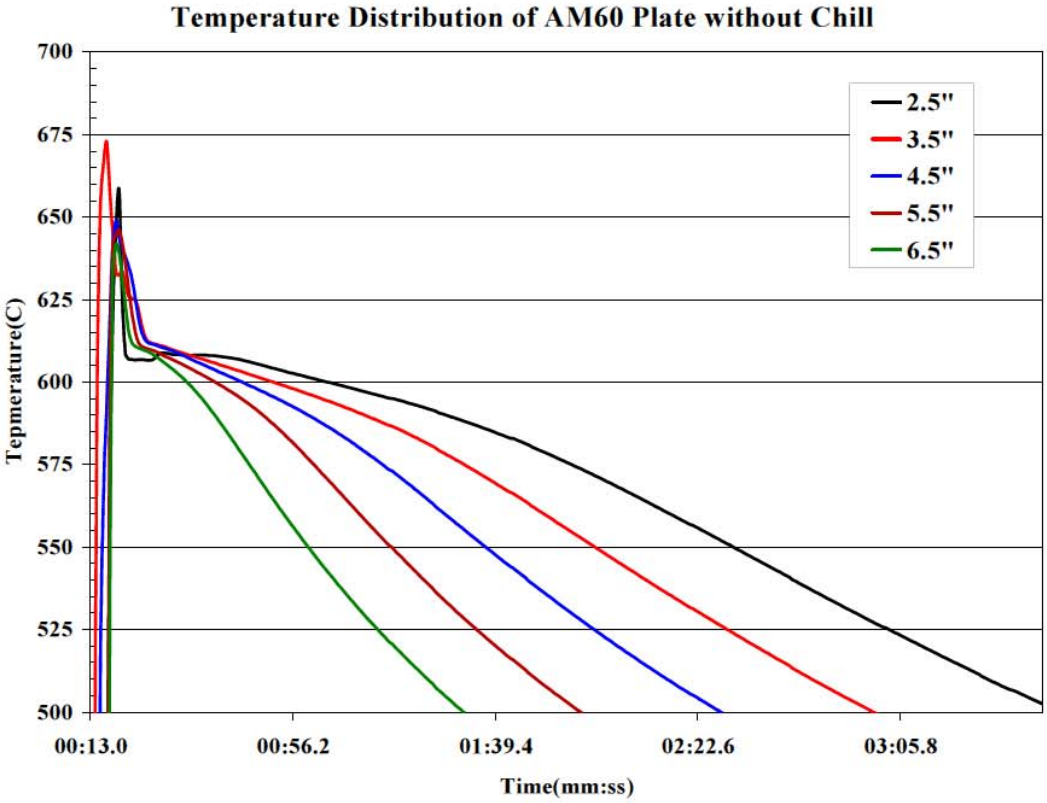
Temperature Distribution of AM60 Plate without Chill
700
675
650
625
600
575
550
525
500
Tepmerature(C)
00:13.0
00:56.2
01:39.4
02:22.6
03:05.8
Time(mm:ss)
2.5"
3.5"
4.5"
5.5"
6.5"

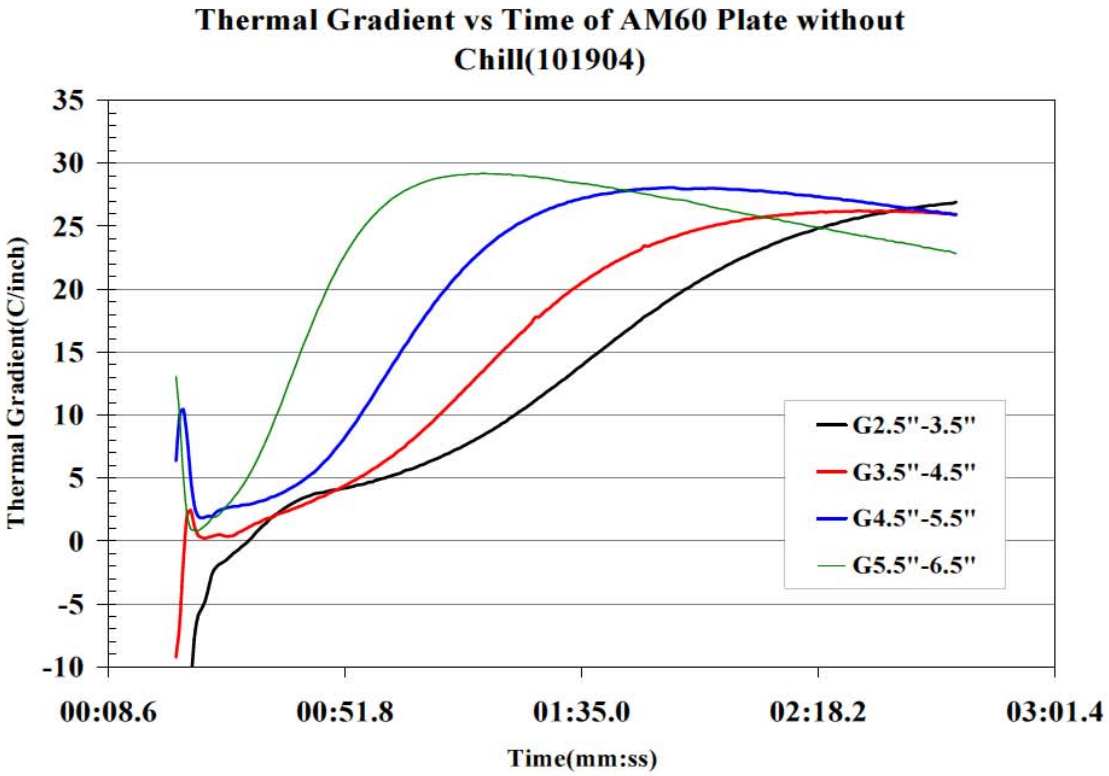
Thermal Gradient vs Time of AM60 Plate without Chill(101904)
35
30
25
20
15
10
5
0
-5
-10
Thermal Gradient(C/inch)
00:08.6
00:51.8
01:35.0
02:18.2
03:01.4
Time(mm:ss)
G2.5"-3.5"
G3.5"-4.5"
G4.5"-5.5"
G5.5"-6.5"

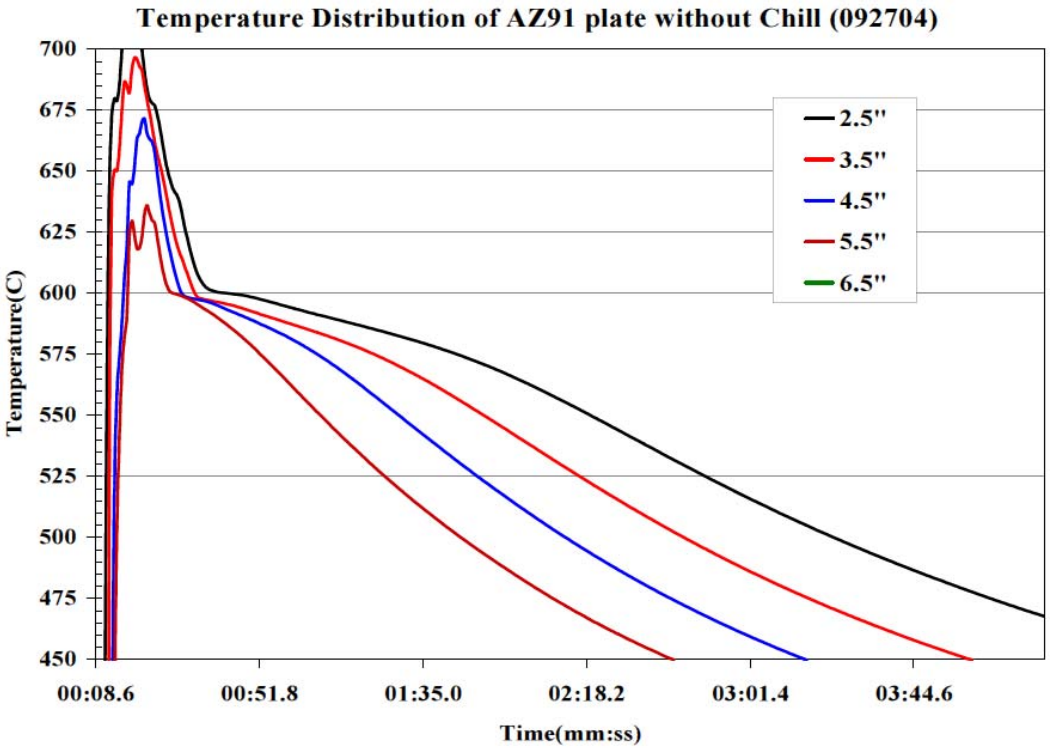
Temperature Distribution of AZ91 plate without Chill (092704)
Temperature(C)
700
675
650
625
600
575
550
525
500
475
450
00:08.6
00:51.8
01:35.0
02:18.2
03:01.4
03:44.6
Time(mm:ss)
2.5"
3.5"
4.5"
5.5"
6.5"

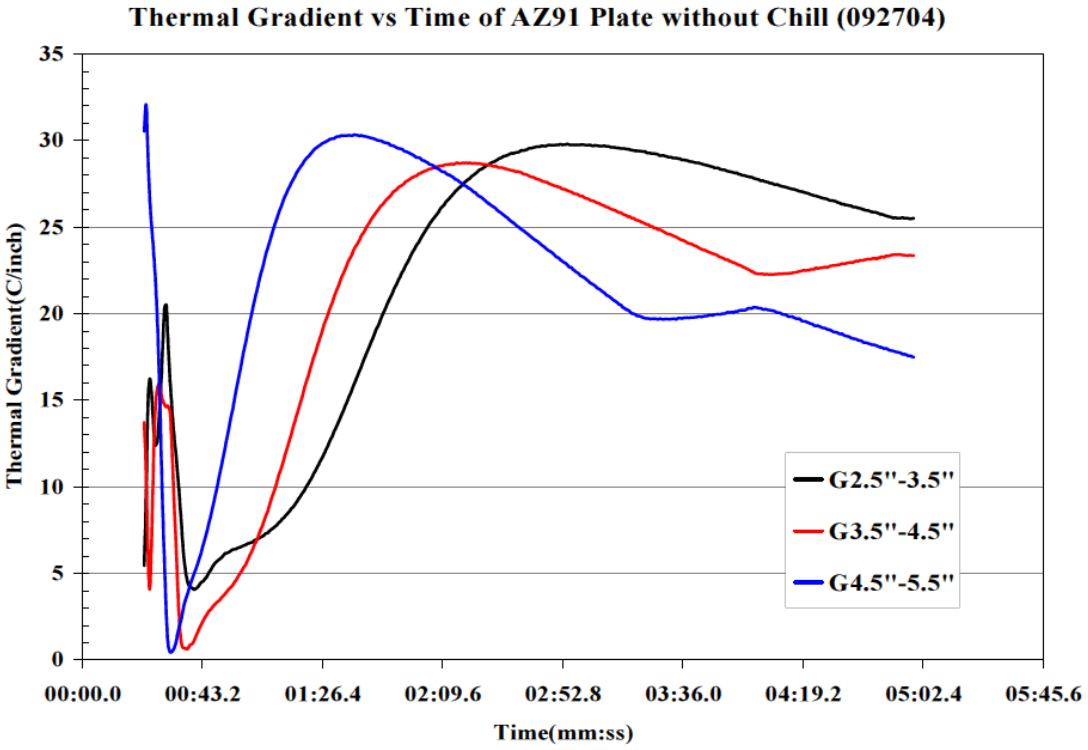
Thermal Gradient vs Time of AZ91 Plate without Chill (092704)
Thermal Gradient(C/inch)
35
30
25
20
15
10
5
0
00:00.0
00:43.2
01:26.4
02:09.6
02:52.8
03:36.0
04:19.2
05:02.4
05:45.6
Time(mm:ss)
G2.5"-3.5"
G3.5"-4.5"
G4.5"-5.5"

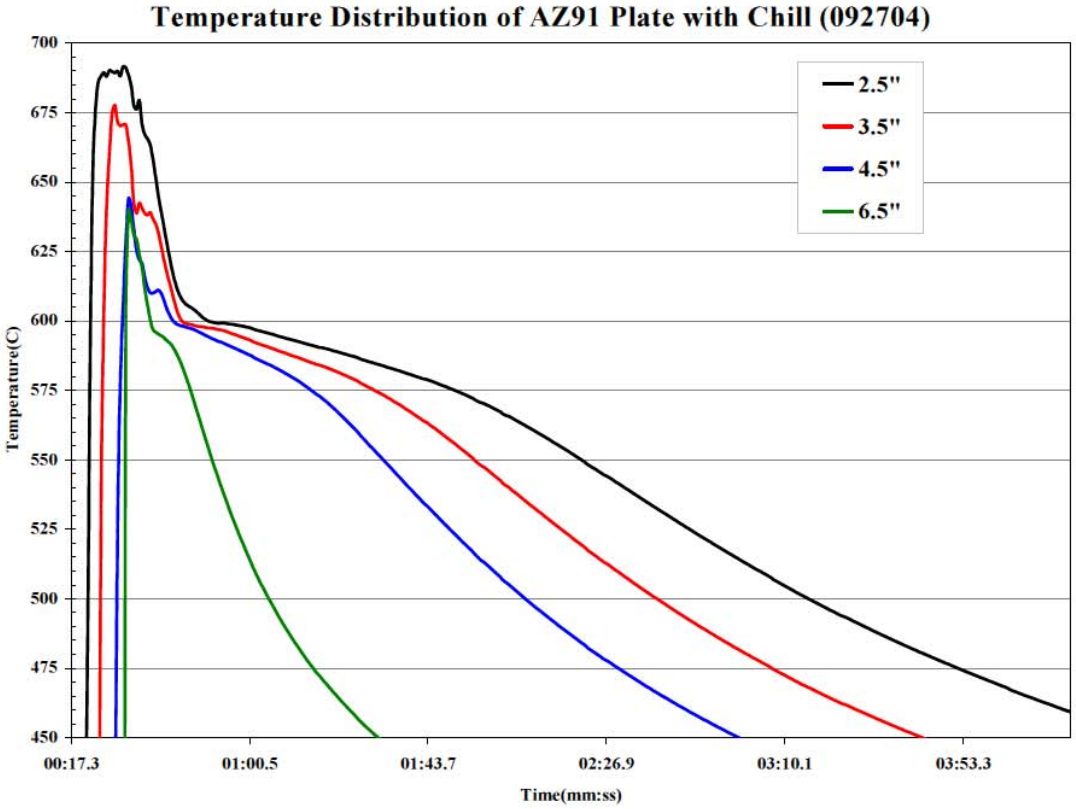
Temperature Distribution of AZ91 Plate with Chill (092704)
Temperature(C)
700
675
650
625
600
575
550
525
500
475
450
2.5"
3.5"
4.5"
6.5"
00:17.3
01:00.5
01:43.7
02:26.9
03:10.1
03:53.3
Time(mm:ss)

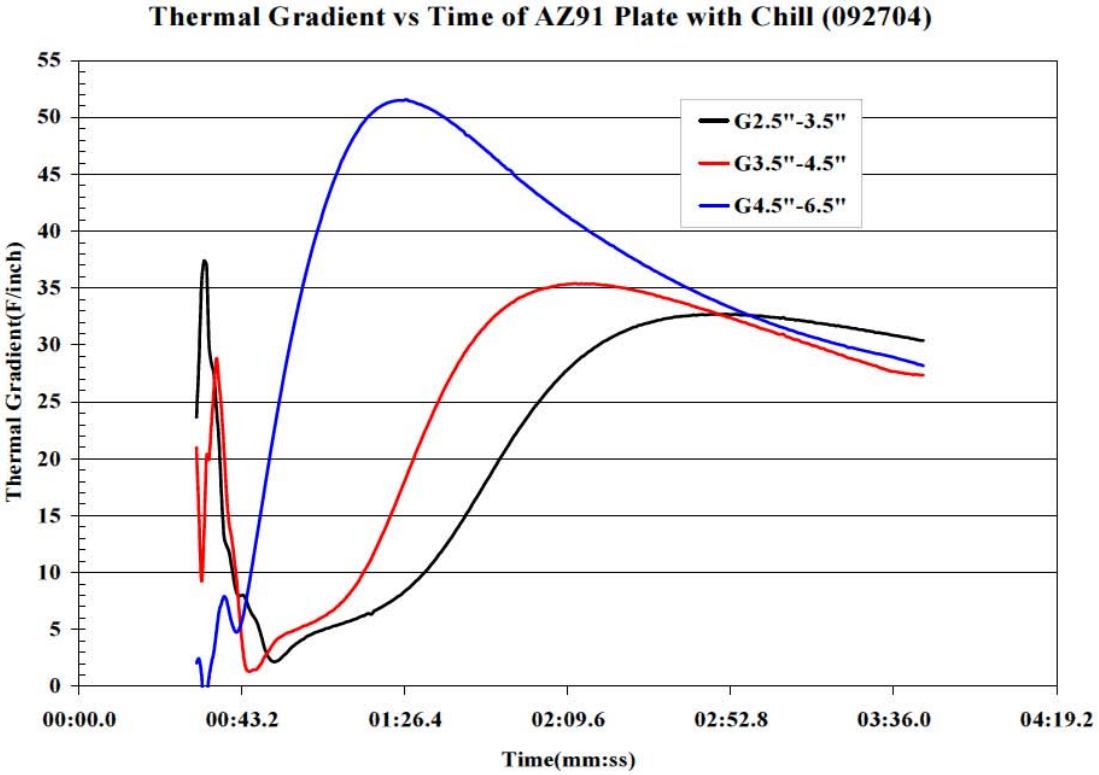
Thermal Gradient vs Time of AZ91 Plate with Chill (092704)
Thermal Gradient(F/inch)
55
50
45
40
35
30
25
20
15
10
5
0
G2.5"-3.5"
G3.5"-4.5"
G4.5"-6.5"
00:00.0
00:43.2
01:26.4
02:09.6
02:52.8
03:36.0
04:19.2
Time(mm:ss)

12 References

1. Robert D. Naranjo, Her-Ping HuangFu, *Lightweight Castings Improving the Fuel Efficiency of America,* 108th AFS/NADCA Conference, 2004.
2. Michael M. Avedesian, and Hugh Baker ed., *ASM Specialty Handbook - Magnesium and Magnesium Alloys* ASM International, Metals Park, OH, 1999.
3. *Standards for Aluminum Sand and Permanent Mold Castings,* 14th Edition, the Aluminum Association, Inc., 2000.
4. Philip D. Harvey ed., *Engineering Properties of Steels,* American Society for Metals, Metals Park, OH, 1982.
5. Stratecasts, Inc. *AFS Metalcasting Forecast & Trends 2004,* American Foundry Society. October. p. 17, 2003.
6. U.S. Department of Energy, Energy Information Administration, *Annual Energy Outlook 2002.*
7. *A SM Handbook Volume 15: Casting,* American Society for Metals, Metals Park, OH, 1998.
8. *Metals Handbook Volume 2 - Properties and Selection: Nonferrous Alloys and Special-Purpose Materials* 10th Edition, ASM International, Metals Park, OH, 1990.
9. *IMA Annual Report: Primary Magnesium Shipments,* International Magnesium Association, Wauconda, IL, 2002.
10. Hugh Baker ed., *ASM Handbook Volume 3: Alloy Phase Diagrams,* ASM International, Metals Park, OH, 1992.
11. J.D. Hannawalt, *SF_6 – Protective Atmospheres for Molten Magnesium,* Paper G775-111, Society of Die Casting Engineers, 1975.
12. G. Schemm, *Sulphur Hexafluoride as a Protection against Oxidation,* Giessrei, Volume58, p 558, 1971.
13. James E. Hillis, *The International Program to Identify Alternatives to SF_6 for Magnesium Melt Protection,* Noranda Magnesium, Inc., 2002.
14. E.O. Hall, *Proc. Phys Soc. London,* Volume 643, p 747, 1951. 15.
15. N. J. Petch, *J. Iron Steel Inst. London,* vol 173, p 25, 1953.
16. Luo Zhiping, Journal of Materials Science Letters. Volume12, p.1490-1492, 1993.
17. D. A. Porter, K.E. Easterling, Phase Transformations in Metals and Alloys, 2nd Edition, Chapman & Hall, London, 1997.
18. John F. Wallace, David Schwam, Yulong Zhu, *The Influence of Potential Grain Refiners on Magnesium Foundry Alloys,* AFS Transactions, Vol. 111, 2003.
19. *Founding of Magnesium Alloys,* Light Metals Vol. 8, No. 84, p. 3-6, London, 1945.
20. R. J. Kissling, J. F. Wallace, *Gas Porosity in Aluminum Castings,* Penton Publishing, Cleveland, 1963.
21. R.D. Green, *Porosity-Free Magnesium Alloy Castings Thermal Requirements,* AFS

Transactions, Vol. 68, pp245 -253, 1960.

22. G.K. Sigworth and C. Wang: Metall. Trans. B, vol. 24B, pp. 349-364, 1993.
23. ASTM, *E8 Standard Test Methods of Tension Testing of Metallic Materials,* Annual Book or ASTM Standards, American Society for Testing and Materials, Vol. 3.01.
24. Galopin, M. et al. *Micro-shrinkage Control in Magnesium Sand Castings.*
25. ASM, *Magnesium and Magnesium Alloys*, ASM International 1999.
26. M. Dierks et.al. *Enhanced Mechanical Properties of Die Cast AM series Magnesium in Attributes of Magnesium for Automobile Design*, SE SP-1022.
27. Z.H. Wang, Y.L.Kang, H.J. Zhao, Y.Xue, *Grain Refinement of Mg-Al Magnesium Alloys by Carbon Inoculation*, Trans. Nonferrous Met. Soc. China, 16 (2006) 1851-1854.
28. L. Lu, A.K. Dahle, D.H. StJohn,*Grain Refinement Efficiency and Mechanism of Aluminum Carbide in Mg–Al alloys*, Scripta Materialia 53 (2005) 517–522.
29. T. Motegi, *Grain-refining Mechanisms of Superheat-treatment and Carbon Addition to Mg–Al–Zn Alloys*, Materials Science and Engineering A 413–414 (2005) 408–411.
30. M. X. Zhang, P.M. Kelly, M. Qian, J.A. Taylor, *Crystallography of Grain Refinement in Mg–Al Based Alloys*, Acta Materialia, 53 (2005) 3261-3270.
31. Q.Jin, J. Eom, S. Lim, Reply to comments on ‘‘*Grain Refining Mechanism of a Carbon Addition Method in a Mg–Al Magnesium Alloy*’’, Scripta Materialia 52 (2005) 421–423.